1-1-2016

A Novel, Ultra-Fast Electrochemical Tool To Study Speciation Of Trace Metals In Aqueous Solution

Pavithra Pathirathna
Wayne State University,

A NOVEL, ULTRA-FAST ELECTROCHEMICAL TOOL TO STUDY SPECIATION OF TRACE METALS IN AQUEOUS SOLUTION

by

PAVITHRA PATHIRATHNA

DISSERTATION

Submitted to Graduate School

of Wayne State University,

Detroit, Michigan

in partial fulfillment of the requirements

for the degree of

DOCTOR OF PHILOSOPHY

2016

MAJOR: CHEMISTRY (Analytical)

Approved By:

_____

Advisor Date

_____

_____

_____

_____

DEDICATION

This dissertation is dedicated:

To my wonderful parents for loving me unconditionally, believing in me always and teaching me how to live life

To my amazing husband for his endless love, sacrificial care and continuous support and encouragement during my time in graduate school

To my little miracle for being so supportive even when it was hard being without Mom and teaching me the way to find joy in the moment

ACKNOWLEDGEMENTS

First, I would like to gratefully and sincerely thank my advisor, Dr. Parastoo Hashemi, for her excellent guidance, unparallel motivation, patience and continuous support throughout my graduate work. Parry, you are the advisor that every graduate student dreams of having. Thank you so much for believing in me and training me, not only as an experimental chemist, but also as an independent scientist. Besides my advisor, I would like to thank Dr. Jennifer Stockdill for providing me an opportunity to join her group and providing me with access to her research facilities. It would not be possible to finish my dissertation without your unwavering support.

I thank all my fellow labmates in Hashemi group, especially Thushani and Shirley, for all the sleepless nights we had in the lab running the experiments. Most importantly, I cherish the everlasting irreplaceable friendship we have built up over the past five years. I would like to thank our former undergraduates, Anisa and Audrey, for teaching me how to make electrodes and helping to set-up the lab. Kevin, Srimal, and Aya, thank you very much for all the valuable discussions and fun we had in the lab together. My sincere thanks also go to Matt, Megan, Rhiannon and Jordan for proof-reading my manuscripts and thesis, and for correcting my mistakes with English grammar. I would also like to thank Michael Rayes for the technical support with electrodes.

I thank my committee members, Dr. Shawn P. McElmurry, Dr. David Crich, Dr. Coolin Poole and previous member Dr. Mary Rodgers for their thoughtful comments and insightful feedback. A special thank goes to Dr.

McElmurry for his continuous support with PHREEQCi analysis and for his valuable suggestions, which encouraged me to think critically and expand my research from various directions. Many thanks also go to Dr. Michael Heien and Dr. Christopher Atcherley for their collaborative research work.

I would also like to acknowledge Nestor O'Campo for his support with software and hardware, Dr. Mike Mei for his help with SEM and XPS analysis, Dr. Chris Thrush for technical support with AFM and XPS, and Dr. Tooraj Hashemi for helpful conversations. I wish to thank all the members of Stockdill group for their great friendship and thoughtfulness. I also wish to express my sincere gratitude for Melissa, Bernie, and Dr. Munk; Melissa for her guidance and support to find the best solution to the problems arose during the last five years in the graduate school, Bernie for her great support with finding the required budget to run last minute experiments, and Dr. Munk for allowing me to work on my dissertation even when I had a tough teaching schedule.

Last but not the least, I would like to thank my family: my parents for their faith in me and the insurmountable support given, my husband for his endless encouragement and unconditional love throughout all good and bad times, my little son for not being so wild especially during my most trying moments, and last but not least, my brother and sister-in-law for always knowing when I needed a little cheering up.

PREFACE

This dissertation is based closely on the following refereed publications:

Chapter 3: P. Pathirathna, Y. Yang, K. Forzley, S. P. McElmurry and P. Hashemi, *Analytical Chemistry*, 2012, **84**, 6298-6302.

Chapter 4: Y. Yang, P. Pathirathna, T. Siriwardhane, S. P. McElmurry and P. Hashemi, *Analytical Chemistry*, 2013, **85**, 7535-7541.

Chapter 5: P. Pathirathna, S. Samaranayake, C. W. Atcherley, K. L. Parent, M. L. Heien, S. P. McElmurry and P. Hashemi, *The Analyst*, 2014, **139**, 4673-4680.

Chapter 6: T. Siriwardhane, A. Sulkanen, P. Pathirathna, A. Tremonti, S. P. McElmurry and P. Hashemi, *Analytica Chimica Acta* - under review.

Chapter 7: P. Pathirathna, T. Siriwardhane, S. P. McElmurry and P. Hashemi, *The Analyst* -under review.

Chapter 8: P. Pathirathna, T. Siriwardhane, S. P. McElmurry and P. Hashemi, *The Analyst* - in preparation.

TABLE OF CONTENTS

LIST OF TABLES

LIST OF FIGURES

LIST OF ABBREVIATIONS

AFM	atomic force microscopy
ASV	anodic stripping voltammetry
BFE	bismuth film electrode
CFM	carbon-fiber microelectrode
CSTR	continuous stirred-tank reactor
CV	cyclic voltammogram
EDS	energy dispersive spectroscopy
EDTA	ethylenediaminetetraacetic acid
DSV	deposition stripping voltammogram
FIA	flow injection apperatus
FAAS	furnace atomic absorption spectroscopy
FSCV	fast scan cyclic voltammetry
FSCAV	fast scan controlled adsorption voltammetry
FSDSV	fast scan deposition stripping voltammetry
ISE	ion selective electrode
LOD	limit of detection
MOPS	3-(N-morpholino)propanesulfonic acid
3-NSA	3-nitrosalicyclic acid
5-NSA	5-nitrosalicylic acid
SEM	scanning electron microscopy/standard error of mean
UPD	under potential deposition
XPS	x-ray photon spectroscopy

CHAPTER 1 INTRODUCTION

1.1 Trace Metals in Biology

Trace metals are vital components in biological systems and are found extensively as structural elements of many metalloenzymes.[1-4] They regulate enzyme-catalyzed biochemical reactions by altering the flow of electrons in enzymes or substrates. Metals such as copper and zinc are present in low concentrations in the brain are thought to serve as neurotransmitters.[5, 6] Recent studies hypothesize that the flow of copper in synapses affects the strength of neuronal connections by changing synaptic plasticity.[7] Further, it is now believed neurotransmission between presynaptic neuron and postsynaptic neurons is disturbed because postsynaptic cells experience low concentrations of copper compared to presynaptic cells. Exposure to excessive levels of copper or deficiency in intracellular copper level leads to the impairments in normal brain development, such as copper accumulation in β-amyloid plaques in Alzheimer's disease.[8, 9] However, these chemical transmissions occur so fast (<seconds) and it has been difficult to monitor these rapid chemical events, mainly due to the inadequate temporal resolution associated with existing analytical tools. Therefore, copper's (and other trace metals) roles in regulating the body's biochemistry has been mostly investigated by comparing animal behavior after exposure to copper. An analytical tool that can provide evidence for rapid copper events would be very useful in understanding underlying copper's physiological mechanisms in biological systems.

1.2 Trace Metals in the Environment

Environmental pollution can result from urbanization and heavy industrialization in modern societies. Trace metals are byproducts of many industrial processes and are major contributors to pollution. The most common sources of harmful trace metals are industrial effluents, fossil fuel combustion, solid waste disposal and fertilizers used in agriculture and mining. These metals bioaccumulate in plants and animals exponentially throughout the food chain and thus humans are highly vulnerable to being exposed via multiple sources. In order to prevent this, environmental engineers have developed robust metal mitigating strategies including active systems such as chelation[10, 11] and amendments,[12-14] and passive systems which employ rain gardens[15, 16] and bioswales.[17, 18] These methods show energy, resource and financial promise; however, because of the complexity of aqueous metal chemistry, these systems are not currently being used at their maximum efficiency.

Trace metals are transported and mobilized during dynamic environmental events such as storms. Because it is very difficult to measure rapidly fluctuating trace metal concentrations, and to define metal speciation on a rapid timescale, it is very difficult to apply existing metal removal systems effectively. Environmental engineers first need to "model" the fate of trace metals during these storm events. The models then can be applied to metal mitigating systems to have them remove trace metals effectively before storm waters are released into natural waters. However the experimental data needed to inform these models remains critically uncategorized because most analytical techniques

cannot monitor trace metals on a rapid temporal scale (<seconds). Fast speciation analysis would greatly aid environmental engineers in their mitigation efforts.

1.3 Trace Metal Detection Techniques

1.3.1 Spectroscopic Methods

Current spectroscopic methods for trace metal detection include atomic absorption spectroscopy,[19, 20] atomic emission spectroscopy,[21, 22] and inductively coupled plasma mass spectroscopy.[21, 23] In many instances, these techniques require the sample to be transferred to the lab for a pre-treatment process before analysis is performed. These methods have high sensitivity, but this comes at the expense of time. Additionally, during sample pre-treatment, speciation is likely altered and only colorless, non-turbid samples can be analyzed without digestion. Two different types of flames are used in flame atomic absorption spectroscopy: An air/acetylene flame is used to quantify metals such as copper, bismuth, and antimony. A nitrous oxide/acetylene flame is used to quantify refractory elements such as aluminum, barium and molybdenum. Graphite furnace atomic absorption spectroscopy is used to achieve higher sensitivity than FAAS as the sample is atomized and condensed in a smaller volume.[24] Finally, large instruments and high maintenance make it challenging to utilize these methods in the field.

1.3.2 Electrochemical Methods

Electrochemistry shows a great deal of promise for trace metal monitoring because the signal generating process occurs on a portable, fashionable, submersible surface, the electrode. The electrode can sample its immediate

environment with little or no disturbance of its surroundings (i.e. speciation). Various electrochemical techniques such as anodic stripping voltammetry and ion selective electrodes have been extensively explored in this context.

1.3.2.1 Anodic Stripping Voltammetry

Anodic stripping voltammetry is one of the most common electro-analytical techniques for trace metal analysis.[25-27] ASV is performed in four steps; first, the working electrode is held at a potential more positive than the oxidation potential of the analyte. During this step, the electrode is cleaned by discharging impurities from the surface. Next, the potential is switched to a negative value to attract positively charged metal ions. During the third step (pre-concentration), the electrode is held at this negative potential for up to 20 minutes to allow electro-reduction of metal ions to a solid deposit on the electrode. Finally, the potential is ramped to more positive potentials, where oxidation (stripping) of the deposited metal from the surface occurs.

The high sensitivity of ASV hinges on two factors: the length of the pre-concentration step and the use of mercury (Hg) electrodes, which limit ASV's application to metal analysis in real systems. Although the pre-concentration step is crucial for sensitive measurements, it comes at the expense of its temporal resolution (minutes). Additionally, anodic stripping voltammetry is mostly performed since Hg forms a stable amalgam with metals.[28, 29] Because Hg is toxic, Hg electrodes are not suitable for analyzing real systems.

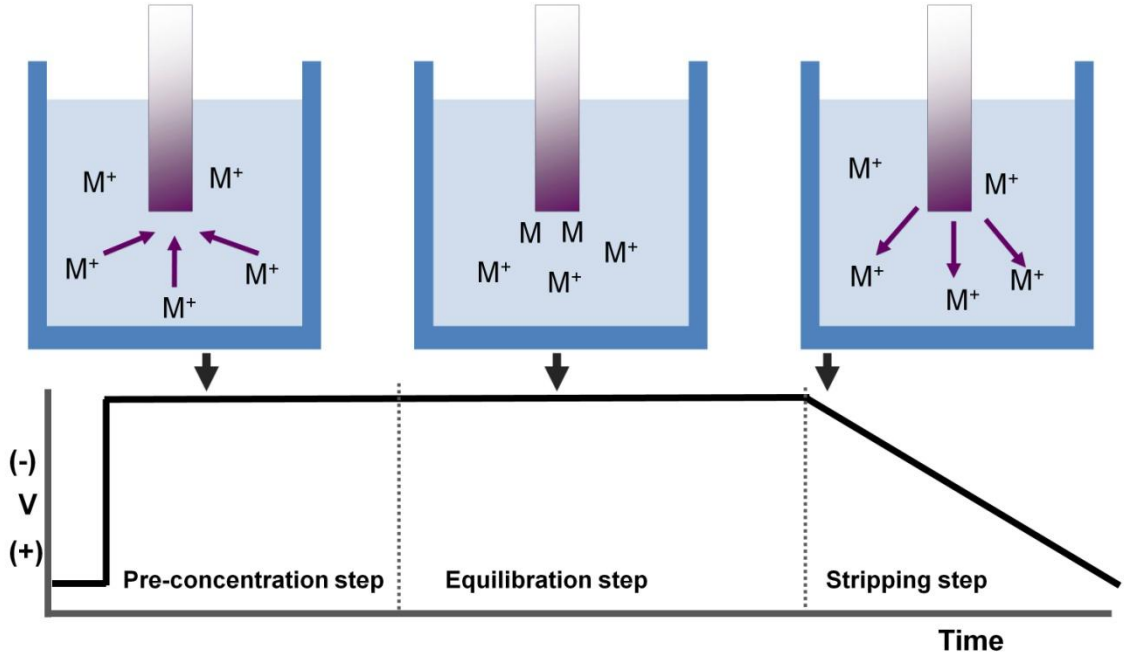

Figure 1.1: Schematic representation of anodic stripping voltammetry

A safer electrode such as the bismuth film electrode is more appropriate for *in situ* monitoring.[30-32] However, the narrow anodic window associated with these electrodes makes it impossible to detect metal ions with higher oxidation potentials than bismuth.[31] Further, BFEs do little to bypass the 20 minute preconcentration period required for sensitive responses.[31] Hence, there is great interest in finding an alternative electrochemical method that is Hg-free and requires a minimal time for pre-concentration.

1.3.2.2 Ion Selective Electrodes

Ion selective electrodes utilize a permeable membrane, incorporating a selective chemical component, which preferentially binds an analyte of interest.[33-35] The membrane's potential changes if this analyte is charged (i.e. positive metal ions) in a predictable way based on concentration of analyte in the membrane.

There are various classes of ISE: glass membrane electrodes, solid state electrodes, liquid-based electrodes and compound electrodes. These electrodes provide a non-destructive, non-contaminating and unaltered by color or turbidity method with good sensitivity and selectivity; however poor stability limits their applicability in-situ.[36, 37] Additionally, ISEs have a temporal resolution of seconds or minutes which further restricts their relevance for rapid metal detection.

1.3.2.3 Fast Scan Cyclic Voltammetry

Cyclic voltammetry is a powerful electrochemical technique because of its simplicity, chemical resolving ability and wide spectrum of applications. It is the most widely employed electroanalytical tool for identifying and quantifying electroactive species.[38-40] In inorganic chemistry, cyclic voltammetry is used to understand various aspects of reaction mechanisms, such as the reaction reversibility, presence and the role of intermediates and electrons, reaction kinetics and fundamental thermodynamic parameters.[41, 42] In biology, cyclic voltammetry is used to determine small concentrations of intracellular and extracellular molecules with high sensitivity.[43, 44]

Julian Millar and colleagues developed fast scan cyclic voltammetry in 1980.[45] As the name implies, it is an extension of cyclic voltammetry with very high scan rates (100 V s^{-1} to 2500 V s^{-1}). Higher scan rates together with a wave form application frequency of 10 Hz allow fast collection of resultant voltammograms at a temporal resolution of milliseconds. Because there is a large, non-Faradic current generated across the electrode surface at higher scan rates, initially the use of FSCV was limited. With the advent of technologically

advanced computers and software, a background subtraction methodology was integrated with FSCV to eliminate interfering non-Faradic signals.[46] This transformative step has rendered background subtracted FSCV one of the most widely accepted electroanalytical techniques among neuroscientists over the last three decades to quantify biomolecules such as neurotransmitters, biogenic amines and other electroactive compounds.[47-51]

In FSCV, a waveform is applied at a specific frequency. In between two cycles, the electrode is held at the resting potential allowing analytes to adsorb onto the electrode. If the potential window is sufficient, adsorbed analytes will repeatedly reduce and oxidize upon raising and lowering the potential on the electrode. This creates an electron flow in the solution and hence a Faradaic current that is measured after background subtraction. Each analyte generates a unique cyclic voltammogram with distinct reduction and oxidation potentials and this signature is used for qualitative purposes. The relationship between the peak current, i_p, and concentration, C is described by Randles–Sevcik equation. (Equation 1: n = number of electron transferred in the redox reaction, F = Faraday's constant, A = electrode area, D = diffusion coefficient, R = universal gas constant and T = temperature). However, in the experiments described in this dissertation, standard solutions are used to construct calibration curves that are used for quantification.

$$\mathbf{i_p = 0.4463\ nFAC\left(\frac{nF\nu D}{RT}\right)^{1/2}} \qquad \text{Equation 1}$$

1.4 Carbon-Fiber Microelectrodes

François Gonon and colleagues first utilization of carbon-fiber microelectrodes in the 1980s[52] was a major breakthrough in the fields of neuroscience and electrochemistry. Carbon-fiber microelectrodes have four fundamental advantages over traditional electrode materials:[53, 54]

1. Hemispherical diffusion of analytes to microelectrode surfaces results in increased mass transfer of analyte to the CFM. This means that there is low ohmic drop across the CFM, hence distortion and separation of the redox peaks in the cyclic voltammogram is minimized

2. The ultra-micron dimensions of CFMs means those invasive measurements in living systems can be achieved with minimal disturbance and damage to the tissue.[55, 56]

3. Since carbon is the most abundant element found in the nature, carbon electrodes are biocompatible and do not induce the body's immune system nor do not they create harmful effects on aquatic systems (as would gold or silver).

4. CFMs oxidize readily at potentials above 1.1 V and subsequently regenerate the surface active groups that enhance the adsorptive properties of the electrode.[57, 58]

Additionally, the broad potential window, wide range of detectable analytes and excellent kinetic properties of CFMs make them a versatile electrode

material. Mark Wightman and his colleagues took a notable step forward by introducing CFMs to FSCV community.[59-61]

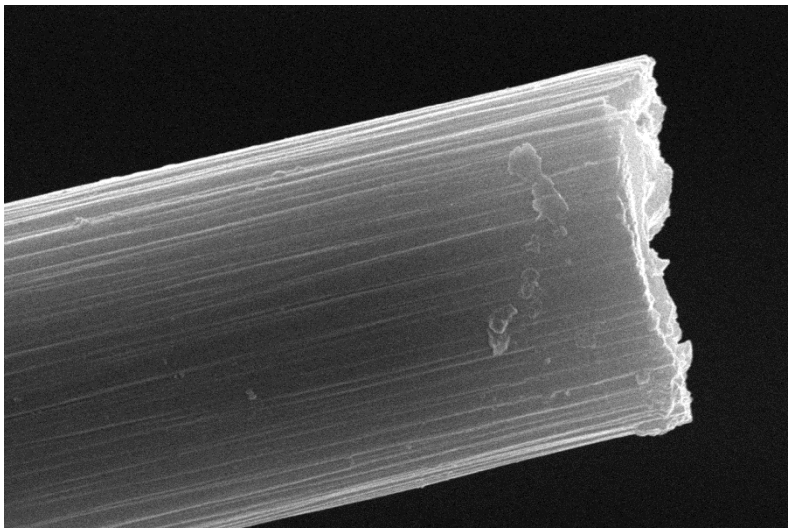

Figure 1.2: SEM image of a carbon-fiber microelectrode.

1.5 Fast Scan Controlled Adsorption Voltammetry

Although FSCV is a successful analytical tool to quantify molecules *in vitro* and in biological systems, because it is background subtracted it cannot report absolute concentrations, just concentration changes. In 2014, Heien and colleagues, developed a modification to allow FSCV to directly measure absolute analyte concentrations *in vitro*, and in collaboration with our group, dopamine *in vivo*.[62] This novel method, fast scan controlled adsorption voltammetry, infers the ability to control the adsorption of analyte at a constant potential without cycling the potential on the electrode.

FSCAV is performed in three basic steps. During the first step, an anlayte specific waveform is applied at high waveform application frequency (100 Hz) at an overoxidizing potential for 2 seconds such that a fresh carbon

surface is generated while analyte adsorption to the surface is minimized. In the second step, the potential is held at a constant potential for a controlled period (10 seconds) during which the analyte is adsorbed onto the electrode surface. The waveform is re-applied during the third step and adsorbed analyte molecules undergo electrochemical redox reactions in the same manner as FSCV. The first or the second cyclic voltammogram collected during step 3 contains chemical information about the adsorbed analyte species. The oxidation/reduction peak is integrated and using Faraday's law, surface concentrations can be calculated. Further, surface coverage can be fit with Langmuir adsorption isotherms to understand the adsorption mechanisms of analytes onto carbon-fiber microelectrodes.[62]

1.6 Motivation

In South West Michigan, natural water pollution is of great concern due to heavy discharge of effluent. This discharge is largely due to insufficient municipal infrastructure and improper release of industrial wastes from automobile manufacturers. Hazardous materials, in particular metals, are heavily used in the automotive and related industries. These include copper as a material for components and catalysts,[63] lead in car batteries and semiconductors[64] and chromium and arsenic in paints and plating.[65] Moreover, older houses in the Detroit area contain lead based paints and plumbing which may contribute to domestic metal contamination. Because the negative consequences of metal exposure are well documented, as described earlier, there have been substantial efforts to mitigate their impact via different metal removal strategies.

At the time I started my PhD research, various types of analytical techniques including spectroscopic and electrochemical tools had been employed to detect and quantify trace metals in aqueous samples. On-site real-time chemical analysis however remained challenging due to given disadvantages discussed above. Therefore, I explored FSCV to identify and quantify two problematic metals, Cu^{2+} and Pb^{2+}. Although my research work concentrated on developing a speciation sensor to analyze Cu^{2+} in environmental samples, our method will be optimized to detect Cu^{2+} in biological samples in the near future.

1.7 Scope of the Dissertation

This dissertation presents the development and optimization of FSCV for ultrafast trace metal monitoring by myself and my colleagues towards development of a real-time speciation sensor. My work concentrates on Cu^{2+} but is applicable to other trace metals. An outline of my dissertation is found below:

Chapter 1 is the introduction

Chapter 2 describes general experimental methods including chemicals and materials, instrumentation, data analysis and software. More specific experimental procedures relevant to each chapter are described within the chapters.

Chapter 3 presents a novel electrochemical approach to detect Cu^{2+} in aqueous samples with FSCV. FSCV was optimized to find unique waveform parameters: a positive and negative potential window, resting potential and scan rate that can generate unique reproducible cyclic voltammograms for copper. The

electrochemical cell was constructed within a flow injection system where tris buffer served as the surrounding matrix. A calibration plot was constructed to determine the sensitivity and the limit of detection for copper with the optimized waveform. Deposition of copper on CFM was illustrated with SEM images and the stability of the technique was confirmed with successive injection of copper into flow injection apparatus. This chapter reports the first evidence of detection of real-time binding of copper and EDTA with an electrochemical technique at a temporal resolution of 100 ms.

Chapter 4 explains the optimization of waveform parameters and solution composition for the detection of Pb^{2+} with FSCV. PHREEQCi, a geochemical modeling software capable of predicting solution chemistry based on thermodynamic equilibrium, was used to mimic the model storm water solution. A Pb-specific waveform was used to analyze real storm water samples spiked with Pb^{2+}.

Chapter 5 reports the investigation of underlying mechanisms of the fast responses in trace metal FSCV. Slow scan Cu^{2+} cyclic voltammograms obtained with a CFM and a gold microelectrode were compared; additional peaks were observed with the CFM. These peaks were further evaluated by changing the scan rate from a 1 mV s^{-1} to 300 mV s^{-1}. We claimed that the origin of these additional peaks was due to the adsorption driven chemistry of copper on the CFM. This adsorption hypothesis was further explored with an array of spectroscopic and electrochemical techniques. FSCAV was utilized to determine the adsorption profile of Cu^{2+} on CFMs and the equilibrium constant for copper

adsorption into CFMs was calculated in two different media: Nacl and tris buffer. We revealed that our system is more sensitive than the solution chemistry predicted by PHREEQCi.

Chapter 6 concentrates on the application of FSCV to study the real-time binding of Cu^{2+} with a model set of ligands in a non-copper binding medium. We developed a kinetic model to assess the hydrodynamic mixing of Cu^{2+}. Our findings point towards the possibility of using our technique to accurately monitor real-time complexation processes with good sensitivity.

Chapter 7 explains in detail the effects of Cu^{2+} complexation with a variety of ligands on the FSCV response. The ligands were chosen to have differing binding abilities and to mimic the full range of complexation equilibria observed in natural waters. We studied the adsorption profiles of Cu^{2+} in the presence of these different ligands with FSACV and showed that the surrounding matrix didn't affect monolayer adsorption properties of Cu^{2+} on CFMs. An interesting mathematical correlation between the literature reported formation constants for Cu^{2+}-ligand binding and FSCV was reported. This correlation allowed us to rapidly predict the formation constant for another model ligand, showcasing the power of FSCV to provide speciation information, in the form of fundamental thermodynamic parameters.

Chapter 8 describes our major step towards a real-time Cu^{2+} speciation sensor. We expanded our previous study detailed in chapter 7 to quantify both the unbound Cu^{2+} level and the overall solution formation constant in the presence of different ligands. We observed strong correlations between the surface charge

determined by FSCAV and the concentration of free Cu^{2+} predicted by PHREEQCi, FSCV response and formation constants for a model set of ligands. We utilized these relationships to predict absolute Cu^{2+} concentration and the formation constant of a groundwater sample spiked with Cu^{2+}. We validated these results are with a ISE. Close agreement between the results obtained with our technique and the ISE reveal the strength of our method to act as a speciation sensor.

Chapter 9 summarizes the conclusions of the research work and future prospectus.

CHAPTER 2 MATERIAL AND METHODS

2.1 Chemicals

All chemicals were purchased from Sigma Aldrich (St. Louis, MO) unless otherwise specified. $Cu(NO_3)_2$ served as the source for Cu^{2+}. The composition of the tris buffer was: Trizma hydrochloride (15 mM), NaCl (140 mM), KCl (3.25 mM), $CaCl_2 \cdot 2H_2O$ (1.2 mM), $NaH_2PO_4 \cdot H_2O$ (1.25 mM), $MgCl_2$ (1.2 mM) and Na_2SO_4 (2.0 mM). EDTA, citric acid, glutamic acid, 5-NSA, and 3-NSA were used as the model ligands for Cu^{2+} - ligand complexation studies. Cu^{2+}-ligand solutions were prepared in 1:1 stoichiometry ratio in NaCl (0.01 M) prior to FIA analysis and sufficient time was given to each solution mixture to reach the steady state. The pH of all solutions was reported at room temperature and atmospheric pressure.

2.2 Carbon-Fiber Microelectrodes

A single carbon-fiber of 3 - 5 µm radius (T-650, Thornel, Amoco Co. / T-650, Cytec Industries, NJ / Goodfellow Corporation, PA, USA) was vacuum aspirated into a glass capillary (0.6 mm external diameter, 0.4 mm internal diameter, A-M Systems, Inc., Sequim, WA). The carbon-glass was made by pulling the fiber-filled capillary under gravity using a micropipette puller (Narishige, Tokyo, Japan), leaving a tapered end. The exposed carbon-fiber was trimmed to approximately 150 µm in length under a microscope. Shorter electrodes with a length of 25 - 30 µm were prepared only for FSCAV experiments.

2.3 Flow Injection Analysis

A custom-built flow injection system served as the electrochemical cell. The carbon-fiber microelectrode was first inserted to a flangeless short 1/8 nuts (PEEK P-335, IDEX, Middleboro, MA) leaving a small portion of the tip (2 mm) outside of the nut. Then the nut containing microelectrode was fastened to one end of a modified HPLC union (Elbow PEEK 3432, IDEX, Middleboro, MA). The other end of the elbow was fastened to the out-flowing stream of the FIA buffer. The reference electrode and the 'waste' of the flow system were incorporated into the union via two holes. The cell was connected to a six-port HPLC loop injector (Rheodyne Model 7010 valve, VICI, Houston, TX) affixed to a two-position actuator (Rheodyne model 7010 valve and 5701 actuator). The flow of buffer was maintained with a syringe infusion pump (KD Scientific, Model KDS-410, Holliston, MA). The analyte was introduced into the flow stream for 10 seconds at a rate of 2 mL min^{-1} *via* the HPLC loop injector as a rectangular pulse.

2.4 Fast Scan Cyclic Voltammetry

All experiments employed a 2-electrode cell consisting of a CFM and an Ag/AgCl reference electrode that was constructed by electroplating Cl^- ions onto a Ag wire (A-M systems, WA). Experiments described in Chapters 3, 5 and 6 were conducted with a custom-built UEI potentiostat and a breakout box (University of North Carolina at Chapel Hill, Department of Chemistry Electronics Facility). Waveform generation, data acquisition, signal processing including back-ground subtraction, signal averaging and digital filtering (4-pole Bessel

Filter, 5 kHz) were performed with a customized software, TH-1 (ESA, Chelmsford, MA) written in LABVIEW (National Instruments, Austin, TX).

The voltammetric experiments described in Chapters 4, 7 and 8 were carried out with another potentiostat (Dagan Corporation, Minneapolis, MN, USA) and a custom-built breakout box. Data acquisition and signal processing were achieved with in-house software, WCCV 2.0 (Knowmad Technologies LLC, Tucson, AZ) written in LABVIEW 2012.

2.5 Fast Scan Controlled Adsorption Voltammetry

A CFM and a reference electrode, Ag/AgCl, were placed in a beaker containing Cu^{2+}- ligand solution. The waveform (-1.0 V – +1.3 V at 100 Hz, resting potential of 0 V, at 600 V s^{-1}) was applied for 2 seconds and the potential was switched to the resting potential with an electronic relay (ADG-419, Analog Device). The adsorption of Cu^{2+} onto the CFM was controlled by applying a constant potential of 0 V for 10 seconds (delay time). The reduction peak on the first background-subtracted copper cyclic voltammogram was integrated with in-house software, WCCV 2.0 (Knowmad Technologies LLC, Tucson, AZ) written in LABVIEW 2012. The surface concentration (Γ_{Cu}) was calculated using Faraday's law. The measured data were fitted with a lineraized Langmuir isotherm (Equation 2) where C is the [Cu^{2+}] in bulk solution, Γ_{max} is the maximum monolayer surface coverage, and K is the equilibrium constant for adsorption.

$$\frac{C}{\Gamma_{Cu}} = \frac{1}{\Gamma_{max}}C + \frac{1}{\Gamma_{max}K} \qquad \text{Equation 2}$$

2.6 PHREEQCi Analysis

The solution chemistry of Cu^{2+} - ligand mixtures in NaCl was predicted with PHREEQCi, a geochemical modeling software based on thermodynamic equilibrium.[66] Equilibrium constants required to evaluate the speciation of each of the mixtures were extracted from MINTEQ.v4 database developed by the U.S. Environmental Protection Agency. The additional constants required to map the complexation processes accurately were modeled in equilibrium with $CO_{2(g)}$ ($10^{-4.8}$ atm.) and $O_{2(g)}$ ($10^{-0.67}$ atm.).[67]

CHAPTER 3 FAST-SCAN DEPOSITION-STRIPPING VOLTAMMETRY AT CARBON-FIBER MICROELECTRODES: REAL-TIME, SUBSECOND, MERCURY FREE MEASUREMENTS OF COPPER

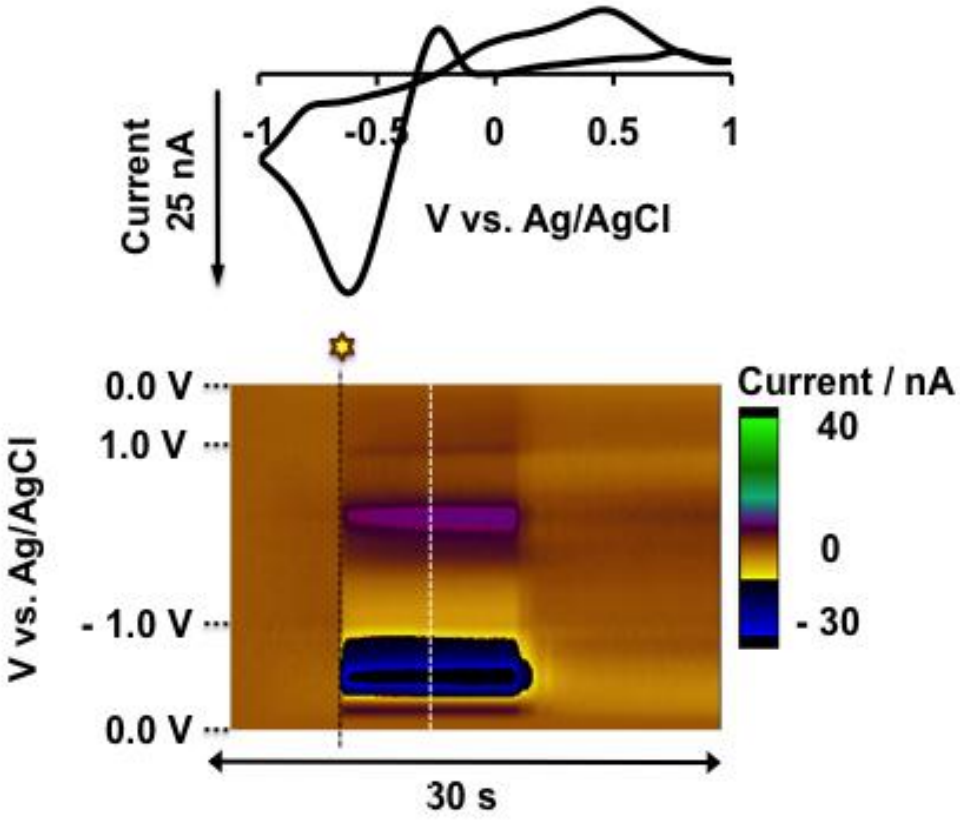

P. Pathirathna, Y. Yang, K. Forzley, S. P. McElmurry and P. Hashemi, *Analytical Chemistry*, 2012, **84**, 6298-6302. Reprinted with permission from Copyright(2012), American Chemical Society.

3.1 Abstract

Elevated concentrations of hazardous metals in aquatic systems are known to threaten human health. Mobility, bioavailability, and toxicity of metals are controlled by chemical speciation, a dynamic process. Understanding metal behavior is limited by the lack of analytical methods that can provide rapid, sensitive, in situ measurements. While electrochemistry shows promise, it is limited by its temporal resolution and the necessity for Hg modified electrodes. In this study, we apply fast-scan deposition-stripping voltammetry at carbon-fiber microelectrodes for in situ measurements of Cu^{2+}. We present a novel, Hg-free technique that can measure Cu^{2+} with ppb sensitivity at 100 ms temporal resolution.

3.2 Introduction

In urban areas, anthropogenic sources of heavy metals are a significant public health concern. Mobility, bioavailability, and toxicity of metals depend on speciation, including complexation with inorganic and organic ligands.[68, 69] The ability to dynamically assess low metal concentrations in aqueous solutions is critical for characterizing environmental processes, assessing risks, and mitigating their impact.

Spectroscopic techniques study heavy metals with high sensitivity.[70-72] These instruments typically have limited portability and require significant sample handling, which may alter speciation. The majority of in situ research, aiming to understand “unaltered” speciation, has aggressively employed electrochemistry[73] with the ultimate goal of a submersible field device (for a review see ref 73).

While ion selective electrodes provide high sensitivity with temporal resolution of seconds, their response time (10−15 s) limits their application for real-time studies.[74] Techniques such as anodic stripping voltammetry have shown promise for environmental applications. ASV involves “deposition” of metal onto an electrode during a negative potential sweep. The metal is subsequently “stripped” off during a positive sweep. A Faradaic current during stripping is typically used to quantify the metal. The extreme sensitivity of ASV has hinged upon two critical factors: (a) Hg (mercury) modification: The “deposition” process can be unstable on conventional electrodes leading to inconsistencies in analyses. Hg on the electrode surface significantly stabilizes this process by creating an amalgam with the depositing metal. (b) Pre-concentration: Conventional electrodes are held at a negative potential for several minutes in order to pre-concentrate the heavy metal on the electrode yielding high sensitivity.[75]

Until now, few alternatives existed that could detect low metal levels without Hg (an environmental hazard) and with high temporal resolution (faster than minutes required for pre-concentration). In this study, we present a Hg-free electrochemical technique that can measure [Cu^{2+}] with environmentally relevant parts-per-billion (ppb) sensitivity and importantly, a temporal resolution of 100 ms. This temporal improvement, of greater than 3 orders of magnitude, allows real-time metal speciation to be studied.

Our method is based on fast-scan cyclic voltammetry at carbon-fiber microelectrodes. FSCV has largely been developed for biological applications[76, 77] and employs scan rates between 400 and 1000 V s^{-1}. The time to acquire one

cyclic voltammogram is approximately 20 ms. A large charging current can be eliminated by background-subtraction when cyclic voltammograms are collected in quick succession (every 100 ms).[78] We now apply this technique, which we refer to as fast-scan deposition-stripping voltammetry, to detect Cu^{2+} in real-time.

3.3 Materials and Methods

Chemicals

All chemicals were obtained as stated in Chapter 2.

Microelectrodes, FIA analysis and FSCV

Fabrication of carbon-fiber microelectrodes and flow injection analysis were performed as described in Chapter 2. Data acquisition and signal processing in FSCV experiments were carried out with a custom-built UEI potentiostat and TH-1 software. (More details can be found in Chapter 2)

3.3.1 Positive and Negative Potential Limits

We were limited by a potential window in order to perform FIA experiments that tested the dependence of current response on positive and negative potential limits. To avoid problems associated with water degradation, the maximum negative potential was limited to -1.4 V. To avoid over-oxidization of the carbon surface, which enhances its absorbtivity and limits its time resolution, the maximum positive potential was limited to 1.3 V. The combinations on the topography were tested in random order to avoid tenting effects and allow us to establish optimal potential limits for Cu^{2+} DSV.

3.3.2 Scan Rate Dependence

We were limited by a maximum scan rate when performing FIA experiments that tested the dependence of current response on scan rate. At scan rates above 1200 V s^{-1}, the charging current on the electrode's surface overloaded our hardware, therefore, analyses at scan rates above this were not possible.

3.3.3 Scanning Electron Microscopy and Energy Dispersive X-ray Spectroscopy

Scanning electron microscopy and Energy dispersive x-ray spectroscopy were performed on a Jeol JSM-6510LV/LGS Scanning Electron Microscope (Peabody, MA). SEM images were collected under high vacuum, using an excitation voltage of 25 kV and Au sample sputtering. EDS data were collected using a SDD detector. EDS spectra were collected at three distinct locations on each electrode and the values for atomic % Copper were averaged.

3.3.4 Cu^{2+} Binding by EDTA

The CFM was immersed into a well stirred solution of Cu^{2+} (20 mL of 200 mM $Cu(NO_3)_2$). EDTA (1 mL of 1 mM) was injected directly into this solution and the CVs were collected upon addition of EDTA.

3.4 Results and Discussion

3.4.1 Fast Metal Voltammetry of Cu

Deposition-stripping voltammograms collected every 100 ms serve two important purposes, identification and quantification, illustrated in **Figure 3.1** Here DSVs were collected for 30 s during a flow injection analysis of Cu^{2+} (10μM) onto a CFM. The potential of the CFM was initially swept in the negative direction

from 0 to −1.0 V and then subsequently reversed to +1.0 V at a scan rate of 400 V s^{-1}. The middle panel of Figure 3.1 provides a representation of all of the background-subtracted DSVs. The interpretation of this color plot is described in detail elsewhere.[79] Cu^{2+} was injected at the time point indicated by the star. **Figure 3.1.A** is one DSV taken during the Cu^{2+} injection, indicated by the vertical white dashed line. Peaks corresponding to deposition (−0.6 V) and stripping (0.5 V) are visible as reduction and oxidation peaks. **Figure 3.1.C** is the current taken at the maximum reduction potential for each DSV plotted with time.

Because we are measuring Cu^{2+} reduction, the current is in the negative direction; however, the signal corresponds to an increase in [Cu^{2+}]. **Figure 3.1.C** can be converted to [Cu^{2+}] first with standard calibrations and then via reversal of the current direction. This analysis now represents the sub-second measurement of [Cu^{2+}] and is shown in **Figure 3.1.D** FSCV at CFM has been found to be highly sensitive for neurotransmitters,[57] and we found the same for Cu^{2+}, in this example 28.7 nA was obtained for a 10 μM Cu^{2+} injection. Hemispherical diffusion of the analyte to the CFM surface creates increased mass transport hence increased response. In addition, Faradic current is proportional to the scan rate for absorbed species and again results in an increased response. Moreover, the increased convection effects of flow injection analysis can contribute to an increased signal.

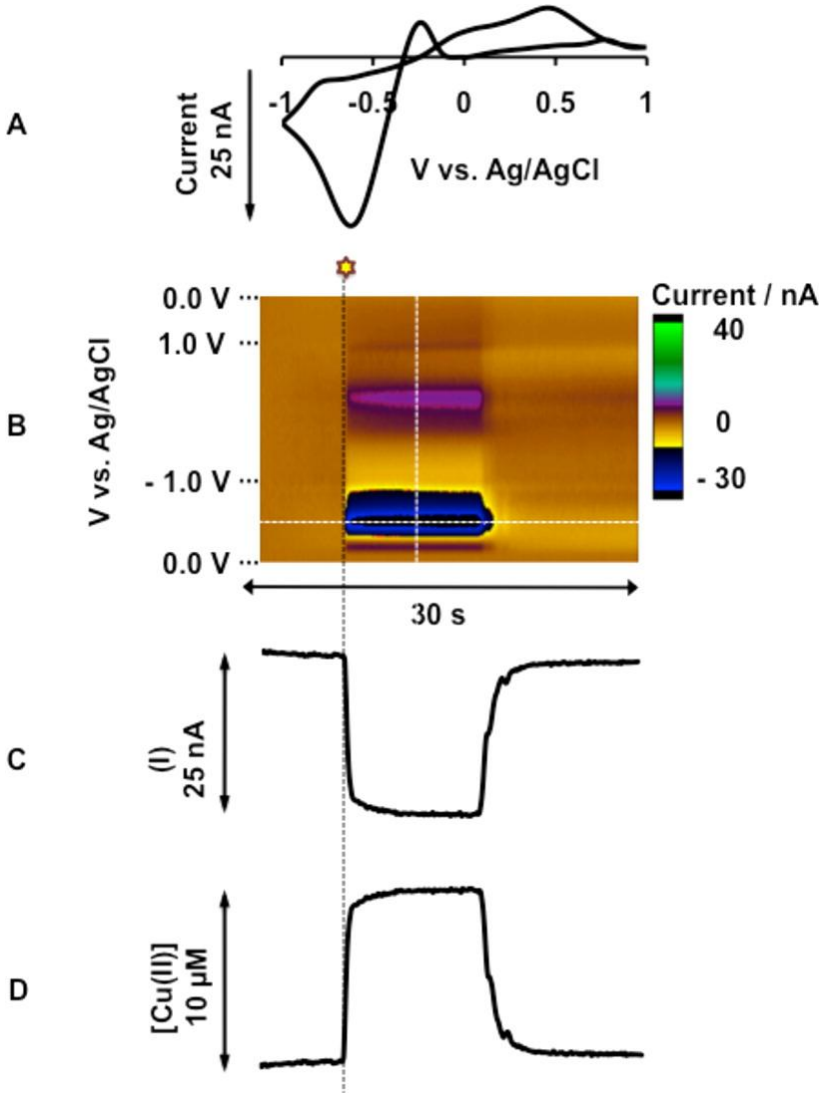

Figure 3.1: (A) DSVs (i vs v) taken and reconstructed from the white vertical dashed line in part B. (B) Color plot with potential on the y-axis plotted against time on the x-axis and the current response represented in false color. Cu^{2+} (10 µM) is injected at the time indicated by the black vertical dashed line and star. (C) i vs time from the horizontal white dashed line at peak reduction potential. (D) $[Cu^{2+}]$ obtained by taking the reverse of part C and standard calibrations.

In classical ASV, the magnitude of the stripping peak is used for quantification; this is because it is not feasible to quantify deposition due to the preconcentration that lasts several minutes. The length of our negative sweep is around 2.5 ms, therefore it is possible to acquire a well-defined deposition peak. This peak is advantageous for two reasons. First, the deposition peak has a

higher magnitude than the stripping peak, presumably due to kinetics (with an optimized waveform described below, deposition and stripping have magnitudes of 55.8 ± 0.96 nA and 18.0 ± 0.39 nA, respectively (n = 50 ± standard error of the mean)), hence, employing the deposition peak for quantification improves sensitivity. Second, this technique has two characteristic voltages by which to identify a process. Our future focus is to characterize multiple metals in environmental samples simultaneously. Therefore having both peaks will be particularly important for distinguishing between them.

3.4.2 Stability of Cu Deposition

To analyze multiple metals with both deposition and stripping peaks, it is essential that deposition is stable over multiple readings in the absence of Hg. To establish whether this holds for CFMs, we tested the reproducibility of $Cu_{(s)}$ electrodepostion on CFMs. We applied −1.4 V to the CFM for 0, 1, 5, and 10 min in a solution of Cu^{2+} (100 μM) and assessed the electrode surface with scanning electron microscopy and energy dispersive X-ray spectroscopy. There is a proportional relationship between the deposition time and % $Cu_{(s)}$ as shown in **Figure 3.2.A**; a visual confirmation of this relationship is observed in the representative scanning electron micrographs for each time group. Here, the SEMs clearly show presence of $Cu_{(s)}$ clusters on the carbon-fiber striations even after 1 min. Trace levels of $Cu_{(s)}$ at 0 min can be attributed to the sample holder material of the instrument. After 1 min, the surface $Cu_{(s)}$ was 1.2 ± 0.2%; after 5 min, 3.2 ± 0.4%; after 10 min, 6.9 ± 1.1%. This shows that we can control the deposition process, an indication of its high stability.

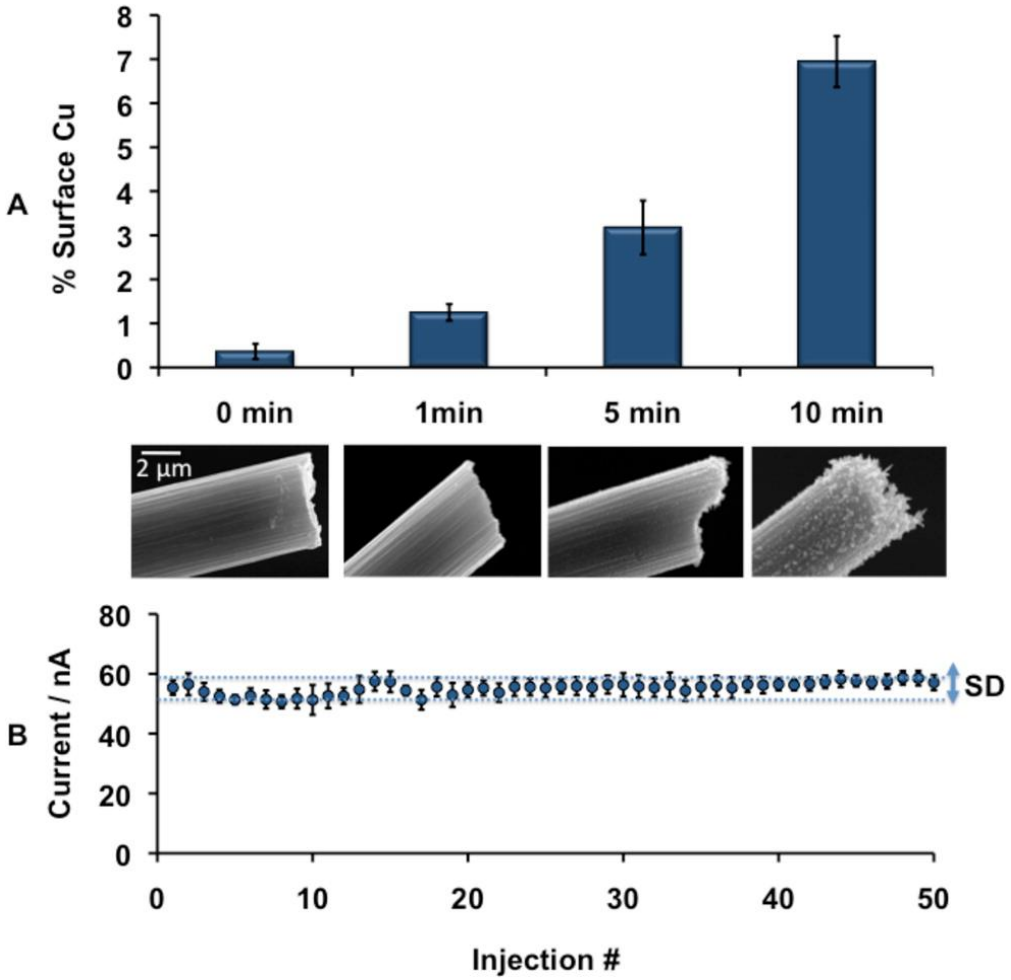

Figure 3.2: (A) Histogram showing % surface $Cu_{(s)}$ vs deposition time (0, 1, 5, and 10 min) (n = 3 ± standard error of the mean). Representative SEMs, taken at 8000× magnification for each group are displayed under each histogram block. (B) Peak reduction current of successive Cu^{2+} (10 µM) injections onto a CFM with FIA. (Positive potential limit +1.3 V, negative potential limit −1.4 V, resting potential 0 V, scan rate 600 V s^{-1}). Horizontal lines indicate SD limits.

To further validate the stability of deposition, we used an optimized waveform (−1.4 to 1.3 V at 600 V s^{-1} with a resting potential of 0 V, as described below), we repeatedly injected Cu^{2+} (10 µM) onto a CFM (50 times), and we recorded the peak reduction current each time. The magnitude of the current observed is plotted against injection number in **Figure 3.2.B**. The response is

55.2 ± 2.1 (standard deviation) ± 0.29 (standard error of the mean) nA (n = 50). The low standard deviation and standard error confirm that this is a stable process. The DSVs exhibited a robust deposition/stripping peak ratio of 3.1 ± 0.03 (n = 50 ± standard error of the mean). Again, the low standard error indicates that deposition is as stable as oxidation, a further index of its high stability.

Cu^{2+} reduction is described below:

$$Cu^{2+} + 2e^{-} \rightarrow Cu_{(s)} \qquad E^{\circ} = 0.34 \text{ V vs. SHE}$$

3.4.3 Optimization of Waveform Parameters

We initially chose waveform parameters that are well established in FSCV.[57] We observed $Cu_{(s)}$ deposition over −0.3 to −0.8 V. The discrepancy may be due to the difference in reference material (SHE vs Ag/AgCl). Another possibility is an iR drop due to slow electron transfer kinetics at high scan rates, during the deposition scan that creates a wide peak separation. The mechanism of this process is a focus of our ongoing studies. With this waveform, the response to Cu^{2+} (10 μM) is 33.9 ± 4.1 nA (n = 4 ± standard error of the mean). We varied our waveform parameters to optimize sensitivity to Cu^{2+}. **Figure 3.3.A** shows the averaged current response to Cu^{2+} (10 μM) when the positive and negative potential limits were varied (n = 4). Each point on the topograph in **Figure 3.3.A** shows the current response at a particular combination of the positive and negative limits. The current is modestly augmented with increasing negative potential; we postulate that this is due to maximized Cu^{2+} adsorption. There is a more defined trend with an increasing positive limit, with two clear

"breaks". First, there is a drop-off at around 0.8 V. This may be due to incomplete stripping, which would reduce the surface available for deposition on subsequent scans. Second, there is an exponential increase after 1.2 V. This has previously been observed for neurotransmitters and is due to overoxidation of the carbon surface. The overoxidation process renders the surface more sensitive due to increased absorption to catalytic oxygen groups[57] and regeneration of the carbon surface with each scan.[58] Therefore, we set the optimal potential limits to −1.4 to 1.3 V vs Ag/AgCl. However, we found that the response to Cu^{2+} (10 μM) at 1.3 V, 53.2 ± 10.9 nA (n = 4 ± standard error of the mean), was variable. The metal has a complex interaction with the carbon surface under these conditions; we are currently studying the surface catalysis at 1.3 V to better understand this. In Figure 3.3.B we varied the resting potential from −0.6 to 0.6 V. We found that the optimal resting potential was 0 V (for 10 μM, 36.1 ± 2.0 nA, n = 4 ± standard error of the mean) with two different slopes governing the drop-off in the positive and negative directions. When the rest potential is held at positive potentials, Cu^{2+} is correspondingly repelled. FSDSV only detects differential responses, therefore, when scanning negatively, there will be a background Faradaic current arising from the deposition that will effectively be subtracted out, manifesting itself as a reduction in signal. Finally, we varied the scan rate from 100 to 1200 V s^{-1}. There is a linear relationship between scan rate and current up to1000 V s^{-1} (**Figure 3.3.C**). The slope of log current vs. log scan rate is 0.9, close to 1, confirming adsorption driven electrochemistry. At 1200 V s^{-1} the current is reduced, possibly because of a temporal limitation for deposition (time for the negative sweep at

this scan rate is less than 1 ms). At 1000 Vs^{-1}, the peak separation was significant enough to cause inconsistencies in the shapes of the DSVs. At 600 V s^{-1}, there were still advantageous current gains, but the shapes of the DSVs were consistent. Therefore, we chose 600 V s^{-1} as our optimal scan rate. Here the current response to 10 μM was 48.7 ± 5.1 nA (n = 4 ± standard error of themean) and the limit of detection was 250 nM or 15.8 ppb.

Therefore, we present a unique, optimized waveform for online Cu^{2+} detection, −1.4 to 1.3 V at 600 V s^{-1} with a resting potential of 0 V. Standard calibrations with this waveform are presented in **Figure 3.3.D** (n = 4 ± standard error of the mean). A linear calibration range up to 5 μM or 318 ppb is suitable for environmental Cu^{2+} analyses; the sensitivity (slope) in this range is 4.9 nA μM^{-1} or 0.077 nA ppb^{-1}.

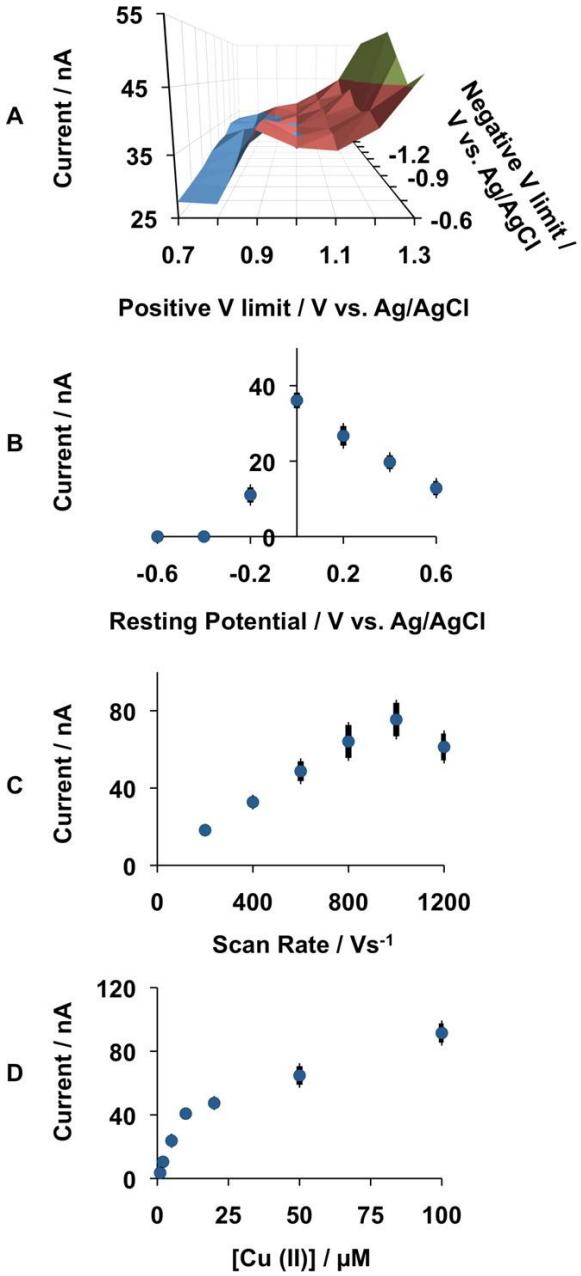

Figure 3.3: (A) 3-D representation of peak reduction current of background-subtracted in vitro DSVs of Cu^{2+} (10 µM) vs positive potential limit (x-axis) and negative potential limit (z-axis) (n = 4).(Resting potential 0 V, scan rate 400 V s^{-1}). (B) Variation in peak reduction current when resting potential is varied (n = 4 ± standard error of the mean). (Positive potential limit +1.3 V, negative potential limit −1.4 V, scan rate 400 V s^{-1}). (C) Variation in peak reduction current when the scan rate is varied (n = 4 ± standard error of the mean). (Positive potential limit +1.3 V, negative potential limit −1.4 V, resting potential 0 V). (D) Standard calibrations (n = 4 ± standard error of the mean). (Positive potential limit +1.3 V, negative potential limit −1.4 V, resting potential 0 V, scan rate 600 V s^{-1}).

3.4.4 Real-time Copper Binding with FSCV

The strength of our technique is its time resolution because it is critical for studying speciation, and we demonstrate this in **Figure 3.4.B**. Here, the CFM was immersed into a well-stirred solution of Cu^{2+}. We injected ethylenediaminetetraacetic acid at the time point indicated by the star and this created an immediate change. The DSV taken at the vertical white dashed line shows the reverse DSV of Cu^{2+} indicating that the concentration of Cu^{2+} decreased (**Figure 3.4.A**). The identity of Cu^{2+} was verified by the close agreement of peak positions in the inset of **Figure 3.4.A** Here, the current of the experimental DSV (black solid) was reversed and superimposed onto an DSV of Cu^{2+} (10 μM) collected in vitro (dashed), both were normalized to the maximum negative current. In **Figure 3.4.C**, the maximum deposition current (reversed) decreased with time reaching a new level indicating less free Cu^{2+}. This is a novel sub-second electrochemical measurement of the Cu^{2+} binding process by EDTA. We repeated this experiment with four different electrodes and found similar results.

Quantitative measurements of Cu-EDTA complexation are routinely performed during titrations, where specific points are monitored at equilibrium. The slope in **Figure 3.4.C** represents the magnitude of Cu^{2+} bound with time or the rate at which EDTA binds Cu^{2+}. This real-time kinetic information is fundamentally novel with electrochemical techniques. Such information is dependent on a complex variety of information about the system, including temperature, flow, pH, ionic strength, and complexation. These can now be

studied using well-established models for Cu^{2+} speciation. Real environmental samples contain a variety of electroactive interferences; therefore, we are currently identifying and characterizing these substances in order to separate out specific effects of interest.

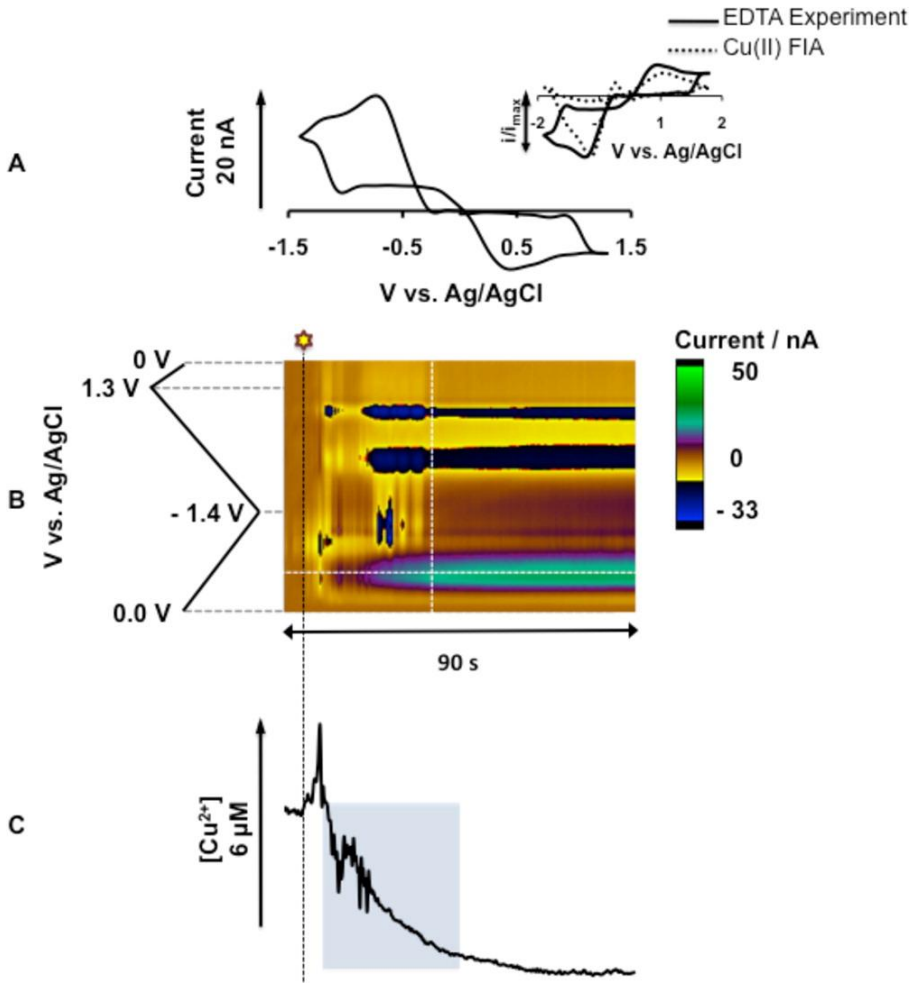

Figure 3.4: (A) DSVs (i vs v) taken and reconstructed from the white vertical dashed line in part B. Inset: DSV of Cu^{2+} (10 µM) taken by FIA (dashed) superimposed on the reverse current DSV taken from white vertical dashed line in part B. (B) Color plot with potential on the y-axis plotted against time on the x-axis, and the current response represented in false color. CFM is immersed into a well stirred solution of Cu^{2+} (20 mL of 200 µM). EDTA (1 mL of 1 mM) is injected at the time indicated by the black vertical dashed line and star.(C) Cu^{2+} vs time taken and reversed from the horizontal white dashed line at peak reduction potential.

3.5 Conclusions

In conclusion, studying metal speciation is essential for mitigating the impact of metals in environmental systems. However field technology that provides real-time information on metal speciation has been limited. While portable and low cost, electrochemical techniques have traditionally been limited by their temporal resolution and necessity for Hg. In this letter, we reported a novel Hg-free technique, FSDSV at CFMs, to perform electrochemical measurements of Cu^{2+} every 100 ms, without toxicity concerns. We anticipate that our technology will open new frontiers for studying speciation, advancing our ability to reduce the environmental impact of metals.

CHAPTER 4 REAL-TIME SUBSECOND VOLTAMMETRIC ANALYSIS OF LEAD IN AQUEOUS ENVIRONMENTAL SAMPLES

FSCV was optimized to quantify Pb in aqueoues water samples. I participated both experimentally and intellectually to develop FSCV to measure Pb and the outcome of this project guided me towards my next projects.

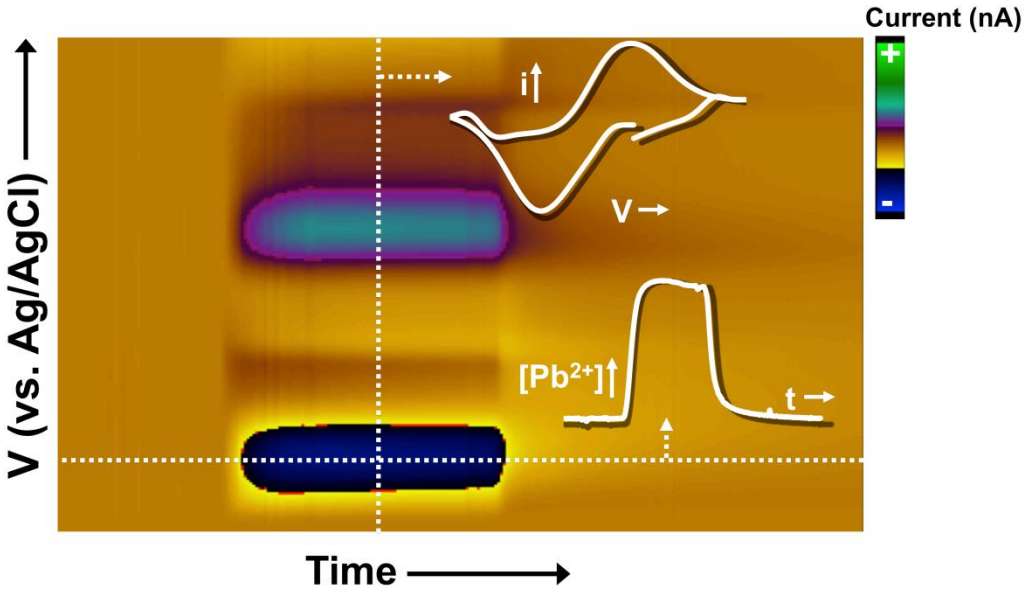

Y. Yang, **P. Pathirathna**, T. Siriwardhane, S. P. McElmurry and P. Hashemi, *Analytical Chemistry*, 2013, **85**, 7535-7541. Reprinted with permission from Copyright (2013), American Chemical Society

4.1 Abstract

Lead pollution is an important environmental and public health concern. Rapid Pb transport during stormwater runoff significantly impairs surface water quality. The ability to characterize and model Pb transport during these events is critical to mitigating its impact on the environment. However, Pb analysis is limited by the lack of analytical methods that can afford rapid, sensitive measurements in situ. While electrochemical methods have previously shown promise for rapid Pb analysis, they are currently limited in two ways. First, because of Pb's limited solubility, test solutions that are representative of environmental systems are not typically employed in laboratory characterizations. Second, concerns about traditional Hg electrode toxicity, stability, and low temporal resolution have dampened opportunities for in situ analyses with traditional electrochemical methods. In this paper, we describe two novel methodological advances that bypass these limitations. Using geochemical models, we first create an environmentally relevant test solution that can be used for electrochemical method development and characterization. Second, we develop a fast-scan cyclic voltammetry method for Pb detection on Hg-free carbon-fiber microelectrodes. We assess the method's sensitivity and stability, taking into account Pb speciation, and utilize it to characterize rapid Pb fluctuations in real environmental samples. We thus present a novel real-time electrochemical tool for Pb analysis in both model and authentic environmental solutions.

4.2 Introduction

Lead is a toxic pollutant commonly found in postindustrial urban watersheds because of its historical use in paints, automotive gasoline and batteries.[80, 81] Despite efforts to reduce Pb loadings to the environment, Pb exposure continues to be of great concern to public health. In particular, there is increasing evidence that children exposed to Pb, even at levels previously considered safe, have a high risk for developing adverse neurological and systemic health problems.[82] These concerns, in addition to newly recognized exposure paradigms,[83] have created a critical interest in better defining Pb cycling in the environment.

One of the most significant transport processes in urban systems is stormwater runoff. Urban stormwater is the primary source of water quality impairments for 13% of all rivers, 18% of all lakes, and 32% of all estuaries in the United States, despite urban land use constituting only 3% of the land cover.5 The discharge of metals in stormwater is one of the primary causes of these water quality impairments.[84] In order to prevent the damaging environmental effects of Pb, it is vital to understand the mechanisms of Pb transport during environmental events such as stormwater runoff where solution chemistry is often in disequilibrium.[85] To understand Pb transport, it is necessary to quantify the interactions of Pb with organic ligands and soils dynamically because these reactions have rapid kinetics.[86, 87] The lack of analytical methods that can continuously monitor Pb in situ with high time-resolution has traditionally limited this goal.

While spectroscopy provides high sensitivity and selectivity, on site analysis is difficult due to limited portability of the instruments. Moreover, sample collection and preparation do not allow in situ analysis. Electrochemistry has shown promise for such measurements[73, 88, 89] because electrochemical reactions occur at a submersible surface. However, concerns about stability, Hg-electrode toxicity, and low temporal resolution have severely limited the application of electrochemistry to environmental analyses.

We recently described the application of fast-scan cyclic voltammetry to real-time, sub-second Cu detection.[90] Our method is fast, robust, and Hg-free. In this work, we applied a similar approach to Pb characterization. We faced two discrete challenges for experimental FSCV analysis. First, aqueous systems were not available to analyze Pb under conditions that are representative of real natural water systems like those in which we ultimately seek to understand Pb's behavior. Because of Pb's limited aqueous solubility, other researchers performing Pb electrochemistry have traditionally utilized test solutions (buffers) at low pH[91-93] or in acetate[94-96] or nitrate rich buffers.[97-99] While such solutions allow electrochemical characterizations, they are not ideal for environmental characterizations. Second, in our prior work, we established a Cu specific electrochemical FSCV waveform[90] but here we discovered that this waveform was not suitable for Pb detection. In this paper, we describe methods to overcome both challenges.

We employed geochemical modeling software to develop a model test solution that mimics stormwater runoff, which we then optimized for

electrochemical analysis. We subsequently optimized a Pb-specific FSCV waveform with high sensitivity and temporal resolution. Finally, we analyzed real stormwater samples spiked with Pb and were able to detect rapidly fluctuating Pb concentrations with the same voltammetric profile as our model solution.

We therefore present a novel experimental method for rapid Pb analysis. We created this system to best mimic stormwater runoff, while retaining sufficient ionic composition required for FSCV analysis. Our novel system will allow researchers to investigate Pb chemistry, kinetics, and transport in model and real environmental systems.

4.3 Materials and Methods

Carbon-fiber microelectrodes, FIA Analysis and Data Acquisition and Analysis with FSCV

Microelectrodes were constructed, FIA experiments were conducted with a custom built electrode cell, and voltammetric experiments (data acquisition and processing) were performed with a custom-built UEI potentiostat and TH-1 software, all as described in Chapter 2.

PHREEQCi Analysis

Solution chemistry was modeled in PHREEQCi as stated in Chapter 2.

4.3.1 Solutions

Stock Pb^{2+} solutions were prepared by dissolving $Pb(NO_3)_2$ (Mallinckrodt Baker Inc., Japan) into different buffer solutions. The composition of our model solutions was based on the geometric mean concentration of major ions observed in stormwaters, as described in the International Stormwater BMP

Database:23 HCO_3^- (1.2 mM), Ca^{2+} (230 mM), Mg^{2+} (33 mM), K^+ (20 mM), NO_3^- (25 mM), and SO_4^{2-} (80 mM). Final solutions were further optimized based on the PHREEQCi modeling results. The Version 1 (V1) model surface water solution was $NaHCO_3$ (0.23 mM), $CaSO_4$ (0.16 mM), $MgCl_2$ (2.2 mM), KCl (0.062 mM), KNO_3 (0.036 mM), and Na_2HPO_4 (0.013 mM) at pH 7.0. The Version 2 (V2) model surface water solution was $NaHCO_3$ (0.0012 mM), $CaCl_2$ (0.23 mM), $MgCl_2$ (0.033 mM), KCl (0.020 mM), KNO_3 (0.025 mM), NaCl (4.0 mM), and Na_2SO_4 (0.080 mM) at pH 6.5. All aqueous solutions were made with deionized water.

4.3.2 Stormwater Collection

We collected stormwater samples during a 30 min runoff event on December 4, 2012 that deposited 0.2 inches of rain over a 45 acre paved parking area in southeast Michigan. Samples were collected in precleaned 1 L bottles using a Sigma SD9000 All Weather-Refrigerated Sampler. Sample bottles were cleaned with soap, phosphate free detergent (e.g., Liqui-Nox soap) and water, rinsed with nanopure water (>18 MΩ), rinsed with 37% trace-metal grade HCl and triple rinsed with nanopure water. Samples were refrigerated (4 ± 1 °C) until they were transported in a dark cooler on ice to the laboratory where they were filtered through a 0.45 µm pore size AquaPrep filter within 6 h. After filtering, no additional alterations were made to the sample and they were stored refrigerated (4 ± 1 °C) in the dark. From these discrete samples, one of the samples collected at an approximate peak flow of the runoff event was selected for voltammetric experiments.

4.3.3 Statistical Analysis

Pooled data is presented with errors signified by the standard error of the mean. Student's t tests were performed on paired data sets; $p < 0.05$ was taken as significant and signified with a star.

4.4 Results and Discussion

4.4.1 Fast Voltammetric Detection of Metals

Electrochemistry has been employed as an important tool for metals detection since Heyrovsky brought polarography to popularity in the 1920s.[100] The most popular polarographic method for metals analysis is anodic stripping voltammetry. The fundamental principle here is that the potential on a Hg droplet is held at a negative value so that metal ions in solution electrodeposit within the Hg matrix, creating an amalgam. If this process is given enough time, it can serve as a powerful preconcentrator of the metal ions on the electrode surface. Thus, when the potential is ramped in the positive direction, the deposited metal is "stripped" off the electrode surface, providing high currents relative to the metal concentration. ASV is an important method for laboratory analysis; however, concerns about Hg toxicity and the portability of the polarographic setup has severely limited the application of ASV for environmental analyses. As such, researchers have explored a variety of safe materials, along with modifications to voltammetric methods in order to create devices more suited to monitor the environment. Among these, the bismuth film electrode is particularly popular.[101-103] The BFE forms "fused alloys" with metal ions, analogous to the formation of an amalgam. Negligible toxicity is its main advantage; however, the

BFE is limited by a narrow anodic range that makes it impossible to detect metal ions with oxidation potentials more positive than Bi (e.g., Cu, Sn, and Sb).[31]

New materials can improve the applicability of stripping methods for environmental studies; however, another ongoing challenge is to improve temporal resolution. This challenge is particularly pertinent during stormwater runoff events where it is important to understand the fate and transport of Pb (e.g., kinetics of metal−organic interactions[104]). Ion-selective electrodes, measuring potential changes due to partition of Pb ions into a selective membrane, have improved temporal resolution.[105-107] However, their response time is still >20 s, and issues with stability and sensitivity create additional challenges for environmental analyses.

We recently described a fast method for Cu detection on carbon-fiber microelectrodes.[90] Our method utilizes the adsorptive capacities of carbon-fiber surfaces to rapidly preconcentrate metal ions onto the electrode surface prior to a fast cyclic voltammetric scan. For Cu, a preconcentration time of 100 ms resulted in ppb (parts per billion) sensitivity.[90] This method is fast, selective, and Hg-free, critical ingredients for an environmental analytical tool.

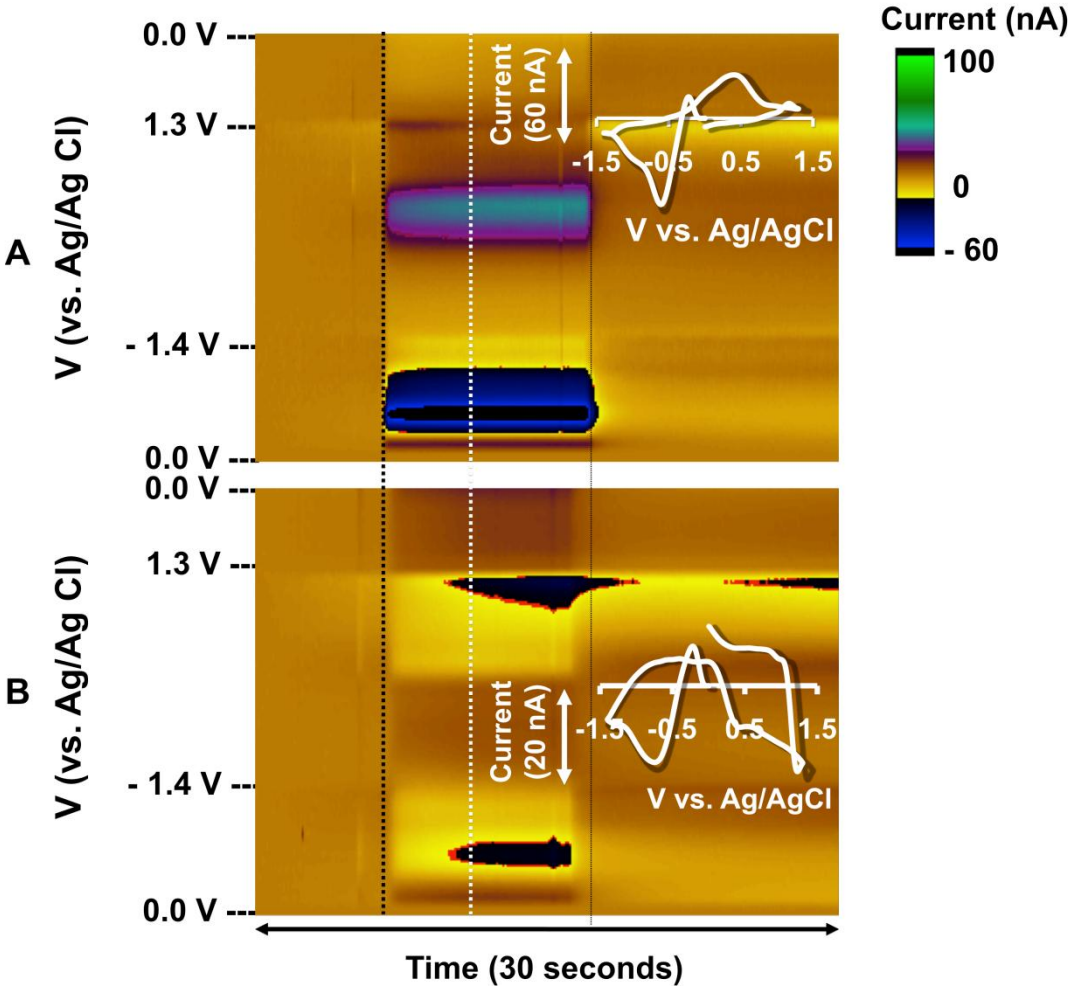

Figure 4.1: Color plots with potential on the y-axis plotted against time on the x-axis and the current response represented in false color. In part A, Cu^{2+} (10 μM) was flow injected onto a carbon-fiber microelectrode and in part B, Pb^{2+} (10 μM) was injected. Insets show CVs taken at the vertical white dashed line.

Using flow injection analysis, we studied the response of our method to Pb^{2+} with our previously established Cu specific waveform.[90] FIA provides reproducible and rapid pulses of analytes to the electrode surface, making it an ideal tool to probe dynamic meta chemistry. The potential was initially ramped in the negative direction from 0 to −1.4 V and then in the positive direction to 1.3 V and finally back to 0 V resting potential. **Figure 4.1.A** shows an injection of Cu^{2+} (10 μM $Cu(NO_3)_2$) onto a CFM. The color plot is constructed by stacking

background-subtracted cyclic voltammograms (y-axis) with time (x-axis) and assigning false color to current changes (z-axis). The start and end of the injection are denoted by the dashed black lines. As we previously found, the voltammetric signature during the injection identifies Cu^{2+} based on the position of the initial reduction and subsequent oxidation peak taken from a CV (inset) during the injection indicated by the white dashed line. In **Figure 4.1.B**, we performed the identical experiment for an injection of Pb^{2+} (10 μM $Pb(NO_3)_2$). Here we encountered two problems. First, Pb^{2+} has limited solubility in Tris buffer, and as such, our standard solutions visibly displayed high levels of precipitation. Second, the $Pb^{2+}_{(aq)}$ in this solution did not give rise to a redox-recognizable process as evidenced by the lack of an oxidation peak (inset CV). This observation was not surprising since Pb^{2+} is larger than Cu^{2+} and necessarily has different absorption and reaction kinetics. This experiment shows that different metals demand unique FSCV waveforms, optimized for their kinetic characteristics. We can employ different FSCV waveforms to provide enhanced selectivity for individual metals. Selectivity can be further improved by using ionophores to preconcentrate metals on the electrode surface prior to the voltammetric scan. This is currently one of our research objectives.

In the following sections, we optimize the test solution to create stability for Pb and create an FSCV waveform for discrete Pb detection.

4.4.2 Model Surface Water Solution for Pb Electrochemistry

Previously, when establishing a Cu^{2+} specific waveform, we utilized a Tris buffer test solution because the majority of FSCV characterizations are carried

out in this buffer system.[57, 77] However metals in natural waters exhibit considerably different speciation than under laboratory conditions. Pb has limited solubility and readily forms carbonate and hydroxy complexes with common buffers.[108] This reactivity makes it difficult to utilize standard laboratory buffer systems for Pb analysis. As such, researchers have traditionally used test solutions at low pH[91-93] and with compositions that are not environmentally relevant.[95-99] Furthermore, it is difficult to compare data between different test solutions because the concentration of free Pb^{2+} can vary due to differences in complexation. Therefore it is important to establish an environmentally relevant model test solution for Pb analysis that can also facilitate electrochemical measurements.

We first created a solution based on the ionic composition of stormwater typical of northern climates where road salt is used.[109] This solution, V1, was at pH 7 with an ionic strength of 4.0×10^{-3} M. When Pb^{2+} was added to this solution to make a standard concentration of 100 μM, we found that the solution was unstable (**Figure 4.2**). With a relevant waveform (we describe full optimization in the next section), the Pb^{2+} standard was successively flow injected onto a CFM. In **Figure 4.2**, the maximum reduction current response to the injection was plotted with the injection number in the blue trace.

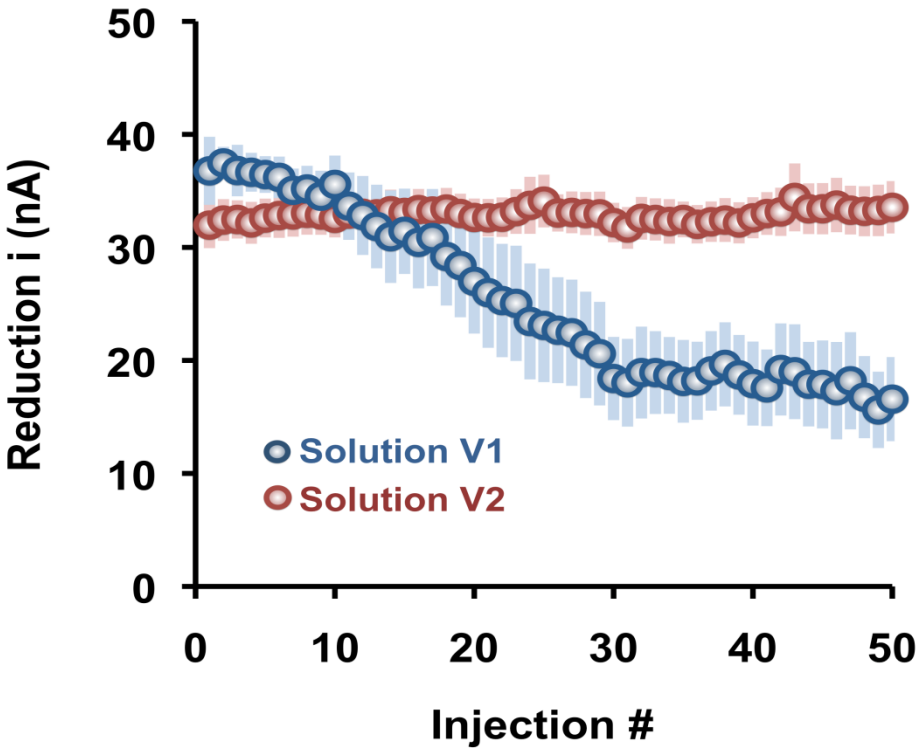

Figure 4.2: Maximum reduction current to successive flow injections of Pb^{2+} in solutions V1 (blue) and V2 (red). Error bars are ±SEM (standard error of the mean).

It is clear that the electrode response decreases with increasing injection number. We have previously shown that FSCV responses to metals are stable with repeated injections;[90] therefore, this decrease in signal is indicative of solution instability. To further validate this hypothesis, test solutions were left overnight, resulting in formation of a white precipitate. After filtering out the precipitate, the FSCV response was no longer detectable, suggesting that the concentration of free Pb^{2+} was dramatically reduced in solution due to precipitate formation. This speculation was confirmed with a PHREEQCi model. The thermodynamic equilibrium described by PHREEQCi predicted that Pb would precipitate as cerrusite ($PbCO_3$) for solutions with this composition and pH until it reached a concentration of 2.6 μM, currently below our detection limit.

To minimize cerrusite formation, we reduced the concentration of bicarbonate, decreased the pH to 6.5, and eliminated phosphate from solution. The ionic strength was similar at 5.3×10^{-3} M (compared to 4.0×10^{-3} M). This solution, V2, displayed increased stability. The red trace in **Figure 4.2** shows successive injections of Pb^{2+} onto the CFM with no loss in response. When this solution was left overnight, no precipitates formed. This result was further verified in PHREEQCi which predicted that this solution should be at equilibrium.

Taken together, these results constitute the first report of a stable solution closely mimicking stormwater composition suitable for Pb electrochemical analysis. Importantly, thi solution resembles the reported makeup of authentic stormwater samples submitted to the International Stormwater BMP database, making it an ideal test solution for environmental analyses. Moreover, the solution has sufficient ionic and buffer capacity to enable accurate fundamental electrochemical characterizations with FSCV.

4.4.3 Optimization of a Voltammetric Waveform for Pb Detection

In **Figure 4.1**, we showed that our Cu^{2+} specific FSCV waveform was not suitable for Pb^{2+} detection. Because the ionic radius of Pb^{2+} is larger than that of Cu^{2+} we expect differences in the FSCV kinetics between the two, thus we expected Pb^{2+} to require different electrochemical detection parameters. To create a unique waveform for Pb^{2+} detection with a robust redox signature, we systematically altered the electrochemical potential limits, the resting potential, and the scan rate. **Figure 4.3** shows the results of this optimization (100 µM Pb^{2+}). The initial cathodic scan induces Pb^{2+} reduction, therefore we increased

the reduction potential window by increasing the resting potential, as shown in **Figure 4.3.A**. We found that, as we increased the potential window, the peak reduction current increased and we were able to capture redox processes on both cathodic and anodic scans. When we increased the positive potential above 0.2 V, we found increase peak separation between the oxidation and reduction peaks. We therefore chose 0.2 V as the ideal resting potential. Here the reduction current was 34.4 ± 2.6 nA (n = 4 ± SEM).

Figure 4.3.B illustrates the effects of varying positive and negative potential limits. **Figure 4.3.B.(i)** displays values of peak reduction current for combinations of positive and negative potential limits when the negative potential limit is plotted on the x-axis while **Figure 4.3.B.(ii)** shows the same when the positive potential limit is plotted on the x-axis. There was not a strong trend when we increased the negative potential window. In **Figure S1.A** in the appendix A, the current at −0.6 V was statistically compared to the current at −1.2 V for every positive potential studied. Only one of the series showed a significant trend. At very low negative potentials (<−1.0 V), O_2 reduction can be observed on CFMs;[110, 111] given that O_2 levels are likely to fluctuate in environmental systems, we chose −0.8 V as our negative potential limit. As the positive potential was increased, there was a significant increase in the signal. We therefore determined that a positive potential limit of +0.8 V would yield high sensitivity and discrete redox peaks.

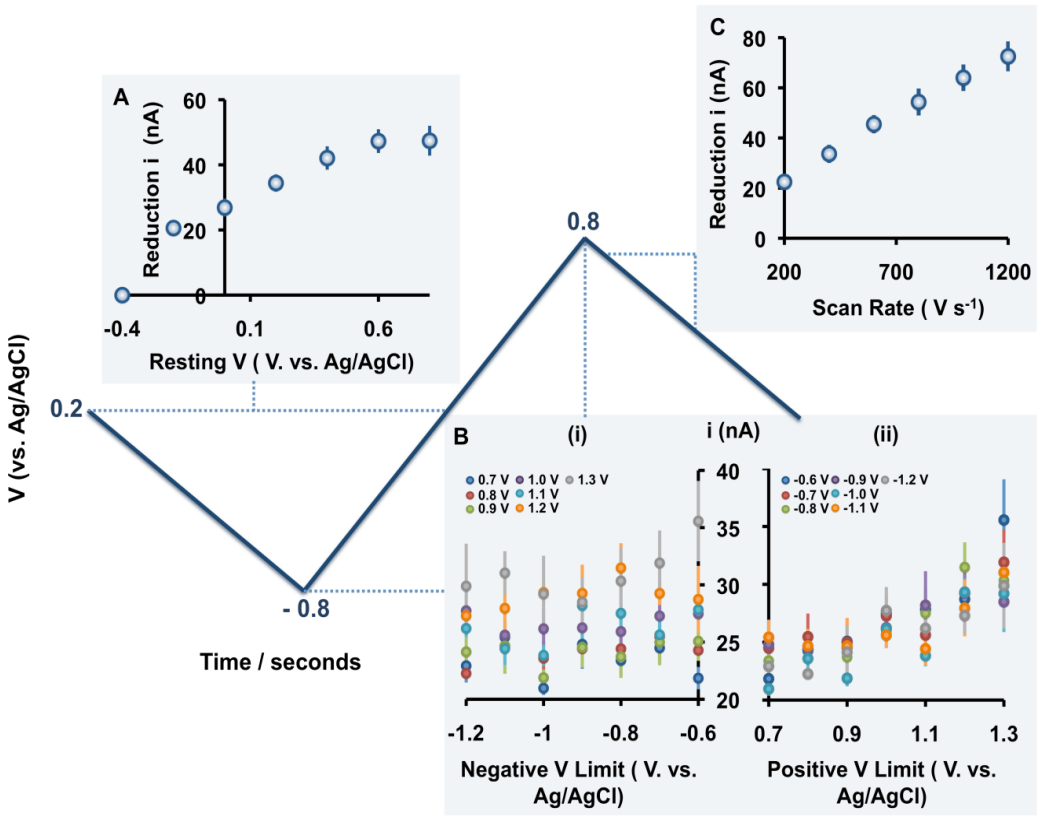

Figure 4.3: Results of waveform optimization. The optimized waveform is shown in blue. Part A shows resting potential dependence on i (scanning from −0.8 to +0.8 V, with a scan rate of 400 V s^{-1}). Part B shows the potential limit dependence. Part B(i) shows values of i for combinations of positive and negative potential limit when the negative potential limit is plotted on the x-axis Part B(ii) shows values of i for combinations of positive and negative potential limits when the positive potential limit is plotted on the x-axis. Part C shows the scan rate dependence on i (scanning from −0.8 to +0.8 V, with a rest potential of 0.2 V).

In **Figure S1.B** in the appendix A, the current at 0.7 V was statistically compared to the current at 1.3 V for every negative potential studied. All but one of the series showed a significant trend due to overoxidation of the carbon-fiber microelectrode surface as described previously.[57, 58] Although the response increased with increasing positive potential limit, at high positive potential limits, oxidation and reduction peaks were undefined and indicated kinetic limitations.

Finally, we confirmed scan rate dependence on current by varying the scan rate from 200 to 1200 V s^{-1}. We found a positive correlation with increasing scan rate; however, the IR drop created by high scan rates increased peak separation and distorted the CVs. We therefore chose 400 V s^{-1} as the optimal scan rate.

Our optimal waveform, shown in **Figure 4.3**, is −0.8 to +0.8 V, resting at 0.2 V, and with a scan rate of 400 V s^{-1}. With this waveform, sensitivity to Pb^{2+} is 0.17 nA μM^{-1} or 0.84 nA ppm^{-1}, the limit of detection is 10 µM or 2.1 ppm, and the linear calibration range is up to 350 µM or 73 ppm.

4.4.4 Optimized Pb Detection Model

We combined our model test solution with our Pb-optimized waveform in order to create a novel Pb analysis method. **Figure 4.4** shows a flow injection analysis experiment where our test solution was used as the flow injection solvent and Pb^{2+} (100 µM) was injected into the flow stream onto a CFM. The color plot (middle panel) shows electrochemical events after injection, and the CV (top panel, extracted from the vertical dashed line) verifies a robust redox process with defined reduction and oxidation peaks at −0.35 and +0.2 V, respectively. Pb^{2+} perturbations on an environmentally relevant temporal scale can be established by extracting i vs t at the peak reduction current (horizontal white dashed line). When compared to calibrations, these data can be turned into [Pb] vs time as previously described,[90] shown in the bottom panel. The entirety of this event lasts 30 s.

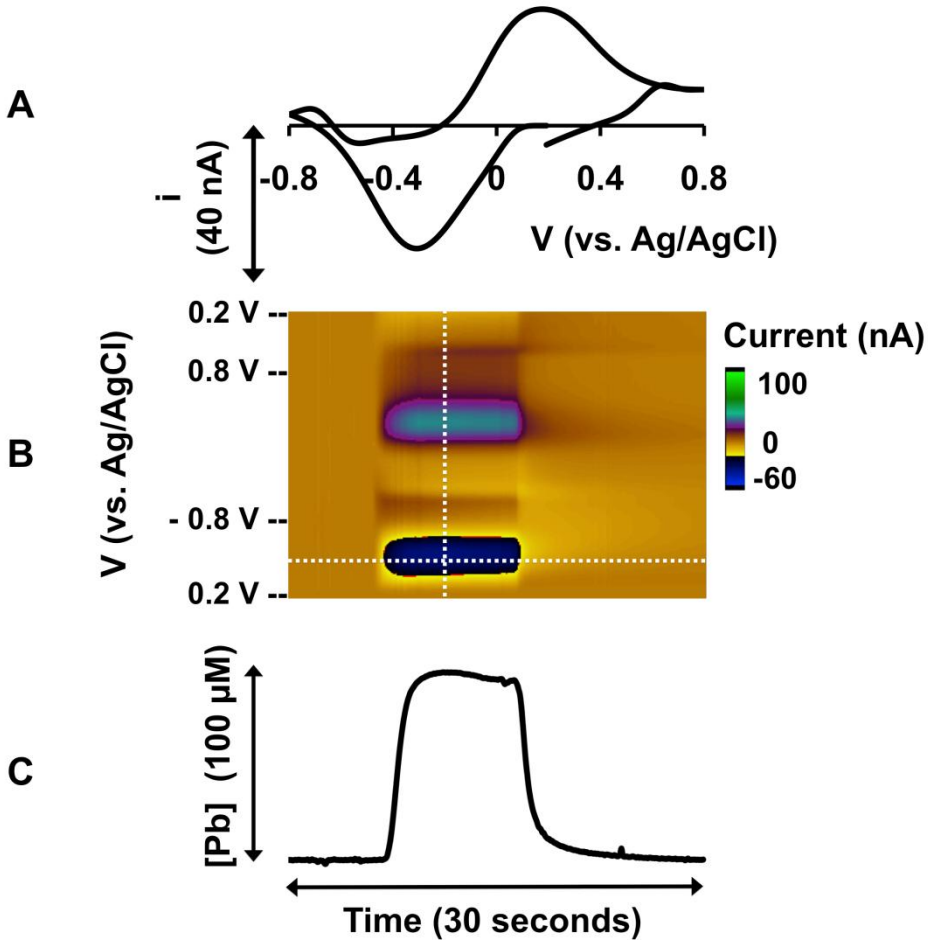

Figure 4.4: A FIA response to Pb^{2+} with optimized test solution and waveform. Part A shows a CV taken at the vertical white dashed line from the color plot in part B. Part C shows a plot of [Pb^{2+}] vs time, which was determined by taking i vs t from the horizontal white dashed line in the color plot. The i vs t trace was reversed to create a positive value (as described in ref 13) and represents 100 µM Pb^{2+}.

Standard Pb calibrations are shown in **Figure 4.5**. Typically calibrations for electrochemical analyses utilize acidified solutions which maximize free Pb^{2+}.[94, 112] In acidic solutions, the [Pb^{2+}] can be considered the same as the total [Pb] However in natural systems, complexation with ligands can reduce [Pb^{2+}]. If

not taken into account, this will result in inaccurate concentration measurements.

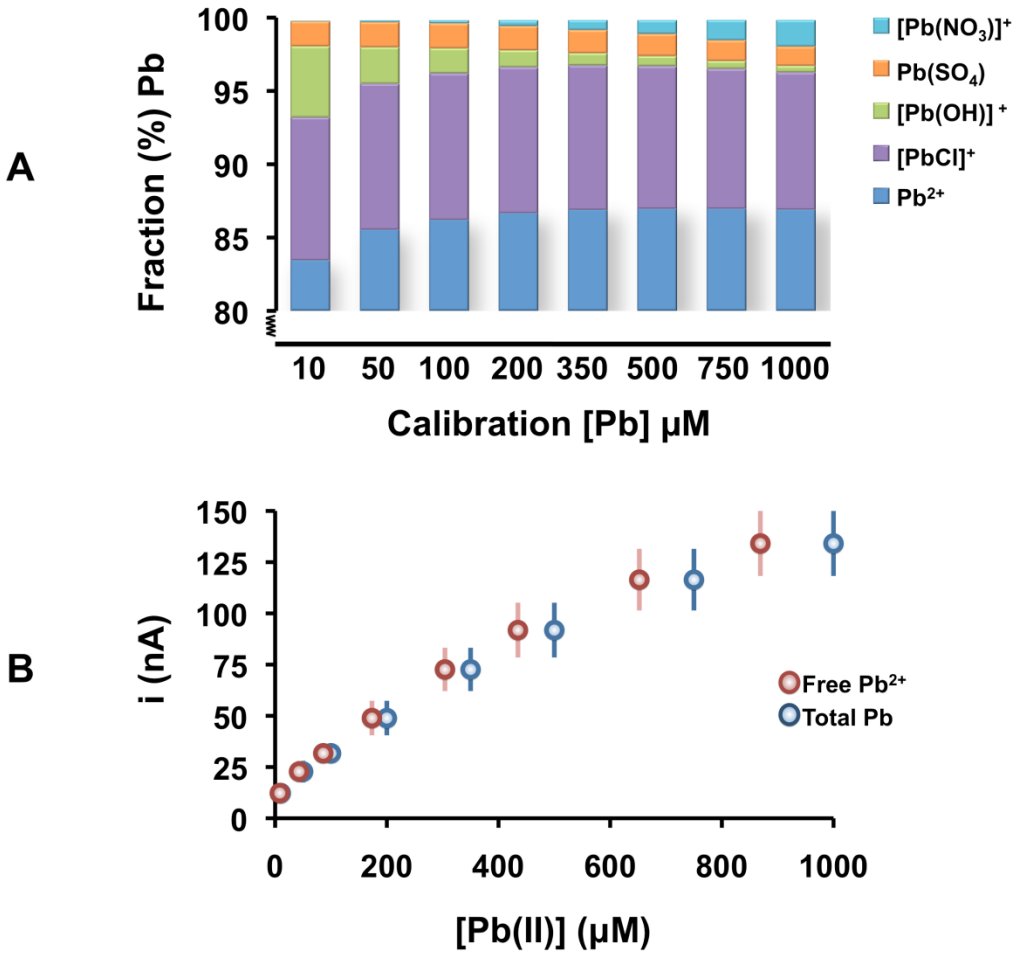

Figure 4.5: Panel A shows the PHREEQCi models predicting the speciation of Pb in terms of the % fraction of Pb in various forms. This speciation information is for Pb in the calibration standards used to construct the calibration curves in Panel B. The blue calibration trace shows total [Pb] in solution while the red trace shows the free Pb^{2+} in solution.

Figure 4.5.A shows the speciation of Pb in each of the calibration standards modeled with PHREEQCi. Our calibration standards ranged in concentration from 10 to 1000 µM Pb. Because of solution composition, the pH of our standards decreased with increasing total [Pb]. When considering speciation, this ΔpH impacts complexation, in particular with respect to hydroxide complexes. As a result, the relative fraction of Pb associated with hydroxides

decreased with increased total Pb, a trend that can be seen by the reduction in the green section of the histogram. Therefore, not only is there a difference between added Pb and Pb^{2+} in solution, this difference is not linear with increasing concentration and needs to be accounted for. Because our sensor responds to Pb^{2+}, it is important to know the concentration of free Pb^{2+} in solution for accurate calibration. **In Figure 4.5.B**, the responses to the total solution Pb are plotted in blue and free Pb^{2+} concentrations are plotted in red. When taking speciation into account, the sensitivity of our method to Pb^{2+} is improved: above, we reported a sensitivity of 0.17 nA μM^{-1} or 0.84 nA ppm^{-1} and an LOD of 10 µM or 2.1 ppm; in actuality the sensitivity is 0.20 nA μM^{-1} or 1.0 nA ppm^{-1} and the LOD is 8.4 µM or 1.7 ppm.

4.4.5 Pb Detection in Real Environmental Samples

We have designed and characterized a robust experimental model for quantifying Pb fluctuations in real-time. While invaluable for studying metals in solutions of known composition, it is important to establish our method's feasibility for studying rea environmental samples of unknown composition.

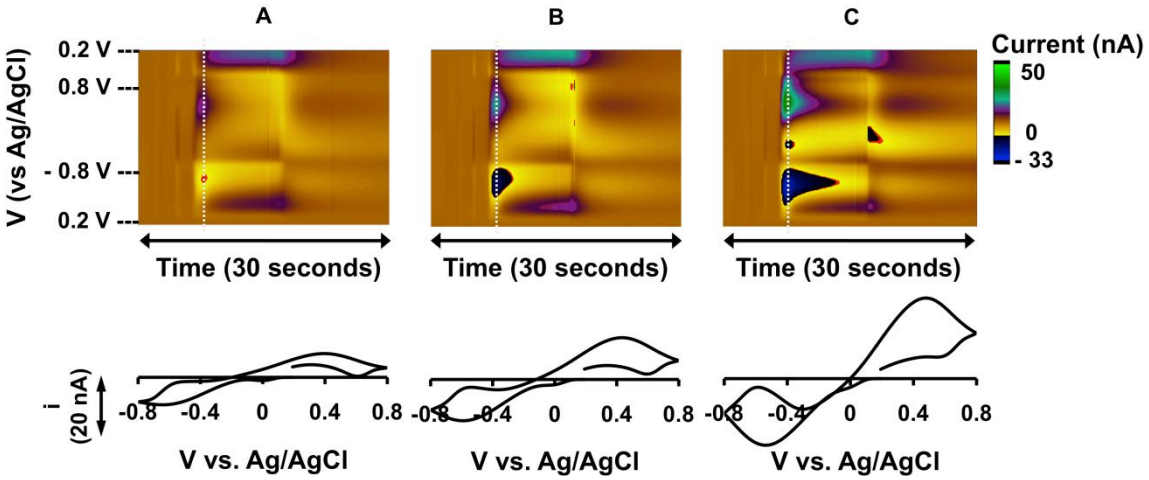

Figure 4.6: FIA of real samples spiked with Pb. The top panel shows color plots during the injection, and the bottom panel displays CVs taken from the vertical white dashed lines. Plots A−C represent responses to different Pb concentrations (20, 50, and 100 μM, respectively).

In **Figure 4.6**, we used real stormwater samples as our flow injection analysis solvent. We spiked the samples with three different Pb^{2+} concentrations ((A) 20 μM, (B) 50 μM, (C) 100 μM) and injected these onto our CFM. The top panel of **Figure 4.6** displays the corresponding color plots, where rapid, concentration dependent Pb responses can be observed. CVs collected from the vertical white dashed lines are displayed in the bottom panel. These CVs resemble those collected with our model solution (**Figure 4.4**); however, the peaks are more separated on the potential axis. This increased separation is to be expected since the solution resistance, which determines the IR drop across the electrode, is different.

We therefore show proof of principle that our method can be applied in real environmental systems to measure rapidly fluctuating Pb.

4.5 Conclusions

It is important to mitigate the impact of Pb on the environment since it is a pressing public health issue. In order to design effective mitigation strategies, it is essential that Pb can be analyzed in dynamic environmental systems. Electrochemical Pb analysis has traditionally been limited by its temporal resolution, Hg toxicity, and stability concerns. In this paper we described safe, stable, and fast analysis of Pb with FSCV. Additionally, we modeled test solutions to mimic environmental stormwater runoff. When coupled to our analysis approach, we showed that our novel method can characterize Pb in model and environmental systems. Our technology heralds a new wave of electrochemical sensors that can ultimately be developed for effective on-site metals analysis.

CHAPTER 5 FAST VOLTAMMETRY OF METALS AT CARBON-FIBER MICROELECTRODES: COPPER ADSORPTION ONTO ACTIVATED CARBON AIDS RAPID ELECTROCHEMICAL ANALYSIS

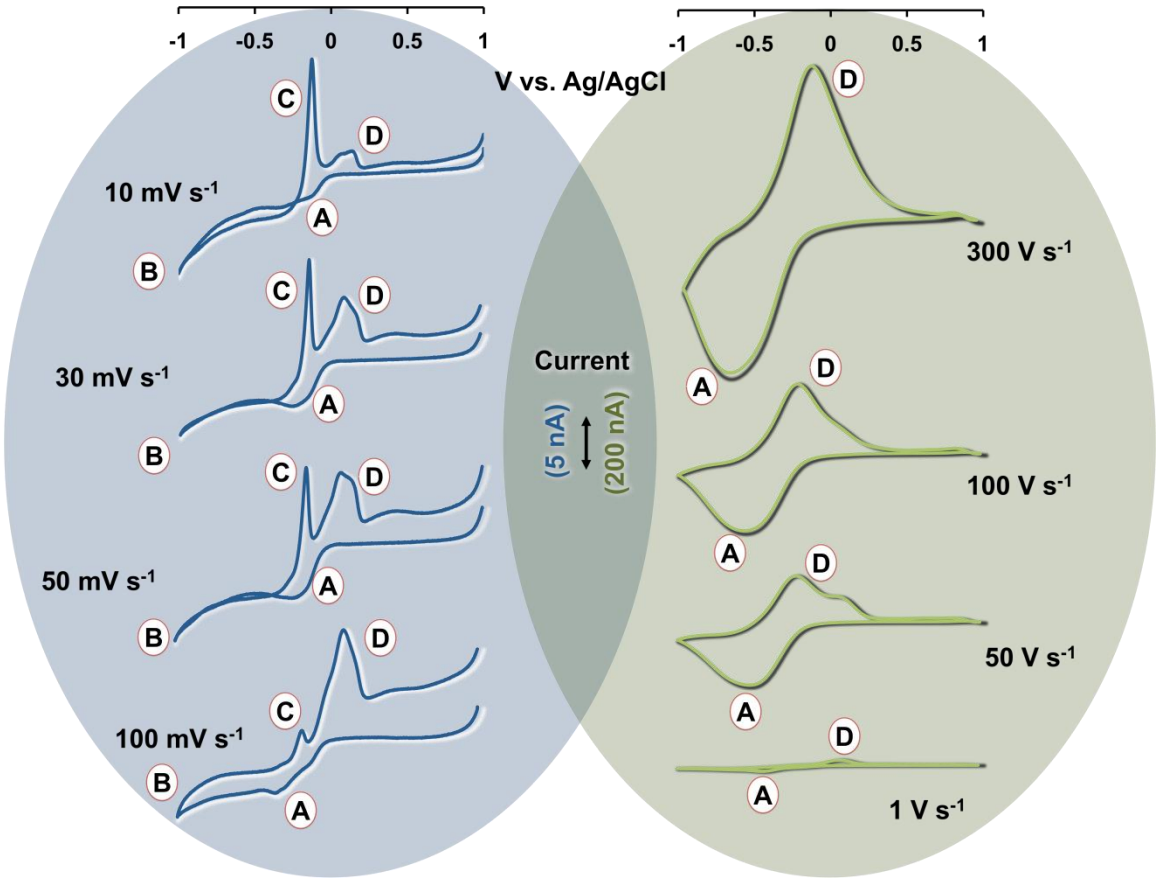

Reproduced from **P. Pathirathna**, S. Samaranayake, C. W. Atcherley, K. L. Parent, M. L. Heien, S. P. McElmurry and P. Hashemi, *The Analyst*, 2014, **139**, 4673-4680 with permission from The Royal Society of Chemistry.

5.1 Abstract

Rapid, *in situ* trace metal analysis is essential for understanding many biological and environmental processes. For example, trace metals are thought to act as chemical messengers in the brain. In the environment, some of the most damaging pollution occurs when metals are rapidly mobilized and transported during hydrologic events (storms). Electrochemistry is attractive for *in situ* analysis, primarily because electrodes are compact, cheap and portable. Electrochemical techniques, however, do not traditionally report trace metals in real-time. In this work, we investigated the fundamental mechanisms of a novel method, based on fast-scan cyclic voltammetry, that reports trace metals with sub-second temporal resolution at carbon-fiber microelectrodes. Electrochemical methods and geochemical models were employed to find that activated CFMs rapidly adsorb copper, a phenomenon that greatly advances the temporal capabilities of electrochemistry. We established the thermodynamics of surface copper adsorption and the electrochemical nature of copper deposition onto CFMs and hence identified a unique adsorption-controlled electrochemical mechanism for ultra-fast trace metal analysis. This knowledge can be exploited in the future to increase the sensitivity and selectivity of CFMs for fast voltammetry of trace metals in a variety of biological and environmental models.

5.1 Introduction

Trace metal analysis in real-time is essential for understanding many biological and environmental processes. For example, trace metals have important functions in biology and are garnering new attention for their roles as neurotransmitters.[113, 114] In Alzheimer's disease for example, copper accumulates in b-amyloid plaques.[115] It is thought that this copper build-up comes at the expense of its normal roles as a neurotransmitter, accounting for some of the disease's neurological deficits.[115, 116] It has been impossible to chemically monitor endogenously acting copper to verify this hypothesis, primarily because chemical transmission occurs so quickly (< seconds).

Rapid metal analysis is also important in the environment, particularly in natural water systems where trace metal contamination is extremely hazardous.[117] The well-documented health consequences of trace metal exposure[118-121] are exacerbated because metals bioaccumulate in plants and animals,[122-125] providing numerous exposure paradigms for humans. Anthropogenic sources of trace metals are commonly mobilized and transported during hydraulic events (storms).[104] It is critical to characterize aquatic trace metals in real-time because their interactions with organic ligands and soils are fast (< seconds).[86] Such rapid metal detection would provide the most efficient implementation of existing metal mitigation systems[126-131] via a diagnostic approach.

Most analytical techniques cannot monitor metals rapidly (< seconds). Spectroscopic techniques are sensitive and selective,[132] however sample

collection and preparation can alter metal speciation and make dynamic measurements difficult.[133, 134] Electrochemical methods are attractive because the chemistry occurs at a submersible or integrated surface that minimally impacts its surroundings. Ionselective electrodes have a temporal resolution of seconds;[135, 136] however it is typically challenging to make measurements in dynamically changing matrices. Stripping voltammetries (such as anodic stripping and adsorptive stripping voltammetry) have extremely high sensitivities.[137] This high sensitivity is largely due to a lengthy pre-concentration step (minutes) that decreases temporal resolution.[138-140] Moreover, anodic stripping voltammetry is most commonly performed at Hg electrodes[141] which have limited portability and pose their own toxicity concerns.

We recently described the use of carbon-fiber microelectrodes to detect copper (Cu^{2+}) and lead (Pb^{2+}) with fast scan cyclic voltammetry at scan rates of 300 – 600 V s^{-1}.[90, 142] Our ultra-fast, Hg-free method can quantify Cu^{2+} and Pb^{2+} concentration changes every 100 ms with parts per billion and parts per million sensitivity, respectively.[90, 142] Our method is highly applicable for studying metals in real time. However it is essential to describe the fundamental mechanisms of this fast voltammetric method before it can be developed into a routine analytical tool for biological and environmental applications. In this paper therefore, we take a multi-faceted approach and establish the underlying mechanisms of fast voltammetry of Cu^{2+} on CFMs in established laboratory test solutions.

We analyzed Cu^{2+}, a biologically relevant[114] and environmentally problematic metal ion[143, 144]with well-known redox chemistry.[98, 144] Besides

classical nucleation, growth and stripping features,[98] we observed new, additional peaks in Cu^{2+} slow scan cyclic voltammograms. These additional peaks were not diminished, as the classical features were, when the scan-rate was increased. In fact, with increasing scan rate, the new features were augmented, as seen previously with neurotransmitters adsorbed to CFM surfaces.[145] We therefore investigated surface adsorption as a fundamental mechanism of the Cu^{2+} FSCV signal. We utilized electrochemical, geochemical, and microscopic tools to describe CFM's surface and thermodynamic mechanisms towards Cu^{2+}. This study provides valuable insight into the adsorption chemistry that governs the FSCV response to metals. Our findings are critical to the future development of the method, namely increases in sensitivity and selectivity, in application to real samples.

5.3 Materials and Methods

Solutions

All chemicals were purchased as described in Chapter 2. Cu^{2+} solutions were prepared by dissolving $Cu(NO_3)_2$ in NaCl (0.01M) and in tris buffer (composition of the buffer can be found in Chapter 2). Solution composition was analyzed with PHREEQCi as detailed in Chapter 2.

Microelectrodes, FIA Analysis and FSCAV

Carbon-fiber microelectrodes were prepared as explained in Chapter 2. Flow injection analysis and FSCAV experiments were conducted as stated in Chapter 2.

5.3.1 Cyclic Voltammetry

All voltammetry employed a 2-electrode system. Cyclic voltammograms were collected on 5 different electrodes and representative examples are displayed. For slow scan cyclic voltammetry (scan rates ≤ 100 mV s^{-1}), microelectrodes were placed into a constantly stirred solution of $Cu(NO_3)_2$ and a triangular wave form (+1 V to –1 V) was applied using custom software, Wildcat CV, written in LAB-VIEW 2012 (National Instruments, Austin, TX). Only solutions for slow scan cyclic voltammetry were nitrogen purged prior to experimentation. The reference electrode was fabricated by electroplating Cl^- on a Ag wire (A-M systems, WA).

For scan rates above 1 V s^{-1}, in-house software, WCCV 2.0, written in LABVIEW 2012 collected background-subtracted voltammograms in a flow injection analysis system.

5.3.2 Electrochemical Pre-treatment

For most experiments microelectrodes were electrochemically pretreated with a Cu^{2+} sensitive triangular waveform as previously described.[90] For experiments comparing electrochemical and chemical pretreatments, the anodic potential/rest potential of the CFMs was varied from +0.4 V to +1.3 V at a constant cathodic potential of -1.0 V at a scan rate of 300 V s^{-1}. Electrodes were treated with each waveform for 10 minutes at 60 Hz and then 10 minutes at 10 Hz.

5.3.3 Chemical Pre-treatment

CFMs were chemically pretreated with a mixture of H_2SO_4 (0.25 M) and HNO_3 (0.25 M) in a 3:1 ratio[146] and washed with DI water prior to analysis.

5.4 Results and Discussion

5.4.1 Slow Scan Cu^{2+} Cyclic Voltammetry at CFMs

During slow-scan Cu^{2+} cyclic voltammetry, a cathodic potential sweep is applied to the electrode at 1 – 10 mV s^{-1}, followed by an anodic sweep that brings the potential back to rest.[98] During the cathodic scan, copper is deposited on the electrode surface following a nucleation and growth mechanism. Copper nucleates over a broad potential range. These nuclei allow more Cu to deposit during a growth phase at any potential sufficient for deposition. Therefore, there are often two broad 'loop' reduction peaks, between the same voltages, on both cathodic and anodic scans.[98] The differences between the nature of the electrode surface and the Cu surface make this nucleation/growth deposition occur at a more negative voltage than the standard Cu^{2+} reduction potential.[147, 148] Indeed when holding a CFM at a constant potential of 0.34 V ($Cu^{2+} + 2e^- \rightarrow Cu_{(s)}$ standard reduction potential), addition of $Cu(NO_3)_2$ induced no change in current. This behavior is true for holding potentials down to -0.1 V (data not shown). During the anodic scan, the deposited $Cu_{(s)}$ is stripped off the electrode surface. Because this happens from a $Cu_{(s)}$ rich surface (a single phase), the stripping or oxidation peak is sharp and its voltage is much closer to the standard equilibrium potential.[147, 148] Metal deposition can also occur via other mechanisms, for example, adsorption, charge transfer, and under potential deposition. [149-151] UPD

is a process by which a metal deposits onto another metal at a more positive electrode potential than the, Nernst potential for bulk deposition.[149]

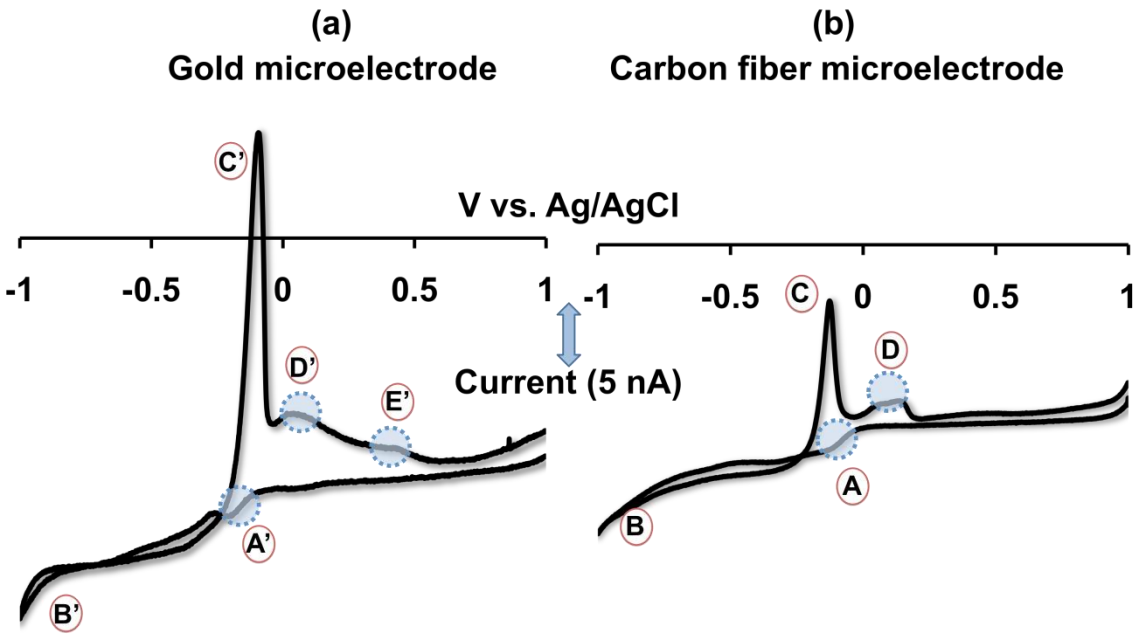

Figure 5.1: Slow scan cyclic voltammograms of $Cu(NO_3)_2$ on (a) AuM and (b) CFM at a scan rate of 10 mV s^{-1} in NaCl. Peaks A' – E' appear on the AuM, whereas peaks A – D appear on the CFM.

CFM slow scan cyclic voltammetry of Cu^{2+} was probed here by comparisons to AuMs. **Figure 5.1** shows representative cyclic voltammograms of $Cu(NO_3)_2$ (100 µM) on a Au Microelectrode (AuM) (a) and a CFM (b) at 10 mV s^{-1} in NaCl. These two voltammograms share common features. For example, Cu^{2+} reduction to metallic Cu begins at -0.1 V (peaks A', A) and continues via a loop formation between -0.4 V and -1.0 V on the cathodic scans (peaks B', B). This loop formation is an indication of nucleation and growth processes and is similar to previous observations.[150] On both AuMs and CFMs, sharp stripping peaks (C', C) and shoulder peaks (D', D) are present between -0.1 to 0.2 V o the anodic

scans. Shoulders accompanying stripping peaks have previously been reported on glassy carbon electrodes[151] and highly oriented pyrolytic graphite electrodes.[150] electrodes[150]. The presence of complexing agents such as chloride and ammonia strongly affect copper redox processes and lead to the observation of shoulder peaks at potentials higher than stripping peaks.[148, 150-154] Shoulder peaks have not been found to be associated with stripping peaks in media containing no complexing agents. [147, 155-158]

A mechanism for shoulder peak formation in the presence of Cl^- has been speculated previously.[151, 154, 156] First, deposited Cu oxidizes to Cu^+, creating a stripping peak (C', C) and forming a barely conductive, passive layer of CuCl according to reaction (1).

$$Cu + Cl^- \rightarrow CuCl + e^- \qquad (1)$$

The CuCl layer shields underlying metallic copper thereby momentarily arresting further oxidation. Dissolution of this passive layer occurs either via direct diffusion or diffusion of a more soluble complex (such as $CuCl_2^-$). Dissolution exposes the remaining underlying metal allowing the electro-oxidation of Cu to continue as shown in reactions (2) and (3):

$$CuCl + Cl^- \rightarrow CuCl_2^- \qquad (3)$$

$$CuCl_2^- \rightarrow Cu^{2+} + 2Cl^- + e^- \qquad (4)$$

We determined whether these processes are responsible for shoulder peaks D' and D by systematically increasing the scan rate as described in the next section. There is an additional peak on the AuM that is not present on the CFM (peak E'). UPD plays a significant role in copper deposition on gold surfaces[149] whereas on

carbon materials, metallic copper follows bulk deposition with no evidence for UPD.[148, 150, 151, 153], [155, 159] Peak E' on the AuM is likely a consequence of anodic processes associated with UPD on gold.[149]

5.4.2 Scan Rate Dependence

The shoulder peak mechanism proposed above was tested on CFMs by progressively increasing scan rate. The rationale here is that by increasing scan rate, nucleation/growth and hence stripping become limited because these processes are mass-transport dependent.[148] Because reactions (3) and (4) rely on the stripping peak, any limitations in stripping should manifest proportionally on the shoulder peak. In this experiment cyclic voltammograms of $Cu(NO_3)_2$ were collected at CFMs at increasing scan rates. From 10 – 100 mV s^{-1}, raw traces were analyzed; however at higher scan rates, the charging current due to double layer capacitance dominates the Faradaic component of the voltammetric signal. Therefore, cyclic voltammograms at 1 V s^{-1} and above were collected in a flow injection system using background subtraction.

Figure 5.2 shows cyclic voltammograms collected at 10, 30, 50 and 100 mV s^{-1} (left, blue panel) and at 1, 50, 100 and 300 V s^{-1} (right, green panel). This experiment illustrates the evolution of a slow scan $Cu(NO_3)_2$ cyclic voltammogram in a typical FSCV signal.[90] Increased peak separation at high FSCV scan rates is due to slow electron transfer kinetics. All peaks are labeled as in Figure 5.1. From 10 – 100 mV s^{-1}, the magnitude of peaks (B) and (C) are greatly reduced such that they are almost absent at 100 mV s^{-1}. This is consistent with the notion that nucleation and growth are mass transport limited

and therefore can be 'outrun' at high scan rates. The magnitude of peaks (A) and (D) however are not subject to the same behavior. Peaks (A) and (D) are present and well defined at 100 mV s^{-1} implying that these features are neither mass-transport limited nor dependent on peaks (B) and (C). The results of these experiments indicate that mechanisms other than those described by Reactions (3) and (4) are responsible for peak (D).

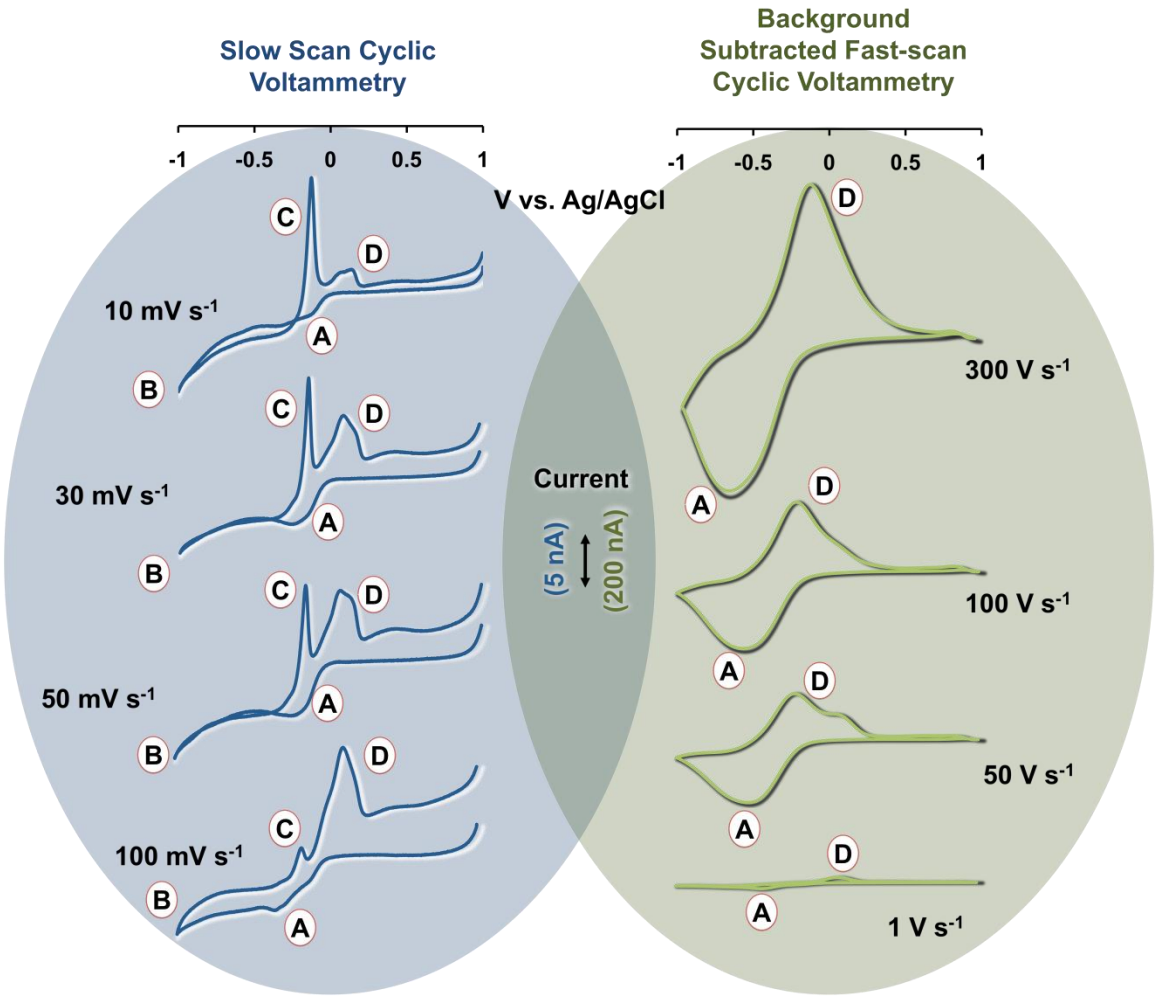

Figure 5.2: Left: Slow scan cyclic voltammograms of $Cu(NO_3)_2$ on CFMs at scan rates of 10, 30, 50 and 100 mV s^{-1}. Right: Fast scan backgroundsubtracted cyclic voltammograms of $Cu(NO_3)_2$ at scan rates of 1, 50, 100 and 300 V s^{-1}.

For adsorbed species, the peak current is proportional to scan rate and we indeed found that from 1 – 300 V s^{-1}, peak amplitudes increased. Furthermore, the slope of a plot of the log current vs. log scan rate for $Cu(NO_3)_2$ was previously reported to be approximately 1 at high scan rates.[90] Taken together, these findings strongly support a hypothesis that peaks (A) and (D) stem from an adsorption controlled process. Adsorption is explored in the following sections.

5.4.3 CFM Over-oxidation Leads to Enhanced Sensitivity

Activated carbon is widely used in wastewater treatment and is the primary purification component of domestic water filters.[159, 160] When carbon is activated (e.g. via heat in the presence of air, or with chemical or electrochemical pretreatments) a wide array of oxygen functionalities are created on its surface.[161] These oxygen moieties adsorb and complex trace metals, removing them from solution.[161, 162]

CFMs are typically electrochemically pre-treated prior to use.[57] Therefore, in analogy to metal adsorption by activated carbon, the oxygen functionalities on the CFM surface may rapidly complex trace metals in solution, pre-concentrating them on the surface. In this experiment, we tested the hypothesis that enhanced surface oxidation is responsible for increased FSCV sensitivity towards Cu^{2+}, presumably due to an increased number of adsorption sites.

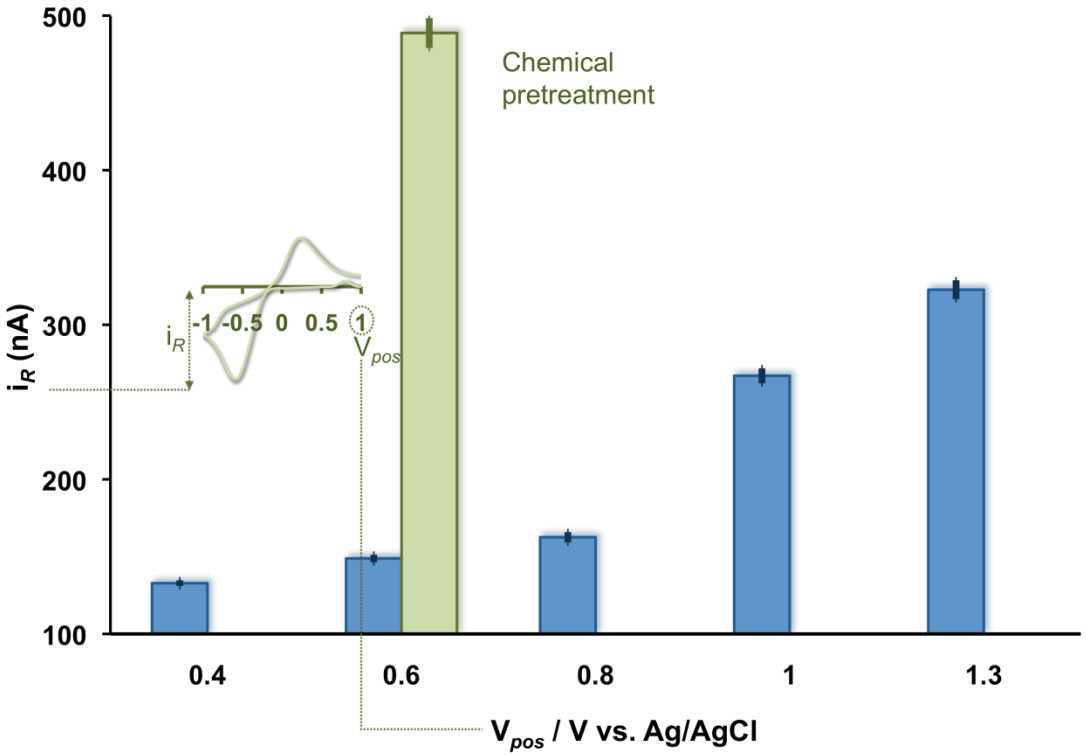

Figure 5.3: Maximum cathodic current of $Cu(NO_3)_2$ (10 μM) fast scan cyclic voltammograms as a function of anodic potential limit (blue series) at 300 V s^{-1} and as a function of acid pretreatment (green).

Using flow injection analysis, we collected background subtracted cyclic voltammograms of CFMs exposed to a bolus of $Cu(NO_3)_2$ (10 μM) with different FSCV waveforms. We systematically increased the anodic potential limit of the waveform at a constant cathodic limit, -1.0 V. **Figure 5. 3** shows the magnitude of cathodic current (demonstrated by the inset cyclic voltammogram) as a function of the anodic potential limit. The cathodic current showed exponential increases with increasing anodic potential. This exact behavior was previously reported with neurotransmitters and attributed to surface 'activation' or over-oxidation.[57] To confirm that the enhanced sensitivity was due to over-oxidation, an alternative method to overoxidize the CFM surface was employed. An acid

pretreatment[146] was applied to the electrode surface prior to use (H_2SO_4 (0.25 M) and HNO_3 (0.25 M) in a 3:1 ratio). An anodic potential limit of +0.6 was used where we previously found negligible effects of electrochemical over-oxidation. The resultant cathodic current is plotted in green on the 0.6 V series. The current here is substantially higher than the non-acid treated CFM confirming that surface activation, by two separate means, begets similar outcomes.

5.4.4 Cu^{2+} Adsorption to CFMs Drives the FSCV Signal

We sought to verify that the enhanced FSCV sensitivity towards Cu^{2+} as a consequence of activation is an adsorption-driven mechanism. This was successfully confirmed by construction of adsorption isotherms using fast scan controlled-adsorption voltammetry on CFMs.[62] Adsorption isotherms describe the thermodynamic equilibrium of Cu^{2+} onto the CFM, providing an index of the amount of Cu^{2+} on the CFM surface with respect to bulk solution via the equilibrium constant, K.

In all experiments described above, we used a simple matrix, NaCl, for characterizations. The adsorption isotherm of Cu^{2+} on CFMs in NaCl is shown in **Figure 5.4.a** (top panel) and follows a Langmuir fit. Authentic biological and environmental matrices are more complicated than NaCl and contain copper binding components. Therefore, we studied whether a complex matrix would affect Cu^{2+} adsorption. We previously characterized copper in tris buffer[90] which has considerable metal binding capacity.[163, 164]. Additionally Tris acts as a model biological medium because it contains amines that mimic proteins. The other salts in the buffer are at a ratio and concentration designed to mimic artificial

cerebrospinal fluid. Many neurotransmitters and other biologically relevant molecules have been characterized in tris *in vitro* [77, 165, 166] therefore adsorption isotherms were additionally constructed in tris buffer, (**Figure 5.4.a** bottom) also following a Langmuir fit.

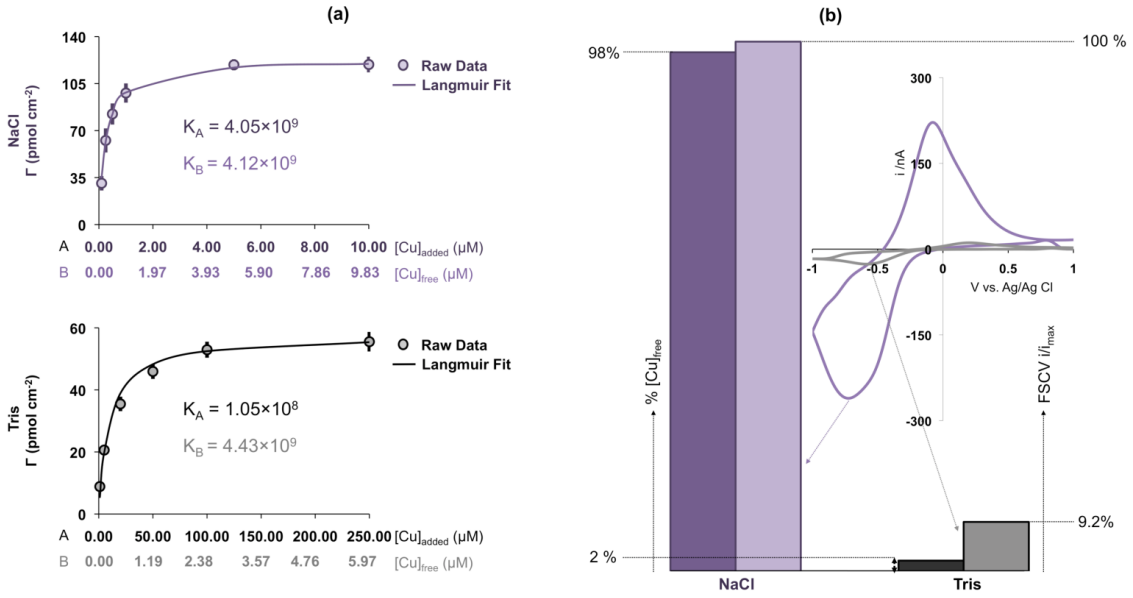

Figure 5.4: (a) Langmuir adsorption isotherms for $Cu(NO_3)_2$ on CFMs in NaCl (top) and in tris buffer (bottom). (b) Histogram showing % $[Cu^{2+}]_{free}$ in solution and % cathodic current of $Cu(NO_3)_2$ (10 μM) in NaCl (purple series) and in tris buffer (black series) at 300 V s^{-1} (% cathodic current is shown by setting the maximum cathodic current with NaCl to 100% and expressing the cathodic current with tris buffer as a percentage of this). The inset background-subtracted cyclic voltammograms are representative examples taken in NaCl (purple) and tris buffer (black).

We previously used a geochemical model to calculate the equilibrium concentrations of free Pb^{2+} in test solutions.[142] We employed the same model here to calculate free Cu^{2+} concentration ($[Cu^{2+}]_{free}$) in NaCl and tris solutions. Our isotherms therefore have two x-axes, (A) denotes the concentration of Cu^{2+} added ($[Cu^{2+}]_{(N)}$) to the test solutions and (B) denotes the free Cu^{2+} concentration $[Cu^{2+}]_{free}$ in solution. For NaCl, the two x-axes values are similar because NaCl

has little Cu^{2+} binding capacity. Therefore when calculating K, there is little difference between the values calculated with $[Cu^{2+}]_{(N)}$ vs. $[Cu^{2+}]_{free}$ (K_A and K_B). For tris the values of axes (A) and (B) are dramatically different because tris has Cu^{2+} binding capacity with K ~ $10^{4.59}$ It is interesting however, that when $[Cu^{2+}]_{free}$ is taken into consideration in the calculation, K (K_B) is similar to the K values in NaCl. Therefore, this complex matrix does not affect the monolayer characteristics of Cu^{2+} adsorption onto CFMs. This experiment further shows that solution complexes and other species do not significantly adsorb to the CFM surface and alter K.

The interactions of the Cu^{2+}- CFM and Cu^{2+} - tris equilibria are complicated. **Figure 5.4.b** is a histogram that compares % $[Cu^{2+}]_{free}$ in solution to the cathodic current of background subtracted cyclic voltammograms of $Cu(NO_3)_2$ in NaCl (purple series) and tris buffer (black series). Shown in the inset are representative examples of cyclic voltammograms of $Cu(NO_3)_2$ in NaCl and tris buffer. In the histogram, we compared the two FSCV signals thus: the maximum cathodic current with tris buffer was normalized to 100% and the current with NaCl was expressed as a percentage of this. It is seen that despite only 2% $[Cu^{2+}]_{free}$ in tris buffer, that the Cu^{2+} signal is 9.2% of the Cu^{2+} signal in NaCl (with 98% $[Cu^{2+}]_{free}$). This discrepancy implies that the two equilibria compete. The equilibrium of Cu^{2+}- CFM complexation is more favorable than Cu^{2+} - tris complexation, and a serendipitous outcome of this effect is high FSCV sensitivity, even in Cu^{2+} complexing matrices. Given the confirmation that our

Cu^{2+} FSCV signal is highly adsorption driven, the nucleation characteristics of the cyclic voltammetry peaks on CFMs were next studied.

5.4.5 AFM Characterization of Cu Nucleation and Oxidation

Changes in the morphology of the CFM surface can be visualized with AFM. AFM is a sensitive surface imaging technique, which employs a cantilevered tip to convert surface contours into images. AFM is routinely used to establish and characterize the formation of metallic copper on electrode surfaces.[147, 148] In **Figure 5.5**, AFM images were recorded at six different points along a slow scan cyclic voltammogram of $Cu(NO_3)_2$ in a complex matrix, tris buffer. Shortly after the start of the scan (i) the striations of the bare CFM surface are well defined. The small round features on the surface are likel solid contaminants. At (ii), metallic copper clusters are present on the CFM surface showing that the eventual cathodic FSCV peak (which evolves from this peak at high scan rates) involves deposition of $Cu_{(s)}$. $Cu_{(s)}$ is more elaborate during nucleation (iii) and after growth (iv) where striations are no longer visible under metallic Cu. After stripping (v), striations are again visible and due to the removal of metallic Cu. During the stripping process, $Cu_{(s)}$ may either be oxidized to Cu^{+} (as discussed above) or directly to Cu^{2+}. The presence of clear carbon striations and the scan rate dependent data provide little evidence for the formation of CuCl. However, the nature of the peak directly proceeding the stripping peak (the eventual anodic FSCV anodic peak) is yet to be determined. One explanation is that this Cu(s) is deposited on specific CFM adsorption sites that have their own

discrete oxidation potentials. The remaining clusters are no longer present at point (vi), confirming that $Cu_{(s)}$ is completely oxidized at the end of the scan.

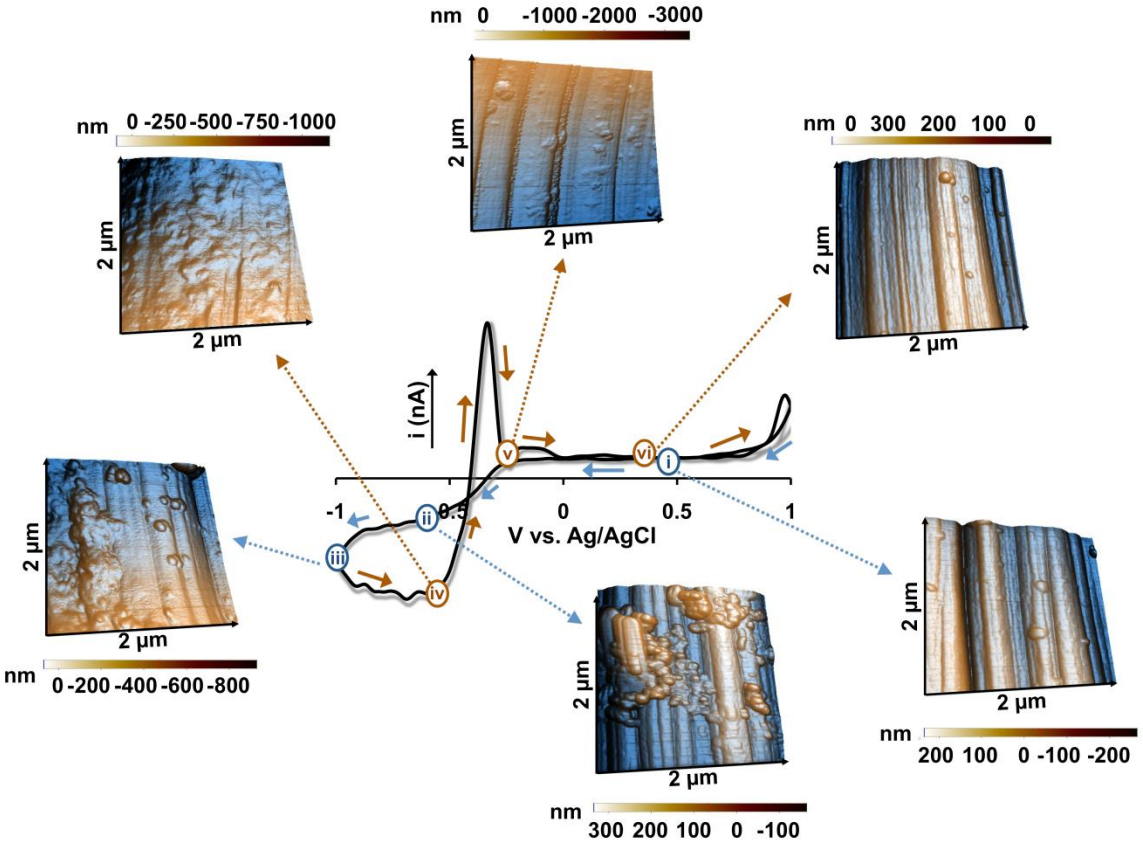

Figure 5.5: AFM images of a slow scan (10 mV s^{-1}) cyclic voltammogram of $Cu(NO_3)_2$ (100 µM) in tris buffer taken at six different points along the scan. On the forward scan, images were recorded at 0.2 V (i), -0.6 V (ii) and -1 V (iii) and on the backward scan at 0.6 V (iv), -0.3 V (v) and 0.2 V (vi). AFM images are 2 µM x 2 µM.

These surface morphology data confirm the nucleation and oxidation of metallic Cu associated with the cathodic and anodic FSCV peaks, i.e., peaks A and B in the FSCV segment of **Figure 5.2** are due to Cu^{2+}+ 2 e^{-}→$Cu_{(s)}$ and the reverse reaction.

5.5 Conclusions

FSCV at CFMs is an excellent tool for fast metal analysis with essential applications in biology and the environment. In this work, we described the fundamental mechanisms of fast scan voltammetry of Cu^{2+} on CFMs. In analogy to metal remediation by activated carbon, we showed that adsorption on CFMs underlies rapid FSCV responses. We ascertained the thermodynamic and physical characteristics of the CFM adsorption mechanism. This study has allowed us to understand the fundamentals of Cu^{2+} FSCV, enabling future improvements in the sensitivity and selectivity of fast metal voltammetry for real-time biological and environmental analysis.

CHAPTER 6 REAL-TIME VOLTAMMETRIC CHARACTERIZATION OF COPPER COMPLEXATION USING A HYDRODYNAMIC AND THERMODYNAMIC EXPERIMNTAL PARADIGM

Cu^{2+} complexation processes are studied with FSCV. I contributed both intellectually and experimentally to this project. The finding of this project made the basis for my next two projects.

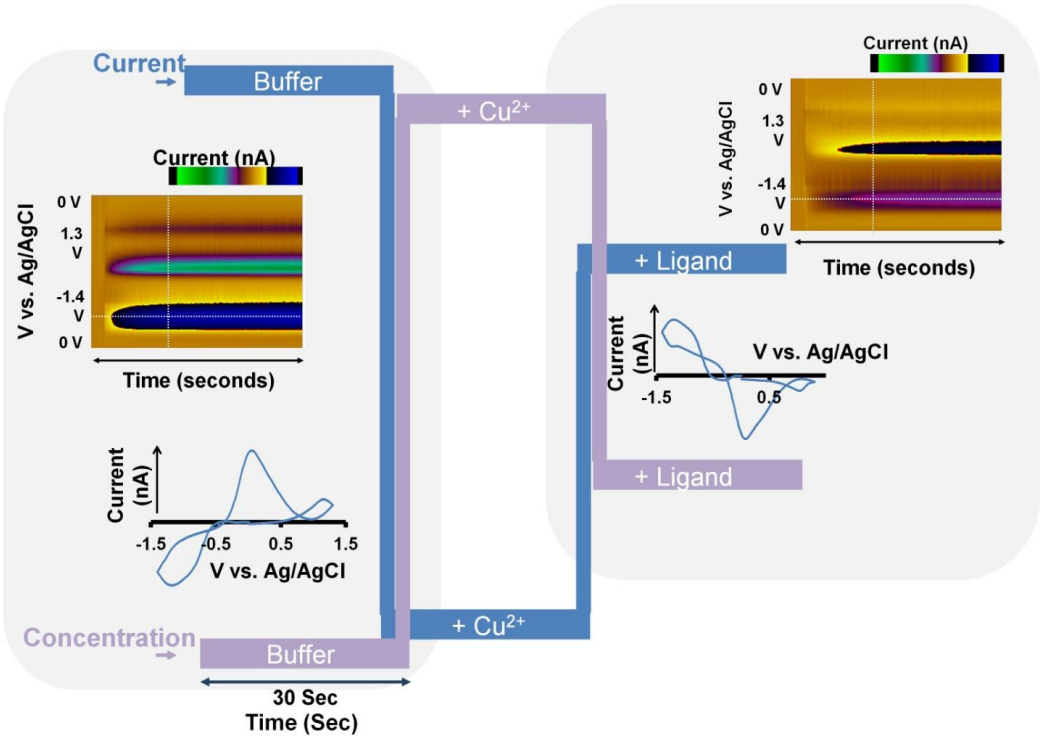

T. Siriwardhane, A. Sulkanen, **P. Pathirathna**, A. Tremonti, S. P. McElmurry and P. Hashemi, *Analytica Chimica Acta* - under review

6.1 Abstract

Many contemporary anthropomorphic practices create effluents rich in trace metals that are harmful to aquatic biota, animals and humans. Metal toxicity is strongly regulated by complexation, and while complexation is well-studied in equilibrium models, trace metal chemistry is ill-defined during dynamic events, such as storms. To better characterize the behavior of metals during these events, we recently described a method, based on fast-scan cyclic voltammetry, that reports trace Cu and Pb concentrations in real-time. In this study we investigate real-time Cu binding with a model set of ligands. We characterize Cu responses in MOPS buffer and develop a kinetic model to describe the hydrodynamic behavior of Cu. Finally, we combine this with a thermodynamic model to accurately capture Cu-binding experiments with our five model ligands. We show that FSCV is a powerful and accurate tool for studying real-time Cu complexation, which is essential for understanding and mitigating dynamic Cu-polluting events.

6.2 Introduction

Modern industrial processes [167-171] and agricultural practices [168, 172-176] produce wastes containing high concentrations of Cu, Cd, Zn and As [177, 178] which pollute aquatic systems. Additional sources of these pollutants include storm water runoff from roads and highways.[179-181] Taken together, these pollutants negatively impact urban lakes, streams, rivers and even on groundwater. The effects of excess trace metals in the environment can be severe and pervasive causing oxidative stress and cellular death in aquatic

organisms.[182] In humans, especially in children, chronic exposure to high enough doses can result in kidney damage and neurological impairment.[183, 184]

The toxicity and mobility of trace metals are controlled by a variety of factors including pH, salinity, and interactions with other substances (e.g., sorption and complexation).[185] Because of its' high toxicity, Cu complexation via organic [186, 187] and inorganic ligands [188, 189] has been well-studied in equilibrium models. However, dynamic environmental events, such as storm water runoff, are responsible for significant amounts of pollutant discharge and transport. Rapid characterization of Cu binding therefore can greatly aid the understanding of Cu mobilization and transport.

We recently described an electrochemical method, fast scan cyclic voltammetry at carbon-fiber microelectrodes for measurements of Cu in real-time. [90] Our method offers 100 ms temporal resolution and parts-per-billion level sensitivity. In this paper we describe the application of FSCV to real-time Cu binding with a model set of ligands representing a range of thermodynamic binding constants expected to be encountered in real environmental systems. We characterize Cu FSCV in a non Cu-binding medium, 3-(N-morpholino) propanesulfonic acid buffer. We develop a kinetic model that describes hydrodynamic behavior of Cu in MOPS and apply this to an experimental evaluation of real-time Cu binding with model ligands. The range of thermodynamic equilibrium constants for five model ligands is mirrored by our experimental data. These findings showcase FSCV's ability to accurately assess

Cu binding in real-time, a critical characterization for future development of this tool for rapid monitoring of environmental pollution events.

6.3 Materials and Methods

Carbon Fiebr Microelectrodes and Data Acquisition and Analysis

Microelectrodes were fabricated as detailed in Chapter 2. FSCV experiments were conducted with customized software, TH-1 written in LABVIEW with a custom-built UEI potentiostat as described in Chapter 2. Data are presented with error bars representing the standard error of mean. Student's t-tests were performed on paired data sets ($p < 0.05$ was taken as significant).

6.3.1 Solutions

A 0.005 M MOPS buffer was prepared using sodium chloride (EMD chemicals Inc, USA) and MOPS Salt (Sigma Aldrich). A stock solution of Cu^{2+} was prepared by dissolving copper nitrate ($Cu(NO_3)_2$) in 0.005 M MOPS buffer to reach a final concentration of 0.3 µM. The model ligands; ethylenediaminetetraacetic acid (Fisher Bioreagents), citric acid (Sigma Aldrich), glutamic acid (Sigma Aldrich), 3-nitrosalicylic acid (Sigma Aldrich), and 5-nitrosalicylic acid (Sigma Aldrich) were prepared in 0.005 M MOPS buffer to reach a final concentration of 0.24 µM at pH 7.25.[190-192]

6.3.2 Geochemical Modeling

Solution chemistry was modeled using PHREEQCi (version 3.1.2, USGS), as explained in Chapter 2.[193] To calculate the composition of solution species, PHREEQCi simultaneously balances equilibrium reactions describing pH, oxidation-reduction, complexation, gas dissolution, precipitation, etc. that are

described in an associated program database. For this study, the database we used was a modified version of the MINTEQ.v4 database, originally developed by the U.S. Environmental Protection Agency [194], that was updated to include protonation and complexation reactions for 3-NSA, 5-NSA and glutamic acid based on literature reported stability constants [195, 196]. Mimicking experimental procedures, individual solutions were modeled independently first and then combined using the MIX routine in PHREEQCi. To account for hydrodynamics, an empirical equation was used to describe the fraction of solutions mixed over time. Consistent with laboratory conditions, all solutions were modeled in equilibrium with $CO_{2(g)}$ ($10^{-3.392}$ atm) and $O_{2(g)}$ ($10^{-0.67}$ atm). The pH of the solutions (buffer, copper nitrate, ligand, and mixtures) was found to be within 0.2 pH units of those predicted.

6.4 Results and Discussion

6.4.1 Copper Electrochemistry in MOPS Buffer

When developing a novel analytical method for metal analysis, it is desirable to fix the pH of the test solution for laboratory characterizations. The most relevant laboratory buffers have considerable metal binding capacity [197-200] which complicates analysis. In the past, we accounted for this using post-hoc geochemical speciation models. [142, 201] In this study however, we are interested in evaluating Cu-ligand binding in real-time. Having multiple competing equilibria complicates such an evaluation; therefore we aimed to employ a buffer solution with negligible metal binding capacity. In 2003, Mash *et al*. reported that MOPS buffer does not bind Cu and is thus an excellent laboratory test solution for Cu

analysis.[198] To assess Cu behavior in MOPS, we separately compared FSCV responses (maximum reduction current) of Cu injection (0.4 M) into two constantly stirred solutions, NaCl and MOPS buffer (0.005 M). **Figure 6.1.A** shows that the Cu response in NaCl is 163.0 ± 4.0 nA (n=7 ± SEM); while in MOPS the response is 148.2 ± 2.3 (n=7 ± SEM). The Cu response in MOPS therefore is significantly decreased (p=0.003) despite the reported inability of MOPS bind Cu.

To test the notion that MOPS does not bind Cu, a CFM was placed in a constantly stirred solution of Cu (0.3 µM) in NaCl and MOPS (0.005 M) was added as shown in **Figure 6.1.B** (blue bar indicates injection time and artifact). We have previously performed this experiment for EDTA [90] and repeat it below with various ligands with different Cu binding capacity. The fact that there is no change in [Cu] strongly suggests that MOPS does not bind Cu. To establish the root of the decreased response therefore, we imaged the CFM at high resolution with scanning electron microscopy. **Figure 6.1.A** (inset) compares an electrode after experimentation in NaCl medium with an electrode after experimentation in MOPS buffer. Substantial build-up is evident on the CFM that was exposed to MOPS which likely accounts for the decline in Cu response. Electrode fouling is not desirable for electrochemical analysis[202], however fouling occurs rapidly and does not generally increase with time.

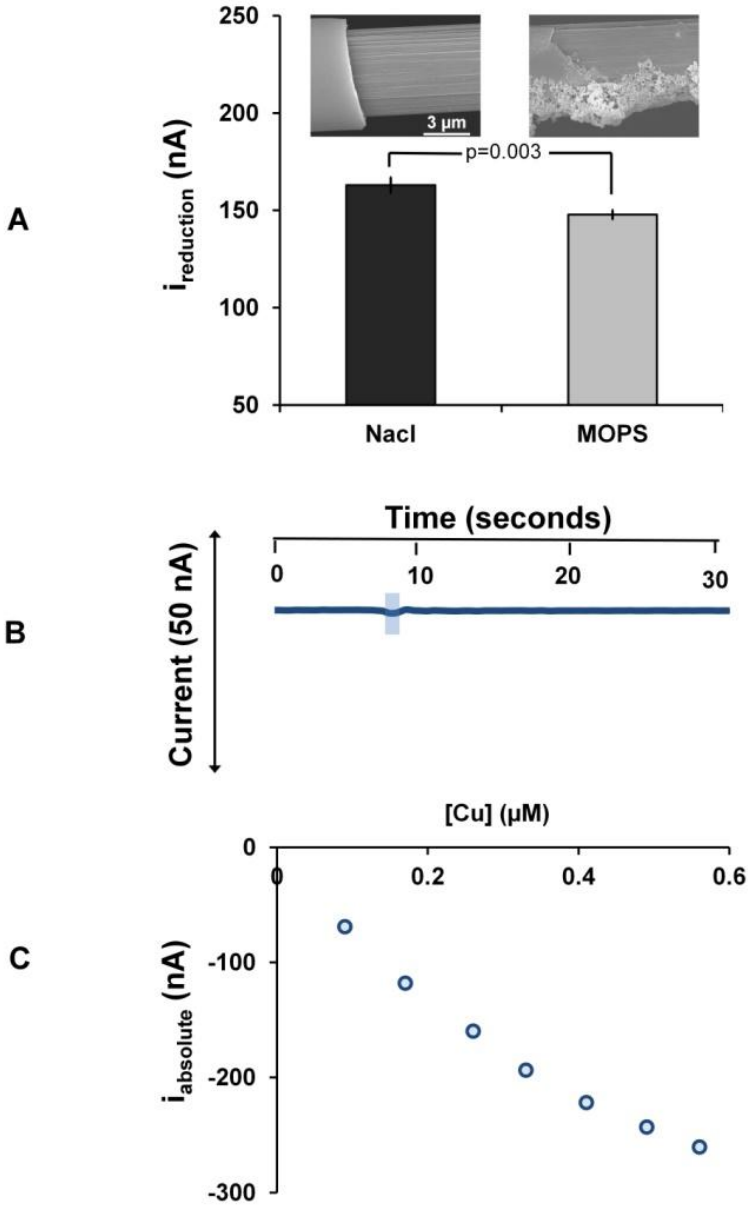

Figure 6.1: (A) Comparison of Cu responses in NaCl and MOPS buffer. The scanning electron microscopy images show the electrode after experimentation in NaCl (left) and MOPS (right). (B) Current measurement during MOPS injection into Cu (blue bar represents the injection time) (C) Cu calibration in MOPS.

The post-fouling sensitivity here for Cu is still very high and sufficient for our characterizations. **Figure 6.1.C** shows a Cu calibration (n=9 ± SEM, the small error bars are not visible under markers) in MOPS, the linear portion of

which is utilized to convert current to Cu concentration ([Cu]) in the proceeding experiments.

With this laboratory tool to measure Cu, we sought to evaluate Cu binding in real-time with well-characterized ligands that have a range of stability constants. However, before we could fully characterize these interactions we had to account for the hydrodynamics inherent to these dynamic experiments.

6.4.2 Hydrodynamic modeling of FSCV Data

The rapid addition of a Cu spike to MOPS does not result in a step-change in the FSCV response. This phenomenon may be due to limited electrochemical kinetics or convection processes. It is unlikely that electrode kinetics is a limitation here because we previously showed square injection responses using flow injection analysis for Cu and Pb.[90, 142] Hence, a hydrodynamic characterization of the FSCV response was performed. In **Figure 6.2**, we rapidly injected a spike of Cu (0.3 µM) into a continuous stirred-tank reactor of MOPS buffer stirring at 0, 200 and 500 rpm.

The lower panel of **Figure 6.2** shows representative FSCV color plots that arise upon spike addition of Cu at different stirring rates. The interpretation of color plots has previously been described.[79] In brief, potential is on the y-axis, time on the x-axis and current is in false color. Conversion of current taken from these color plots to Cu concentration [Cu] was also described previously.[90] Concisely, currents taken from the horizontal dashed lines (peak reduction current) were converted to concentration via the calibration curve in **Figure**

6.1.C. The concentrations were averaged between 5 electrodes for each stir rate and displayed in the main graph in **Figure 6.2**.

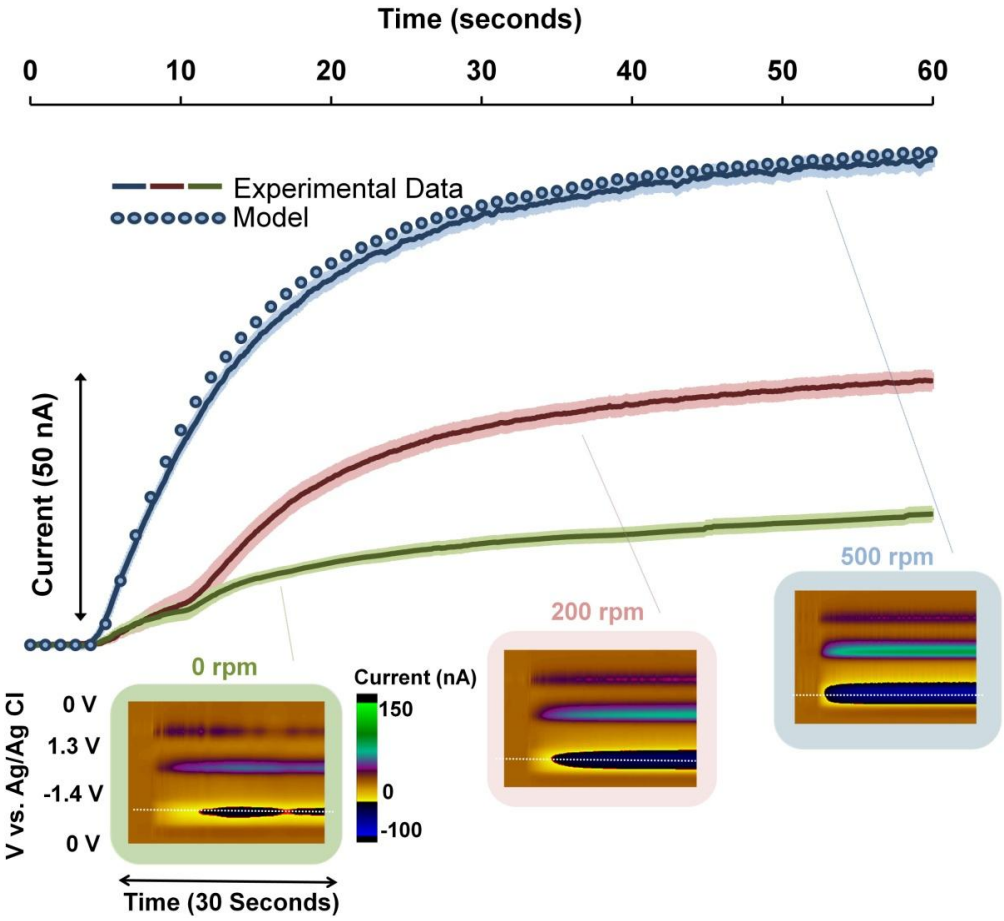

Figure 6.2: Injections with different stir rates (0 rpm- green, 200 rpm-red, 500 rpm-blue).The blue dotted trace shows the PHREEQCi modeled mixing data which used to develop the hydrodynamic model.

We found that hydrodynamics significantly control the FSCV response. The effect of increasing the stirring speed to 500 rpm was to produce the most rapid and high amplitude response as a higher rate of analyte is delivered to the electrode surface. Stirring speeds of more than 500 rpm were not feasible due to physical limitations of our prototype CSTR and fiber electrode; therefore we

utilized this mixing speed in our subsequent experiments. To account for this hydrodynamic behavior, an empirical equation was derived to model the response, described by equation 3:

$$f_{mix} = \frac{[0.0295\ln(t) + 0.017] - r_{bl}}{r_{std}} \qquad \text{Equation 3}$$

where the fraction mixed (f_{mix}) is a function of time (t) normalized by the baseline response (r_{bl}) and electrode response to the 0.3 μM Cu spike (r_{std}). In **Figure 6.2**, the model (blue dotted trace) accurately describes the deviation from a theoretical step-change response due to mixing (r^2 = 0.99). This hydrodynamic model was then used to account for mixing during subsequent ligand binding experiments.

6.4.3 Measurement of Cu Complexation in Real-time

To understand Cu mobilization and transport in environmental systems, it is necessary to characterize rapid interactions of Cu with ligands. It has previously been difficult to observe changes in free Cu during complexation at environmentally relevant levels. Above we described a model solution for a hydrodynamic analysis of real-time Cu detection with FSCV. We now apply this experimental paradigm to the analysis of dynamic Cu binding with a variety of model ligands.

Figure 6.3 shows our experimental paradigm for Cu complexation. FSCV is background subtracted to remove a large, non-faradic current that arises because of the high scan rates employed. For background-subtraction to be effective, files can be collected for a maximum of 60 seconds while the

background is stable. Because of this, our experimental paradigm is a two-step process. The first file is taken for 60 seconds during which a Cu spike is added after 5 seconds to MOPS buffer stirred at 500 rpm. The color plot on the left is a representative example of Cu addition to MOPS and the cyclic voltammogram taken from the vertical dashed line is a characteristic Cu CV previously observed. [90, 201] Also on the left of **Figure 6.3** are displayed the expected current and [Cu] traces after Cu addition (current and concentration have an inverse relationship as previously described) [90], whereby an increase in reduction current corresponds to an increase in [Cu].

In the second step, another file is taken for 60 seconds during which a ligand is added to the Cu-MOPS solution after 5 seconds. The color plot on the right is a representative example of ligand addition to Cu-MOPs solution and the CV taken from the vertical dashed line is the inverse Cu CV, showing that [Cu] has decreased. Here an increase in current corresponds to a decrease in [Cu] as it is complexed by the ligand. We used this paradigm to characterize Cu-ligand binding in real-time.

We deliberately chose 5 ligands to mimic the properties of ligands found naturally with Cu-ligand equilibrium (complexation) constants ranging from $10^{8.1}$ to $10^{20.5}$. EDTA, citric acid and glutamic acid were chosen for their well-established thermodynamic characteristics, while two salicylic derivatives (3-NSA, 5-NSA) were intended to mimic humic acids, the major organic ligand found in environmental systems. The salicylic compounds investigated both

contain a phenolic and a carboxylic functional group, which are common in humic substances.[203]

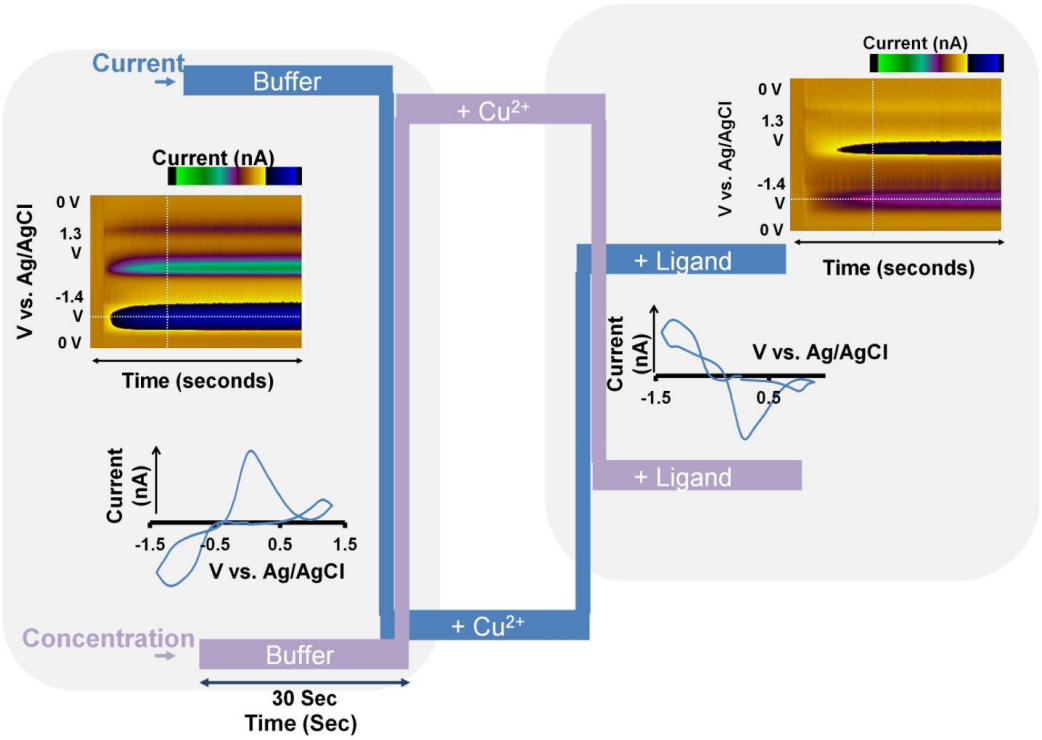

Figure 6.3: Modeled two step Cu-ligand complexation experimental paradigm. The current and concentration are shown in blue and purple, respectively. The color plot (left) represents the Cu injection and the characteristic CV for Cu is below this. Ligand addition is defined by the color plot (right) and the decrease in free Cu in the solution is characterized by the inverse of the Cu CV under this.

Figure 6.4.A shows an averaged Cu injection into MOPS stirred at 500 rpm (n=25 ± SEM) (blue solid) with the hydrodynamic model superimposed on top (blue dots).

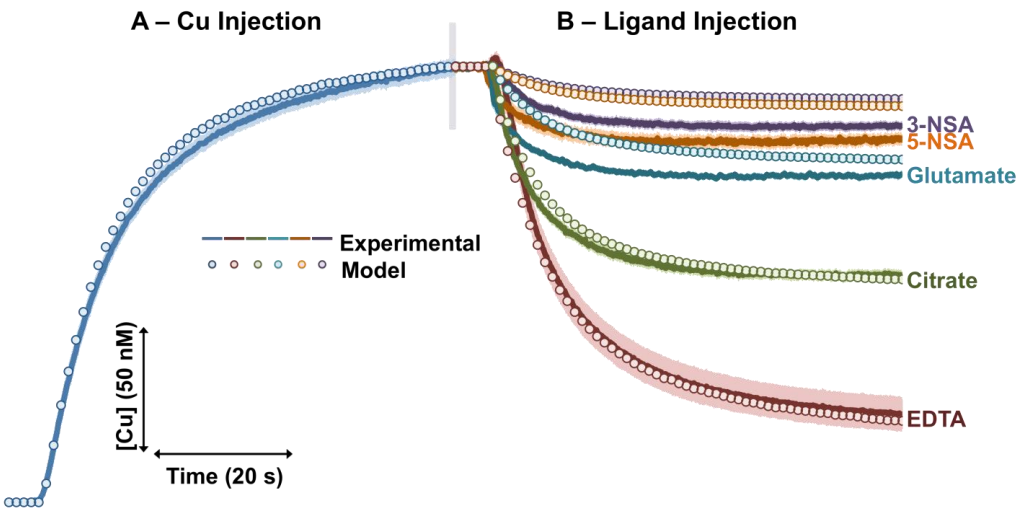

Figure 6.4: (A).Blue solid line shows the average Cu injection into MOPS buffer. Blue dotted trace shows the hydrodynamic model for the Cu addition. (B). Decrease in [Cu] after addition of ligands (step two), EDTA (burgundy), citrate (green), glutamate (teal), 5-NSA (orange), 3-NSA (purple) is shown by the solid lines. The corresponding dotted lines show modeled data.

Figure 6.4.B is the result of addition of the five ligands (5 injections onto 5 separate electrodes) to the Cu-MOPS solution (solid purple, orange, teal, green and burgundy). Each ligand caused the Cu levels to drop as Cu was complexed. As expected, the ligands with greater Cu complexation/stability constant (K) were found to result in greater decreases in Cu levels. For example, 3-NSA ($K=10^{8.1}$) bound 0.0220 +- 0.001 µM (n=5 ± SEM) Cu, while 5-NSA ($K=10^{8.4}$) bound 0.0274 ±0.001 µM (n=5 ± SEM). An important strength of our method is that even the smallest differences in K (i.e. $10^{8.1}$ vs. $10^{8.4}$) are mirrored by experimental data that shows 5-NSA binds more Cu than 3-NSA. Glutamic and citric acid showed moderate Cu binding of 0.0407 ± 0.001 and 0.0787 ± 0.001 µM (n=5 ± SEM), respectively. EDTA ($K=10^{20.5}$), a multidentate ligand exhibited the greatest ability to bind Cu, a consequence of the high entropic and kinetic driving forces that

favor multidentate chelation. Here, 0.1307 ± 0.005 µM of Cu (80% of Cu in solution) was bound. Our experimental data clearly correlates Cu-ligand to Ks; we further verified that the experimental data accurately describes Cu complexation via an equilibrium model. Previously we utilized PHREEQCi, a thermodynamic based geochemical model to describe free Pb and Cu levels in our test solutions.[68, 142, 201] Here we developed a PHREEQCi model to predict, based on reported Ks and our hydrodynamic model, Cu binding after addition of the 5 ligands.

Using the empirical hydrodynamic model derived above (equation 3), fractions of solutions were sequentially mixed. At each time-step, the model calculated new equilibrium conditions based on the solution composition which were then saved and used during the next mixing step. The purple, orange, teal, green and burgundy dots superimposed onto the solid lines describe model results. The model predictions closely align with Cu concentrations observed during complexation with EDTA and the citrate. Modeling results for the remaining 3 ligands are in the correct order (3-NSA>5-NSA>glutamate), however appear to under-predict the extent of complexation observed in the experimental data. While the model accounts for changes in experimental conditions (e.g. ionic strength, pH), the Ks used for 5-NSA, 3-NSA and glutamate were determined under different experimental conditions.[195, 196]

To obtain a more accurate K that reflects our experimental conditions, we utilized our model to back-predict K values. Because PHREEQCi balances numerous chemical reactions during each time step, we opted to modify only a

single K value for each ligand during this exercise. Since the pH remained fixed during experiments and was far from acid dissociation (pK_a) for each ligand, these parameters remained fixed. Based on the experimental results observed using FSCV, Ks for 3-NSA, 5-NSA and glutamate were predicted (**Table 6.1**). The Ks derived for glutamate ($K=10^{9.165}$), 5-NSA ($K=10^{8.61}$) and 3-NSA ($K=10^{8.35}$) now more closely reflected our experiment. Based on these results, this approach also provides a means of estimating Ks for unknown ligands and demonstrates the power of the combined hydrodynamic and thermodynamic experimental paradigm.

Table 6.1: Reported stability constants used during modeling (Figure 6.2) and derived based on experimental results

Ligand	Reaction	Log K (literature)	Log K (model)
3-Nitrosalicyclic Acid	$Cu^{2+} + C_7H_3NO_5^{2-} \leftrightarrow Cu\text{-}C_7H_3NO_5$	8.1[a]	8.35
5-Nitrosalicyclic Acid	$Cu^{2+} + C_7H_3NO_5^{2-} \leftrightarrow Cu\text{-}C_7H_3NO_5$	8.3[a]	8.61
Glutamate	$Cu^{2+} + C_5H_7NO_4^{2-} \leftrightarrow CuC_5H_7NO_4^{2}$	9.17[b]	9.165

[a] Merce, et al. [195], [b] Smith, et al. [196]

6.5 Conclusions

Trace metal pollutants are toxic to aquatic and terrestrial ecosystems. Toxicity of metal pollutants is largely a function of complexation and while complexation equilibrium models are well characterized, it is difficult to study trace metal behavior during rapid transport events. In this study using FSCV, we evaluated real-time Cu complexation with a model set of ligands in MOPS buffer. We developed a kinetic hydrodynamic model to describe Cu addition to a CSTR. By combining our hydrodynamic model with an equilibrium model, we closely modeled our experimental data and back-calculated complexation/stability

constants for the ligand interactions. FSCV is a uniquely important tool for studying Cu complexation in real time.

CHAPTER 7 FAST VOLTAMMETRY OF METALS AT CARBON-FIBER MICROELECTRODES: ULTRA RAPID DETERMINATION OF SOLUTION FORMATION CONSTANTS

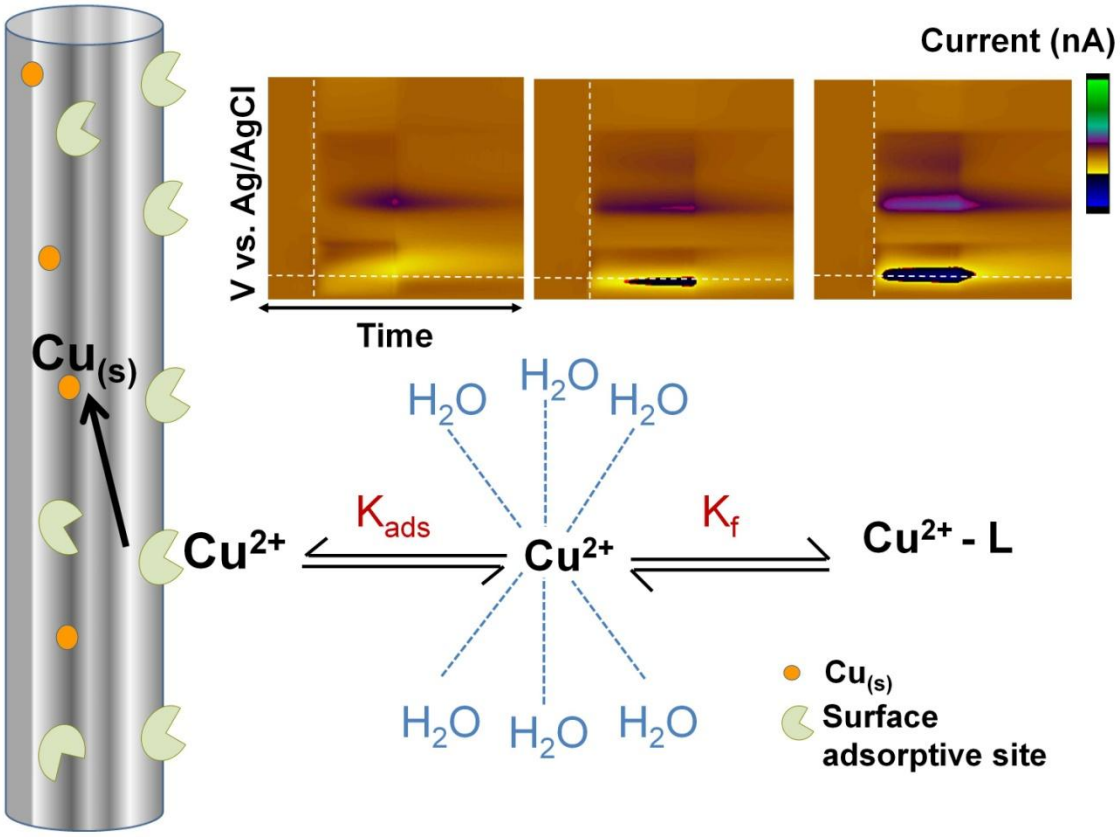

P. Pathirathna, T. Siriwardhane, S. P. McElmurry and P. Hashemi, *The Analyst* - under review.

7.1 Abstract

The roles and mechanisms of trace metals in biological and environmental systems depend on metal speciation. To better define the behavior of trace metals in real systems, therefore, it is desirable to rapidly measure metal interactions with surrounding complexing ligands. Fundamental thermodynamic parameters, such as a formation constant of metal-ligand equilibria provide useful speciation information. Although this information can be determined by spectroscopic techniques with high accuracy, it comes at the expense of time and cost. In this work, we studied Cu^{2+} complexation with different ligands using an ultra-fast method, fast scan cyclic voltammetry at carbon-fiber microelectrodes. We observed a correlation between FSCV response and previously reported Cu^{2+}- ligand equilibrium constants. This relationship allowed us to predict the K_f associated with a model ligand. We hence present an essential proof of principle study that highlight's FSCV's capability to prove speciation information in real time.

7.2 Introduction

Trace metals play fundamental and dynamic roles in biological and environmental systems. In biology, trace metal homeostasis is responsible for maintaining many aspects of the body's biochemistry.[204-206] In the environment, endogenous and anthropogenic sources of trace metals can be rapidly mobilized and transported into natural waters, where they create harmful and persistent contamination. The behavior of metals in biology and in the environment is fundamentally dependent on speciation, to which complexation is a major

contributor.[207-209] Thus to better understand the mechanisms and impact of trace metals on human and environmental health, it is desirable to define metal speciation *in situ* in delicate, dynamically changing and often harsh systems.

Fundamental thermodynamic elements, such as equilibrium constant of metal-ligand equilibria, provide an index of the relative strength of intervening complexation reactions in aqueous solution. While spectroscopic methods can deliver this information with high accuracy, the secondary methods required are technically laborious and time consuming.[210, 211] A rapid delivery of this parameter would provide key diagnostic information with which to better tackle physiological and environmental issues.

We recently described real-time analysis of Cu^{2+} and Pb^{2+} using fast scan cyclic voltammetry at carbon-fiber microelectrodes.[90, 142] We found that the endogenous adsorptive properties of an activated carbon-fiber microelectrode afford extreme sensitivity to the FSCV measurement.[201] We attributed the high sensitivity of the response to a CFM – Cu^{2+} adsorption equilibrium on the surface of the microelectrodes that competes with solution equilibria to shift towards more Cu^{2+} on the CFM surface.[201] This phenomenon is not only auspicious in providing enhanced detection sensitivity but, as we explore in this paper, can also be exploited to provide rapid information about overall formation constants.

Here using FSCV, we study Cu^{2+} complexation with a variety of model ligands that encompass a wide range of Cu^{2+} - ligand equilibrium constants (Ks). We find a strong correlation between the Cu^{2+} FSCV response and Cu^{2+} -ligand formation constants, which importantly allows us to rapidly predict the K_f

associated with a further model ligand. We thereby present an essential proof of principle study to showcase FSCV's versatility in providing, not only chemical but also, speciation information in real-time. Our data represent an important first step towards a real-time speciation sensor.

7.3 Materials and Methods

Microelectrodes, voltammetric experiments and solution analysis

Carbon-fiber microelectrodes were prepared as detailed in Chapter 2. FSCV and FSCAV experiments were conducted as explained in Chapter 2. PHREEQCi analysis was performed to predict the solution chemistry in each of the solution mixtures (more details can be found in Chapter 2).

7.3.1 Solutions

All chemicals were purchased from Sigma-Aldrich (St. Louis, MO) unless otherwise specified. The source of Cu^{2+} was $Cu(NO_3)_2$. ethylenedaminetetraacetic acid, citric acid, 5-nitrosalicylic acid, 3-nitrosalicylic acid and glutamic acid served as the model ligands for Cu^{2+} - ligand complexation processes. The Cu^{2+} - ligand mixtures were prepared in 1:1 stoichiometric ratio in NaCl (0.01 M) prior to flow injection analysis at ambient temperature and pressure. Each solution mixture was allowed sufficient time (>2 hrs) to come close to steady-state equilibrium prior to experimentation. The pH of each mixture was recorded, and incorporated into geochemical modeling performed using PHREEQCi.

7.4 Results and Discussion

7.4.1 Effect of Mass Transport Rate and Waveform Application Frequency on FSCV Response

The CFMs utilized in this study have a cylindrical geometry and sit in a hemispherical diffusion field within the FIA flow cell, where the mass transport of Cu^{2+} to the electrode surface occurs primarily via convection and diffusion. Since we previously observed a higher FSCV sensitivity to Cu^{2+} than expected from the levels of free, unbound Cu^{2+} in Tris buffer,[201] we hypothesize that the CFM - Cu^{2+} adsorption equilibrium might yield a predictive relationship between solution K and FSCV response. However there are fundamental experimental parameters of our system, namely waveform application frequency and rate of mass transport that necessarily affect the CFM - Cu^{2+} equilibrium, that need to be addressed before focusing on our hypothesis.

In the FIA system utilized, flow follows a well-defined laminar profile thus the rate of mass transport can be controlled by varying the flow rate of the FIA system. Our prior experiments and the experiments in this paper are at a flow rate of 2 mL min^{-1}, consistent with other literature reports.[77] In **Figure 7.1** (left segment) are displayed maximum cathodic FSCV currents (i_c) of FIA of a 1:1 stoichiometric ratio of Cu^{2+} - EDTA with systematic increase of flow rate from 0.5 mL min^{-1} to 8 mL min^{-1}. As expected a higher FSCV response is concomitant with increased flow because of increased rate of mass transport. The highest response (98.2 ± 1 nA) was found at our routine flow rate of 2 mL min^{-1}, after which the response began to decrease likely due to physical limitations of our flow cell (pressure limit).

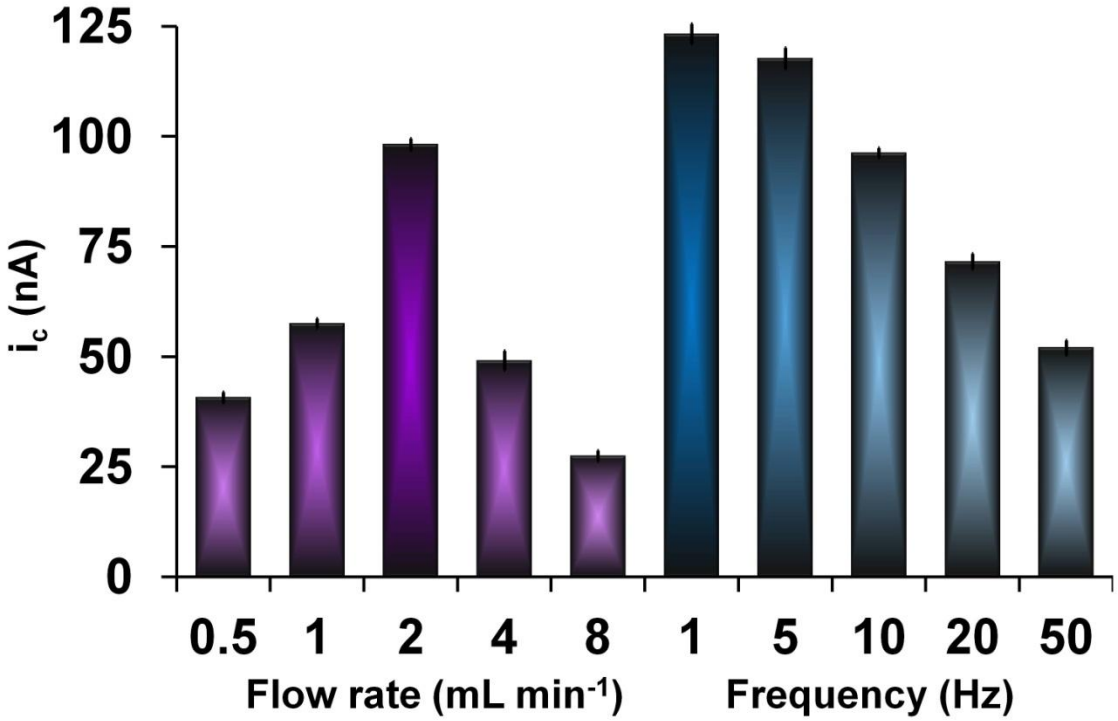

Figure 7.1: Left: Maximum cathodic current (i_c) for Cu^{2+} voltammograms obtained from Cu^{2+}- EDTA mixture at a flow rate of 0.5, 1, 2, 4, and 8 mL min^{-1}. Right: Maximum cathodic current for Cu^{2+} voltammograms obtained from Cu^{2+}- EDTA mixture in FIA system at frequencies of 1, 5, 10, 20, and 50 Hz.

We next addressed how the waveform application frequency affects FSCV response. The same analyte was injected into a flow stream at 2 mL min^{-1} while waveform application frequency was varied from 1 Hz to 50 Hz. The hypothesis here was that by increasing application frequency, adsorption time becomes limited resulting in lower surface adsorbed Cu^{2+} and hence a lower FSCV response. This phenomenon has previously been observed for neurotransmitters[62, 212] and is consistent for Cu^{2+} as shown in the right segment of **Figure 7.1** where maximum current was observed for lower application frequencies. However, this increase in signal comes at the expense of the

temporal resolution therefore we chose to maintain 10 Hz as our FSCV waveform application frequency.

This experiment shows that, as expected, both mass transport rate and the waveform application frequency affect the FSCV response because of different Cu^{2+} adsorption profiles on the CFM surface. Importantly, the high reproducibility of the response per parameter (small error bars on **Figure 7.1**) shows that with a given set of parameters, Cu^{2+} adsorption is consistent. This allows us to confidently set the flow rate and waveform application frequency for the remaining experiments in this paper at 2 mL min^{-1} and 10 Hz respectively, providing experimental accuracy in the following Cu^{2+} - ligand comparison studies.

7.4.2 FSCV Response, Free Cu and Computationally Derived Ks

We previously noted higher than expected FSCV sensitivity towards Cu^{2+} in a solution of Tris buffer where approximately 98% of Cu^{2+} was bound.[201] We sought to observe whether this phenomenon holds in other Cu^{2+} binding media. We made solutions with differing degrees of Cu^{2+} binding ability, indicated by K_f for Cu^{2+} - ligand complexation. Those were 1:1 mixtures of Cu and EDTA (log K_f = 20.3), citric acid (log K_f = 13.2), and 5-NSA (log K_f = 8.3) in NaCl. We performed FSCV on each solution and present the raw data in the color plots in Figure **7.2.A**. The maximum cathodic current from the cyclic voltammograms extracted from the color plots is shown in table in **Figure 7.2.B**. These data follow our previous observation with Tris buffer[201] and support our hypothesis that the CFM - Cu^{2+}equilibrium shifts, according to Le Chatelier's principle,

towards the left as depicted in **Figure 7.2.B** below, resulting in higher than expected (from a pure solution chemistry perspective) FSCV signal. We illustrate this effect further, by using the PHREEQCi model to predict the % free [Cu^{2+}] in each of the Cu^{2+} -ligand mixtures, which is presented in the table in **Figure 7.2.B**. In all cases, Cu^{2+}equilibrium shifted towards the CFM and it is of particular note that even with the EDTA complex, where only 0.02% Cu is unbound, there is appreciable FSCV signal (208.9 ± 4 nA). Furthermore, there is an apparent relationship between FSCV response and K_f.

These experiments strongly support our postulation that the CFM- Cu^{2+} adsorption pulls Cu through the associated aqueous phase equilibrium resulting in an apparent increase in signal, and we next seek to find whether their relationship is predictable. However, before this data can be used for predictive modeling, it is critical to show that the CFM - Cu^{2+}adsorption equilibrium is consistent between media.

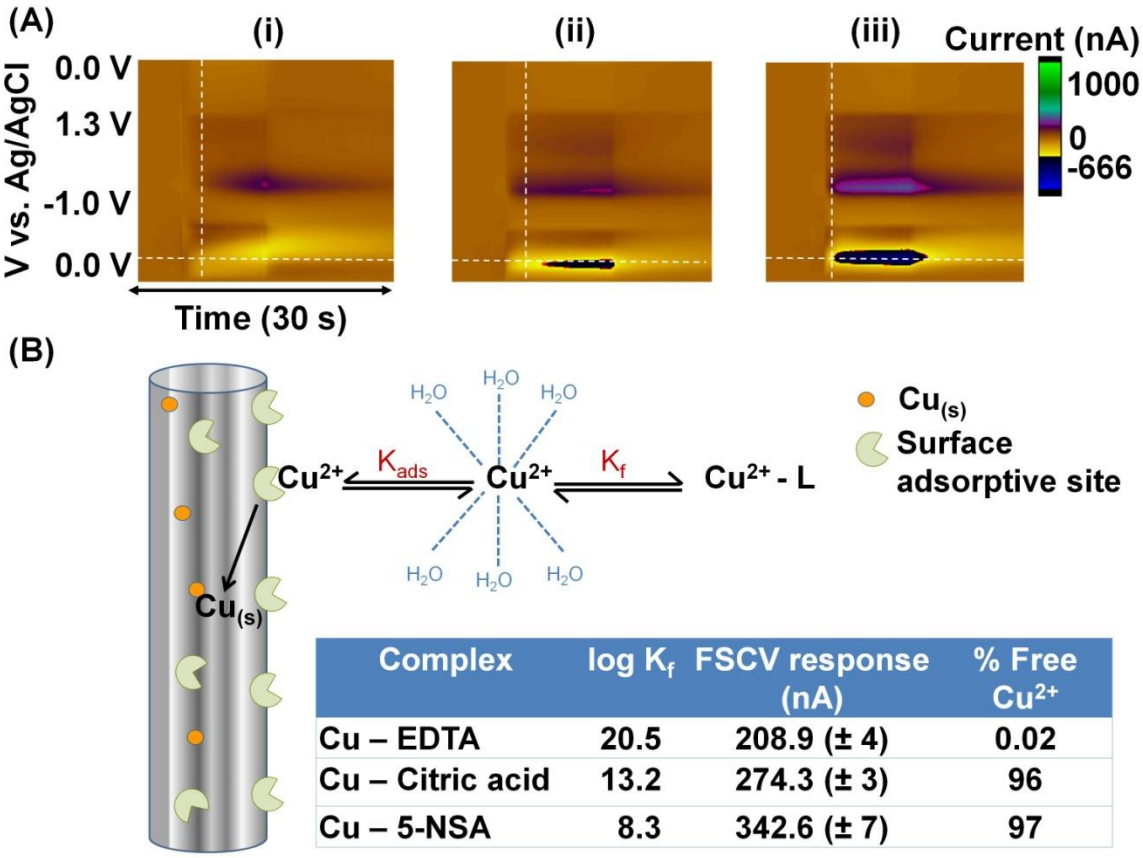

Complex	log K_f	FSCV response (nA)	% Free Cu^{2+}
Cu – EDTA	20.5	208.9 (± 4)	0.02
Cu – Citric acid	13.2	274.3 (± 3)	96
Cu – 5-NSA	8.3	342.6 (± 7)	97

Figure 7.2: (A): Representative color plots obtained after injection of (i) Cu^{2+} - EDTA, (ii) Cu^{2+}- citric acid and (iii) Cu^{2+}- 5-NSA complexes into FIA system. White horizontal dashed line indicates the Cu^{2+} electroreduction vs. Ag/AgCl electrode. White vertical dashed lines indicate injection time. (B): Schematic illustrating Cu^{2+} - CFM and Cu^{2+} - ligand equilibria in aqueous solution.

7.3 Adsorption Isotherms

By constructing adsorption isotherms, we can calculate the equilibrium constant (K_{ads}) accompanying CFM - Cu^{2+} monolayer adsorption. We previously created such isotherms for Cu^{2+} in NaCl and Tris buffer[62] and we followed the same procedure here. **Figure 7.3** shows the Langmuir fits to the adsorption isotherms with two x-axes. These represent the concentration of Cu^{2+} added to solution $[Cu^{2+}]_A$ and the level of unbound Cu^{2+} as predicted with PHREEQCi $[Cu^{2+}]_B$. As expected the difference between the two x-value series is highest in

the presence of EDTA for the Cu^{2+} - EDTA solution, since only 0.02% Cu^{2+} is free whereas citric acid and 5-NSA leave 96-97% Cu^{2+} unbound. K_B is the K_{ads} calculated via $[Cu^{2+}]_B$ and importantly shows good agreement between the 3 ligands and with the K_{ads} that we previously reported for Cu^{2+} - NaCl and Cu^{2+} - Tris mixtures.

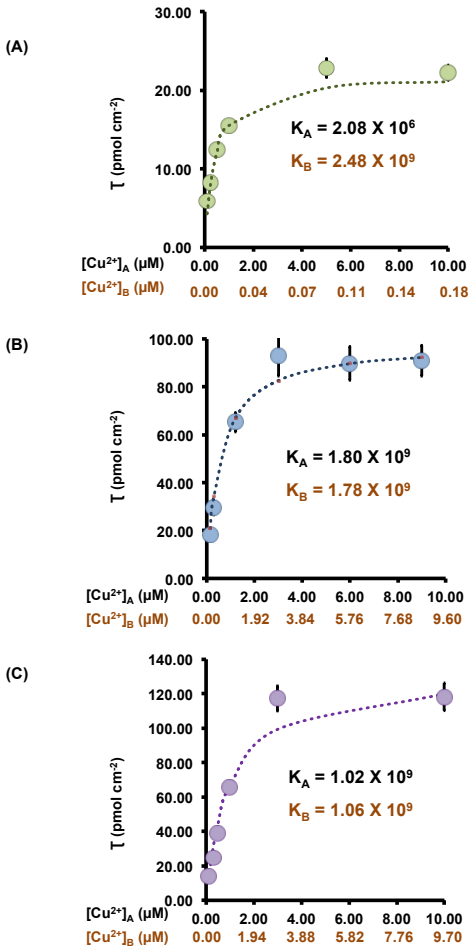

Figure 7.3: Langmuir adsorption isotherms (A) Cu^{2+} - EDTA (B) Cu^{2+}- citric acid and (C) Cu^{2+} - 5-NSA mixtures in NaCl. $[Cu^{2+}]_A$ represents the added $[Cu^{2+}]$ and $[Cu^{2+}]_B$ represents the free $[Cu^{2+}]$ calculated from PHREEQCi. K_A and K_B are equilibrium constants for Cu^{2+} adsorption onto CFM with respect to $[Cu^{2+}]_A$ and $[Cu^{2+}]_B$.

This experiment verifies that Cu^{2+} monolayer adsorption is not restricted or promoted significantly by the surrounding matrix and allows us to pursue whether a predictive relationship exists between the FSCV response and solution K_f.

7.4 Predictive Relationship between Solution K_f and FSCV response

K_f expresses the relative strength of the interaction between two species. Determination of K_f values, particularly for metals, are essential to different applications including chelation therapy,[213-215] MRI contrast production processes,[216, 217] the detergent industry,[218, 219] and ion selective electrode manufacturing processes.[220] Moreover, K_f values allow the calculation of thermodynamic properties like entropy and enthalpy, providing additional significant information of interest.

Because of the wide interest in determining solution K_f, the precision and accuracy of traditional K_f measurements has been greatly enhanced from the first method introduced by Jannik Bjerrum,[221] although the principle of the method remains the same. In brief, an acidic solution of a protonated ligand and metal is titrated and the activity or the concentration of hydrogen ions is measured with a glass electrode. However, glass electrodes fail to monitor some reactions and alternative procedures become necessary. These alternate methods include spectroscopic techniques such as absorption, fluorescence and NMR spectroscopy.[222-224] Although glass electrodes and spectroscopic techniques provide sensitive and accurate information, these procedures are offline, lengthy and can be laborious. If we were to find a predictive relationship between FSCV

response and K_f, we could report solution K_f with the ultra-fast temporal resolution of FSCV.

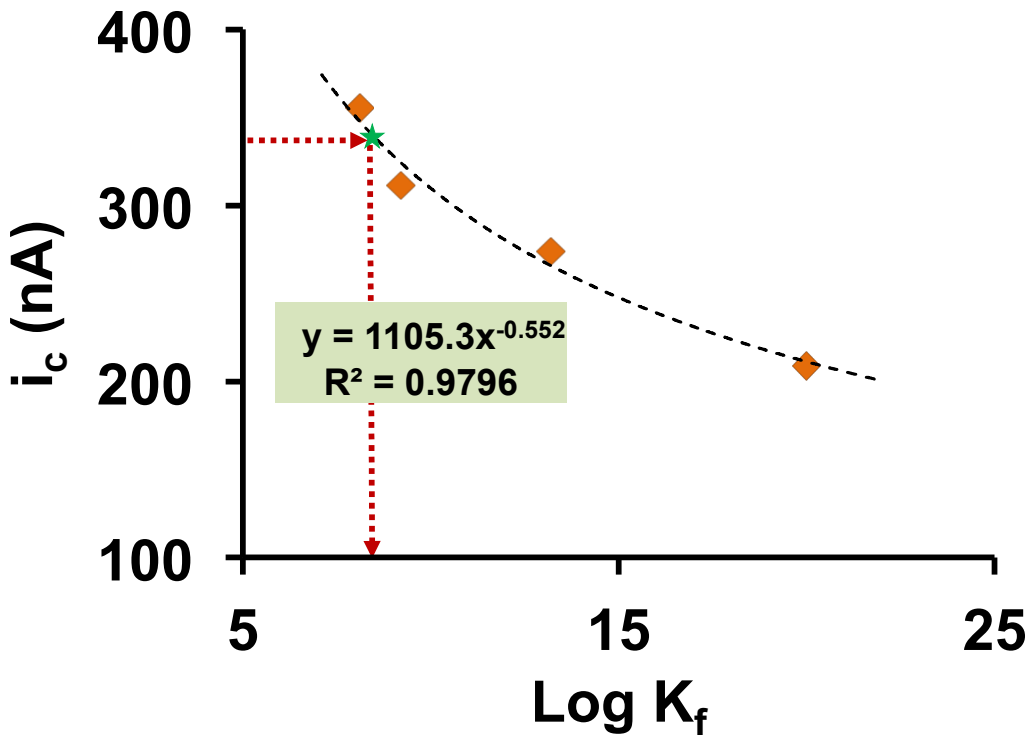

Figure 7.4: Correlation between cathodic current (i_c) and log formation constant, K_f for Cu^{2+}- ligand complexes. Exponential fit is with respect to responses for Cu^{2+} - EDTA, Cu^{2+} - citric acid, Cu^{2+} - gluatamic acid, and Cu^{2+} - 3-NSA (orange diamonds). Green star is FSCV response for Cu^{2+} - 5NSA and the exponential relationship is used to predict log K_f of Cu^{2+} - 3NSA complex.

As proof of principle that FSCV can achieve this type of measurement, we employed 5 different ligands and created mixtures with Cu^{2+} in the same manner described earlier; EDTA, citric acid, glutamic acid, 5-NSA and 3-NSA. We plotted the maximum FSCV cathodic current for Cu^{2+} - EDTA, Cu^{2+} - citric acid, Cu^{2+} - glutamic acid, and Cu^{2+} - 3NSA vs. the log of the corresponding literature K_f values (**Figure 7.4**). We found a clear relationship that we fit in a simple fashion

with an exponential function, yielding an R^2 of 0.98. This level of analysis is not sophisticated; however as a proof of principle experiment, an excellent fit to experimental data is achieved.

Furthermore, we used this model to predict the log K_f of 5-NSA by using the observed FSCV response for Cu^{2+} - 5-NSA mixture as the y component (plotted on **Figure 7.4** as the green star data point). Agreeably, our model yields log K_f as 8.34, which agrees well with previously reported values.[225] An important caveat here is that this model can only currently function when the $[Cu^{2+}]_{added}$ is a known (in this case, the same) value. In our future work, we are working to incorporate an ambient $[Cu^{2+}]$ measurement that would afford speciation information in authentic samples of unknown Cu^{2+} concentration. Nonetheless we present here an important laboratory tool for ultra rapid delivery of speciation information.

This is exciting data that, for the first time, highlights FSCV's power for providing speciation information about the matrix surrounding the CFM, in real time.

7.5 Conclusions

Copper-ligand complexation equilibria can be studied at high time resolution with FSCV. In this work we observed a strong relationship between FSCV response for different Cu^{2+} - ligand solutions and their corresponding equilibrium constants. We predicted the K of another model ligand, a key parameter in speciation studies. This study is proof of principle that FSCV can be utilized to study speciation on rapid time scales.

CHAPTER 8 FAST VOLTAMMETRY OF METALS AT CARBON-FIBER MICROELECTRODES: TOWARDS A REAL-TIME SPECIATION SENSOR

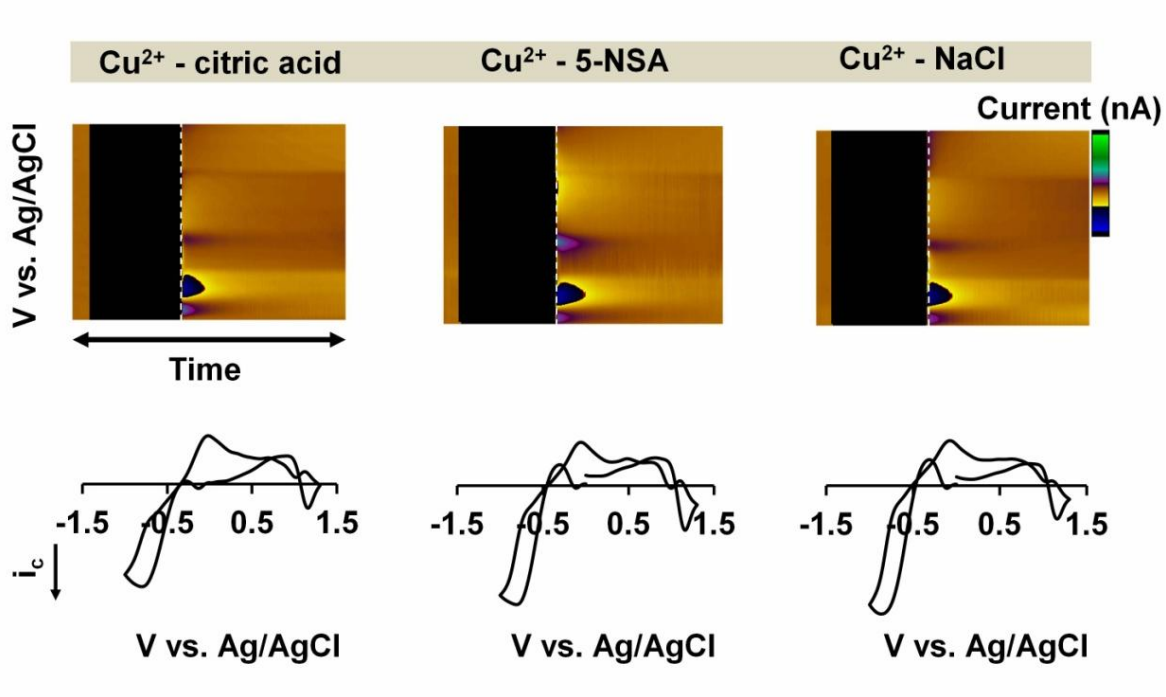

P. Pathirathna, T. Siriwardhane, S. P. McElmurry and P. Hashemi, *The Analyst* - in preparation.

8.1 Abstract

Trace metals play important roles in both biological and environmental systems. In biology, they are responsible for controlling many physiological processes including neurotransmission. Environmental trace metal pollution caused by mobilization of trace metals into natural waters is a significant public health issue. Studying metal speciation is important in understanding the behavior of metals in these real systems. Thus, there is great demand for rapid speciation analysis.In this study, we describe the application of fast scan cyclic voltammetry and fast scan adsorption controlled voltammetry to speciation analysis. We show that the same cyclic voltammograms define the FSCAV response to Cu^{2+} in different matrices. Using geochemical modeling, we show that matrices with different Cu^{2+} binding ability do not affect the equilibrium of Cu^{2+} adsorption onto CFMs, hence surface coverage can be utilized to predict free Cu^{2+} in solution. We show that a simple relationship can be established between the FSCV, FSCAV and K_f response for various different concentrations of solutions of Cu^{2+} complexes. Using our analytical methods and this relationship, we were able to instantly predict the free Cu^{2+} and K_f of a real groundwater sample spiked with Cu^{2+}. We validated our results with a commercially available Cu^{2+} ion selective electrode. This study presents proof of principle experiments that showcase fast voltammetry's potential as a rapid speciation sensor.

8.2 Introduction

Speciation controls the behavior of metals in real biological and environmental systems. Particularly, it is free, unbound metals in aquatic environments that are readily uptaken by aquatic organisms and plants, where at sufficient concentrations they can be pervasively detrimental. Similarly, unbound metals play fundamental roles in biological systems, acting as important signaling molecules.[114] In both environmental and biological systems the concentrations of unbound metals fluctuate dynamically, making it very difficult to define the exact nature and roles of metals in these networks.

Electrochemistry is a promising tool for metal analysis in real, dynamically fluctuating systems because the analysis occurs at a surface that can be fashioned into a variety of, minimally invasive, shapes and sizes. This surface or electrode can easily be submersed or integrated into the system of interest where, importantly, sample collection can be avoided. While Hg electrodes continue to provide unparalleled sensitivity, they are not easily portable and may pose health hazards. Thus, ion selective electrodes have been intensively used by environmental scientists to investigate metal speciation.[226-228] However, the temporal resolution of ISEs cannot capture dynamic events where metals are rapidly mobilized and transported into environmental water (e.g. within seconds during storms). Additionally ISE's are not generally suitable for monitoring physiological chemistry in intact systems because of their large dimensions (tissue damage).

In recent years, we pioneered fast scan cyclic voltammetry at carbon-fiber microelectrodes for real-time measurements of Cu^{2+} and Pb^{2+}.[90, 142] A robust adsorption equilibrium on the CFM surface allowed us to study Cu^{2+} complexation with a range of ligands and create a predictive model correlating the FSCV response to overall solution formation constant, K_f.[229] Here, we expand our study to rapidly and simultaneously report the unbound copper concentration and the K_f of a given sample. We achieve this by investigating the Cu^{2+} FSCV and FSCAV responses in a variety of media with different Cu^{2+} binding abilities. Based on these results, we construct models relating the FSCV and FSCAV response to free Cu^{2+} levels and K_f. We hence report the K_f and free Cu^{2+} concentration in a real environmental sample spiked with Cu^{2+}. Our measurement of free Cu^{2+} is validated with a commercially available ISE and the close agreement between two responses highlights the potential of our method as a real-time minimally invasive speciation sensor.

8.3 Materials and Methods

Microelectrodes, FSCV, FSCAV Experiments and Solution Analysis

CFMs were fabricated as stated in Chapter 2. Voltammetric experiments: FSCV in FIA system and FSCAV experiments and PHREEQCi analysis of each solution mixure were performed as explained in Chapter 2.

8.3.1 Solutions

All chemicals were purchased from Sigma-Aldrich (St. Louis, MO). Cupric nitrate ($Cu(NO_3)_2$) served as the source of Cu^{2+} and EDTA, citric acid, 5-NSA, 3-NSA and glutamic acid served as the ligands to bind Cu^{2+}. All Cu^{2+} - ligand

mixtures were prepared in 1:1 stoicheometric ratio in NaCl (0.01 M) prior to FSCAV and FSCV experiments at room temperature and pressure. Sufficient time was given for each solution mixture to reach the steady-state equilibrium prior to experiments. Solution pH was recorded and accounted for in proceeding PHREEQCi analyses.

8.3.2 Cu^{2+} Ion Selective Electrode

Cu^{2+} calibration curve was constructed with a Copper Combination Ion Selective Electrode (model 4230-A49, Thomas Scientific,Swedesboro, NJ,USA). A series of concentrations of Cu^{2+} solutions were prepared from a standard Cu^{2+} solution (1000 ppm, Thomas Scientific,Swedesboro, NJ,USA). All solutions were stirred well and allowed 20 mins before taking the stable measurements.

8.4 Results and Discussion

8.4.1 Voltammetric Determination of Unbound Cu^{2+}

In both environmental and biological systems, there is a discrepancy between the total concentration of Cu^{2+} and the concentration of Cu^{2+} available to engage in chemical processes. Biologically, Cu^{2+} is rapidly stabilized by proteins, thus only a small percentage of the total Cu^{2+} in the brain is thought to be unbound and participating in dynamic processes such as neurotransmission.[230, 231] Environmentally, many natural organic and inorganic ligands bind Cu^{2+}, while it is generally the free Cu^{2+} that is readily transported between systems creating harmful, toxic effects. Thus, to decipher the roles of Cu^{2+}, it is important to measure its unbound levels and such an analysis should be performed as rapidly as possible. Several analytical approaches have been taken to examine this type

of speciation in a variety of matrices including copper-ISEs, potentiometry, cation exchange resins and charge separation techniques.[226, 232, 233] These methods generally do not have adequate time resolution to assess the dynamic changes we are interested in deciphering.

In this work we utilized FSCAV, an extension of the FSCV method, developed by Atcherley *et al.*[62] to quantify ambient analyte levels. In FSCAV, a controlled adsorption time period allows ambient Cu^{2+} to come to equilibrium at the CFM surface, with an equilibrium constant that we refer to as K_{ads}, and thus directly reports the unbound analyte concentration surrounding the CFM. The temporal limitations here are those of file collection and controlled adsorption times such that readings can be taken every 30 seconds. Compared with the 10 s of minutes required to reach steady state for other speciation analysis methods (*vide supra*), this temporal resolution represented an improvement of orders of magnitude. To illustrate the applicability of FSCAV to Cu^{2+} speciation analysis, 1:1 mixtures of Cu^{2+}-NaCl, Cu^{2+}-Citric and Cu^{2+}-5-NSA, where Cu^{2+} was added at a concentration of 0.05 µM, were analyzed. The presence of a characteristic reduction event in the same position on all three color plots (**Figure 8.1.A**) and the cathodic peak around -0.7 V on all three CVs (**Figure 8.1.B**) confirms detection of the same specie (Cu^{2+}) in each mixture.

The differences in the peak height are likely caused by differences in $[Cu]_{free}$ due to the different inherent binding capability of each mixture and excitingly could potentially be used to quantify free Cu^{2+} in each solution. However, to accurately translate the FSCAV response to $[Cu]_{free}$, it is critical to

show that the Cu^{2+} - CFM equilibrium (K_{ads}) is not affected by the differing equilibria present in different solutions. We address this issue in the next section.

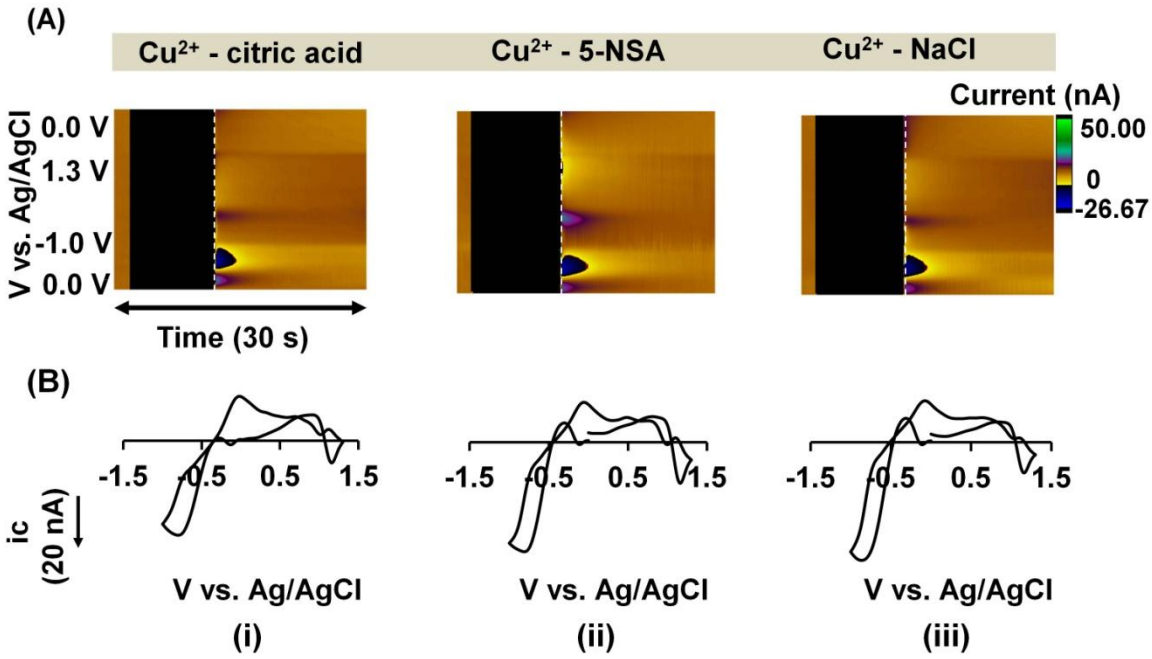

Figure 8.1: Top (A): Representative color plots obtained for the (i) Cu^{2+}-citric acid, (ii) Cu^{2+}-5-NSA and (iii) Cu^{2+}-NaCl complexes with FSCAV. Bottom (B): Buffer subtracted first CV taken at the vertical white dashed lines on the colour plots for (i) Cu^{2+}-citric acid, (ii) Cu^{2+}-5-NSA and (ii) Cu^{2+}-NaCl complexes.

8.4.2 K_{ads} of CFM - Cu^{2+} is Consistent in Different Model Solutions

$[Cu^{2+}]_{free}$ in solution depends on a variety of factors, including the inherent binding ability of the matrix. In **Figure 8.1**, differences in FSCAV peak height implied differences in $[Cu^{2+}]_{free}$, but to pursue the FSCAV response as a basis for quantifying $[Cu^{2+}]_{free}$ one must assume that different matrices do not alter the K_{ads} of the Cu^{2+}- CFM equilibrium. This assumption can be held true if we find that for the same $[Cu^{2+}]_{free}$ in different solutions, the CFM surface coverage of Cu^{2+} is the same. Thus we prepared solutions of different $[Cu^{2+}]$ in NaCl, Citric acid and 5-

NSA since these matrices have different affinities for Cu^{2+}. In **Figure 8.2** we utilized PHREEQCi to calculate $[Cu^{2+}]_{free}$ in each solution and plotted this on the x-axis vs. surface coverage, as calculated via Faraday's law and integration of the FSCAV peak. It can be seen that the same $[Cu^{2+}]_{free}$, regardless of matrix, yields the same CFM surface coverage, demonstrating that the matrices employed in this study do not affect CFM-Cu^{2+} K_{ads}. We can thus utilize the FSCAV response (surface coverage calculated from peak integration) to report $[Cu^{2+}]_{free}$ in different solutions.

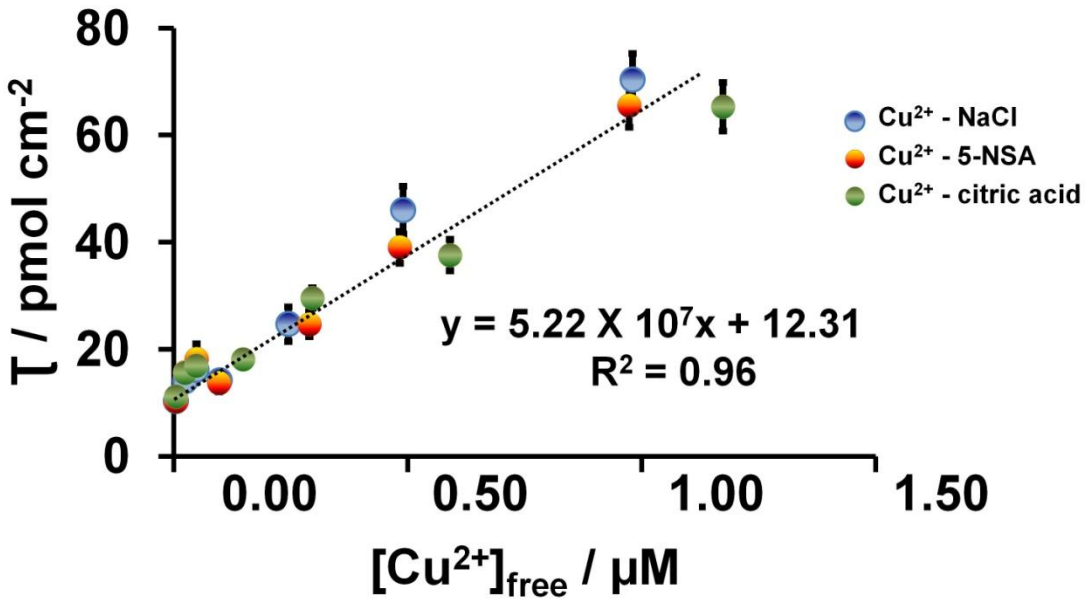

Figure 8.2: Correlation between surface concentration (Γ_{Cu}) vs. free copper [Cu^{2+}] in Cu^{2+}-NaCl, Cu^{2+}-citric and Cu^{2+}-5-NSA mixtures.$[Cu^{2+}]_{free}$ (x-axis) is calculated by PHREEQCi software and the surface concentration (y-axis) at each concentration is calculated by integrating cathoodic peak on respective CVs obtained with FSCAV.

The ability to report $[Cu^{2+}]_{free}$ is a powerful analytical development. We previously reported a simple model that could predict the overall solution K_f from

FSCV response.[229] Below we illustrate how this relationship is dependent on $[Cu^{2+}]_{free}$ and thus how FSCV and FSCAV can be utilized to provide multiple levels of speciation information by reporting $[Cu^{2+}]_{free}$ and overall solution K_f.

8.4.3 FSCV and FSCAV for Multi-Leveled Speciation Analysis

In a previous study, we showed that the FSCV response could predict the overall Kf of solution by performing experiments where we separately pre-mixed four different ligands with a known concentration of Cu^{2+}, performed FIA and obtained a FSCV response.[229] We then constructed a plot between FSCV response and literature reported formation constants and we successfully predicted the K_f of a solution of Cu^{2+} - 5-NSA with our model.[229] However, the FSCV response depends on two factors; the $[Cu^{2+}]_{free}$ and the K_f. Although it is possible to calculate $[Cu^{2+}]_{free}$ via PHREEQCi in a solution whose composition is known (which we did in our prior study), for analysis of real samples this approach is not appropriate since the matrix composition is unknown. Therefore, we sought to extend the prior relationships that we found to include $[Cu^{2+}]_{free}$. In this way, analysis of an unknown sample could yield values for $[Cu^{2+}]_{free}$ and K_f.

We prepared five different 1:1 concentration series (0.10, 0.30, 0.50, 0.80 and 1.0 µM) of Cu^{2+}-ligand solutions with known K_f of Cu-Ligand binding. We analyzed each mixture with FSCAV and FSCV respectively, with FSCAV providing a value for $[Cu^{2+}]_{free}$. We found a simple relationship between $[Cu^{2+}]_{free}$ FSCAV response, FSCV response and K_f which we present in **Figure 8.3**. In this plot, the ratio between FSCV response and log $[Cu^{2+}]_{free}$ on x-axis is plotted vs. the ratio between FSCV response and log K_f on the y-axis for each mixture

(different colors signify the different ligands). There is a simple, linear relationship corresponding to the experimental data in this plot. We next use this relationship to predict the $[Cu^{2+}]_{free}$ and K_f in real environmental sample spiked with Cu^{2+}.

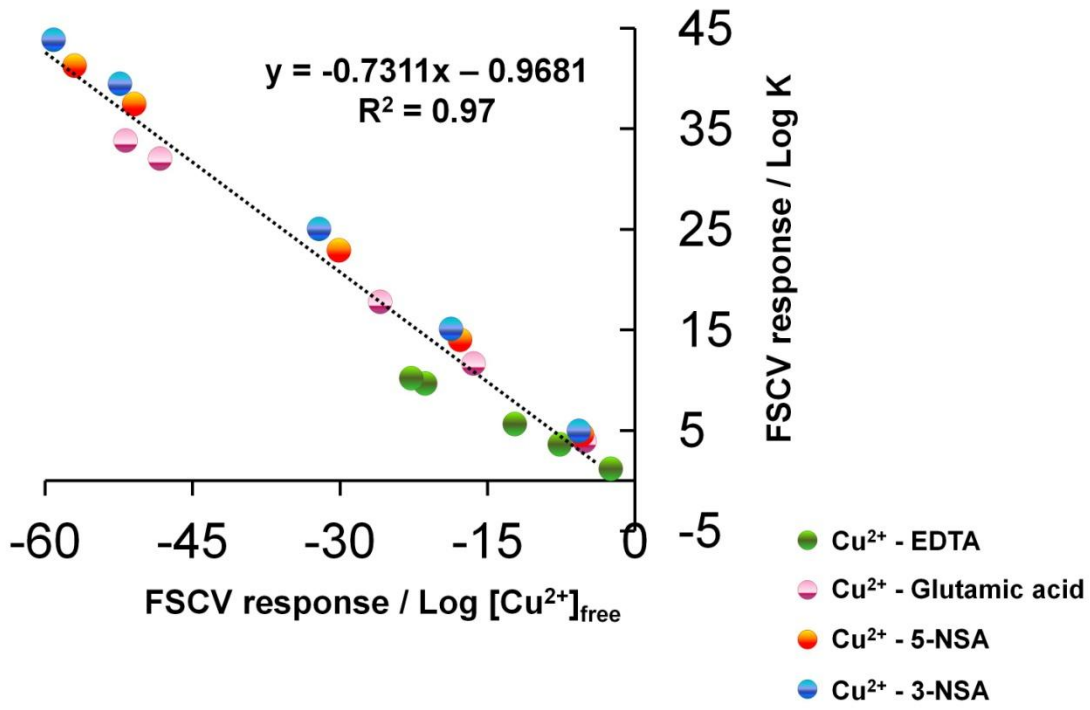

Figure 8.3: Correlation between FSCV response, $[Cu^{2+}]_{free}$ and formation constant, K_f. x-axis represents the ratio between FSCV response and log $[Cu^{2+}]_{free}$ and y-axis represents the ratio between FSCV response and log K obtained for four solutions ; Cu^{2+}-EDTA, Cu^{2+}-Glutamic acid, Cu^{2+}-5-NSA and Cu^{2+}-3-NSA.

8.4.4 Analysis of $[Cu^{2+}]_{free}$ and Overall Solution K in a Real Environmental Sample

We obtained a groundwater sample collected from Indian springs metro park, MI. We tested this sample with FSCV and FSCAV and found no detectable levels of Cu^{2+}; therefore, we spiked this same water sample with 0.5 µM Cu^{2+}. FSCV and FSCAV were performed on this spiked sample (4 electrodes (3

replicates on each)) and the average surface concentration was calculated for a total of 12 replicates. $[Cu^{2+}]_{free}$ was determined with FSCAV to be 0.1±0.01 µM. The difference in $[Cu^{2+}]_{added}$ and $[Cu^{2+}]_{free}$ is due to the removal of $[Cu^{2+}]_{free}$ via complexation ligands present in the groundwater sample. We further validated this result with a commercially available copper ISE.

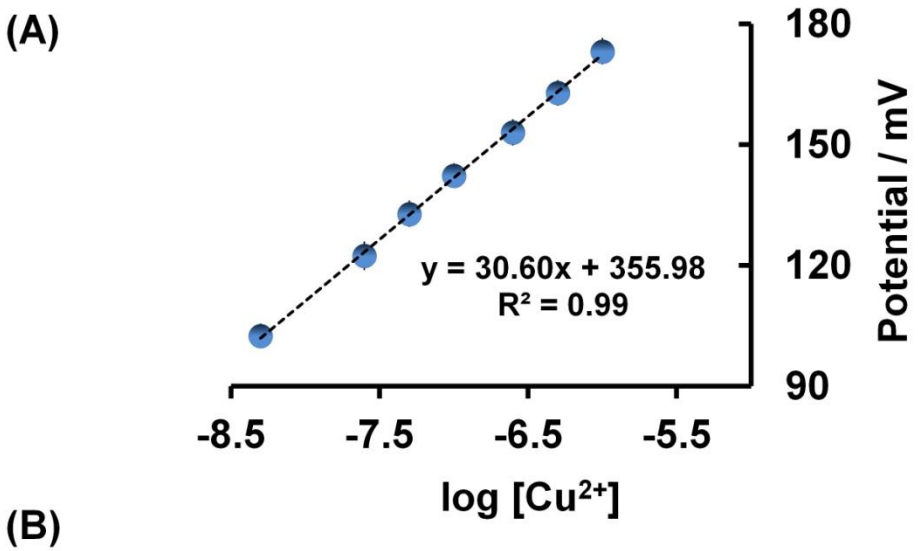

(B)

Real ground water sample	FSCAV response (pmol cm^{-2})	$[Cu^{2+}]$ from FSCAV calibration (µM)	ISE response (mV)	$[Cu^{2+}]$ from ISE calibration (µM)
	16.2 (±0.5)	0.10 (±0.01)	139.3 (±0.3)	0.10 (±0.0007)

Figure 8.4: (A) Calibration curve obtained for Cu^{2+} ISE. Line equation represents a perfect Nernstian response with a slope of 30 mV indicating the accuracy of Cu^{2+} ISE. (B) Summary of $[Cu^{2+}]_{free}$ in a groundwater sample calculated using FSCAV and ISE.

Figure 8.4.A represents the calibration curve we constructed for the commercially available Cu^{2+} ISE after an equilibrium period of 20 minutes. A slope of 30 mV in the line equation indicates a linear Nernstian response for Cu^{2+}. As is observed in the table in **Figure 8.4.B**, close agreement between our prediction of $[Cu^{2+}]_{free}$ and the ISE validates the accuracy of FSCAV. Having

established $[Cu^{2+}]_{free}$ in this solution, we next used the correlation we constructed in Figure 3 to predict the overall Kf of this solution as log K_f = 13.7.

Although our findings show a great promise in predicting speciation information, future experiments are needed to study the dependency of various stoichemoetric ratios between Cu^{2+} and ligand and the effect of pH on FSCV and FSCAV responses. Further, a comprehensive mathematical study is required to incorporate all possible variables into future correlations that could potentially affect our responses thus to predict speciation information in real systems.

8.5 Conclusions

In this paper we described the application of fast voltammetric tools to speciation analysis. We showed that by using FSCAV Cu^{2+} could be measured in different matrices. We found that matrices with different Cu^{2+} binding ability did not affect the equilibrium of Cu^{2+} adsorption onto CFMs, and thus predicted free Cu^{2+} in solution. We found a simple relationship between the FSCV, FSCAV and K_f response for different Cu^{2+} complexes. Via this relationship, we instantly predicted, and validated the free Cu^{2+} and K_f of a real groundwater sample spiked with Cu^{2+}. We thus present FSCV and FSCAV's promise towards a rapid speciation sensor.

CHAPTER 9 CONCLUSIONS AND PROSPECTUS

Trace metals play important roles in both biological and environmental systems. In biology, they are responsible for controlling many physiological processes including neurotransmission. Environmental trace metal pollution caused by mobilization of trace metals into natural waters is a significant public health issue. Studying metal speciation is important in understanding the behavior of metals in these real systems. Thus, there is great demand for rapid speciation analysis.

At this time existing metal analysis techniques including spectroscopic methods and conventional electrochemical tools cannot provide rapid speciation information because of inadequate temporal resolution, complex sample preparation and pre-concentration steps, high-cost, low portability instruments and use of hazardous materials.

In this dissertation, I described the development and application of an ultra-fast electrochemical technique using FSCV to identify and quantify Cu^{2+} and Pb^{2+} in aqueous samples. Adsorption was determined to be the fundamental mechanism governing the fast electrochemical response and the thermodynamic profile of Cu^{2+} adsorption onto CFMs in different matrices studied using spectroscopic and electrochemical tools. Additionally, we investigated complex formation of Cu^{2+} with a range of ligands with different formation constants for the Cu^{2+}-ligand complexation process. From this, two strong correlations were observed and used to predict the solution formation constant and the concentration of free Cu^{2+} using a combination of FSCV and FSCAV responses.

Our findings showcase the power of our technique as a rapid, robust, real-time speciation sensor with high sensitivity, we must next perform a series of experiments before a field or *in vivo* device can be developed.

In our study, the stoichiometry between Cu^{2+} and the ligand was maintained at 1:1 since most of the ligands studied were proven to make complexes with Cu^{2+} in 1:1 molar ratio. In the future we would like to study the impact of stoichiometric ratio on FSCV and FSCAV responses using a series of solution mixtures with differing molar ratios of Cu^{2+} and a ligand. Further, the pH of our solutions were varied between 4.00- 5.50 in the presence of NaCl, however in real systems, the pH is slightly more basic than this. It would be appropriate to include the dependency of pH in further reported correlations. The selectivity of our technique should be addressed properly with the surface modification of electrodes with Cu^{2+} ionophores, without compromising electrode temporal resolution. The steady-state approximations need to be further evaluated by studying adsorption profiles at different time scales. An in depth mathematical analysis should be performed to correlate all possible variables that could potentially have an impact on FSCAV and FSCV responses. The knowledge of microfluidics is essential to incorporate FIA system into a miniaturized device.

APPENDIX A

Pb Analysis Supplemental Data

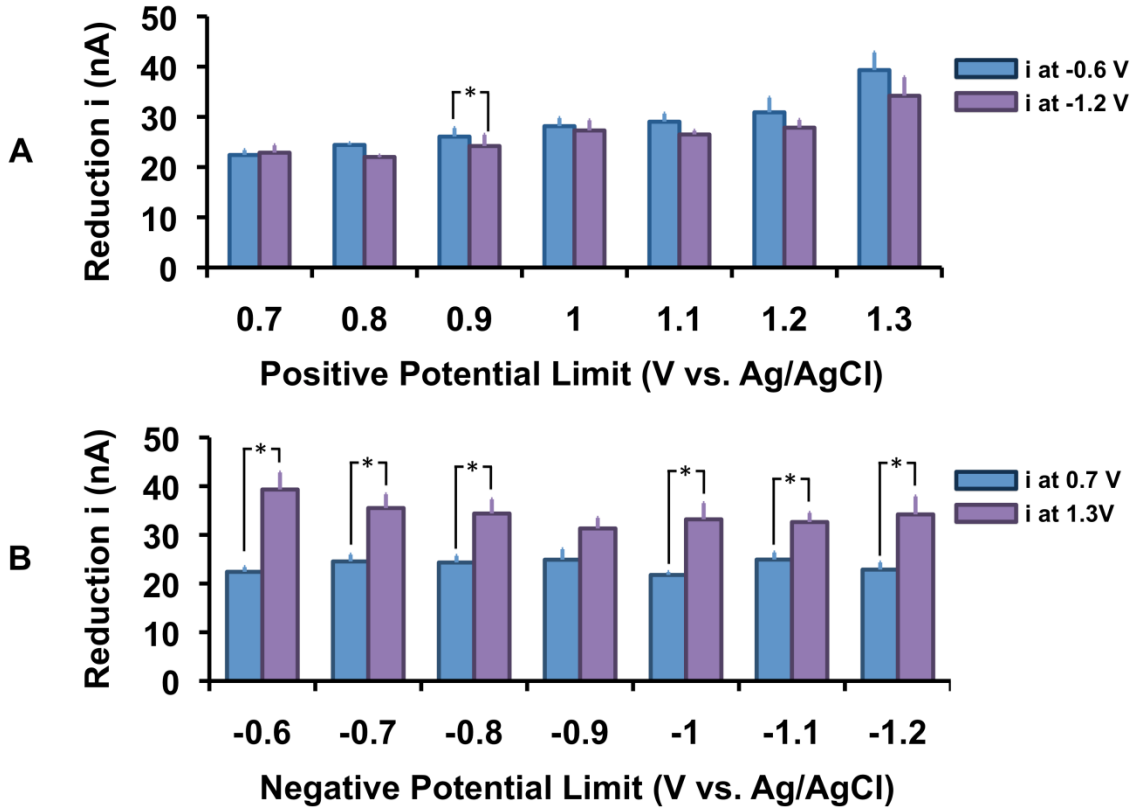

Figure S1: (A) Maximum reduction current at -0.6 V (blue) compared to the current at -1.2 V (purple) for every positive potential studied and (B) maximum reduction current at 1.3 V (purple) compared to current at 0.7 V (blue) for every negative potential studied: stars signify statistically different values.

APPENDIX B

Permission obtained from American Chemical Society to reprint the article in Chapter 3

Title:	Fast-Scan Deposition-Stripping Voltammetry at Carbon-Fiber Microelectrodes: Real-Time, Subsecond, Mercury Free Measurements of Copper
Author:	Pavithra Pathirathna, Yuanyuan Yang, Kristen Forzley, et al
Publication:	Analytical Chemistry
Publisher:	American Chemical Society
Date:	Aug 1, 2012

PERMISSION/LICENSE IS GRANTED FOR YOUR ORDER AT NO CHARGE

This type of permission/license, instead of the standard Terms & Conditions, is sent to you because no fee is being charged for your order. Please note the following:

- Permission is granted for your request in both print and electronic formats, and translations.
- If figures and/or tables were requested, they may be adapted or used in part.
- Please print this page for your records and send a copy of it to your publisher/graduate school.
- Appropriate credit for the requested material should be given as follows: "Reprinted (adapted) with permission from (COMPLETE REFERENCE CITATION). Copyright (YEAR) American Chemical Society." Insert appropriate information in place of the capitalized words.
- One-time permission is granted only for the use specified in your request. No additional uses are granted (such as derivative works or other editions). For any other uses, please submit a new request.

APPENDIX C

Permission obtained from American Chemical Society to reprint the article in Chapter 4

Title:	Real-Time Subsecond Voltammetric Analysis of Pb in Aqueous Environmental Samples
Author:	Yuanyuan Yang, Pavithra Pathirathna, Thushani Siriwardhane, et al
Publication:	Analytical Chemistry
Publisher:	American Chemical Society
Date:	Aug 1, 2013

PERMISSION/LICENSE IS GRANTED FOR YOUR ORDER AT NO CHARGE

This type of permission/license, instead of the standard Terms & Conditions, is sent to you because no fee is being charged for your order. Please note the following:

- Permission is granted for your request in both print and electronic formats, and translations.
- If figures and/or tables were requested, they may be adapted or used in part.
- Please print this page for your records and send a copy of it to your publisher/graduate school.
- Appropriate credit for the requested material should be given as follows: "Reprinted (adapted) with permission from (COMPLETE REFERENCE CITATION). Copyright (YEAR) American Chemical Society." Insert appropriate information in place of the capitalized words.
- One-time permission is granted only for the use specified in your request. No additional uses are granted (such as derivative works or other editions). For any other uses, please submit a new request.

APPENDIX D

Permission obtained from The Royal Society of Chemistry to reprint the article in Chapter 5

Fast voltammetry of metals at carbon-fiber microelectrodes: copper adsorption onto activated carbon aids rapid electrochemical analysis

P. Pathirathna, S. Samaranayake, C. W. Atcherley, K. L. Parent, M. L. Heien, S. P. McElmurry and P. Hashemi, *Analyst*, 2014, **139**, 4673

DOI: 10.1039/C4AN00937A

publications or in a thesis or dissertation provided that the correct acknowledgement is given with the reproduced material.

Reproduced material should be attributed as follows:

- For reproduction of material from NJC:
  [Original citation] - Reproduced by permission of The Royal Society of Chemistry (RSC) on behalf of the Centre National de la Recherche Scientifique (CNRS) and the RSC
- For reproduction of material from PCCP:
  [Original citation] - Reproduced by permission of the PCCP Owner Societies
- For reproduction of material from PPS:
  [Original citation] - Reproduced by permission of The Royal Society of Chemistry (RSC) on behalf of the European Society for Photobiology, the European Photochemistry Association, and RSC
- For reproduction of material from all other RSC journals:
  [Original citation] - Reproduced by permission of The Royal Society of Chemistry

If you are the author of this article you still need to obtain permission to reproduce the whole article in a third party publication with the exception of reproduction of the whole article in a thesis or dissertation.

Information about reproducing material from RSC articles with different licences is available on ourPermission Requests page.

REFERENCES

1. B. L. Vallee and R. Williams, *Proceedings of the National Academy of Sciences*, 1968, **59**, 498-505.
2. K. D. Karlin, *Science*, 1993, **261**, 701-708.
3. M. Fontecave and J.-L. Pierre, *Coordination chemistry reviews*, 1998, **170**, 125-140.
4. M. Yim, P. B. Chock and E. Stadtman, *Journal of Biological Chemistry*, 1993, **268**, 4099-4105.
5. J. R. Prohaska, *Physiological reviews*, 1987, **67**, 858-901.
6. W. R. Markesbery, W. D. Ehmann, M. Alauddin and T. Hossain, *Neurobiology of aging*, 1984, **5**, 19-28.
7. M. L. Schlief, T. West, A. M. Craig, D. M. Holtzman and J. D. Gitlin, *Proceedings of the National Academy of Sciences*, 2006, **103**, 14919-14924.
8. P. S. Donnelly, Z. Xiao and A. G. Wedd, *Current opinion in chemical biology*, 2007, **11**, 128-133.
9. C. S. Atwood, R. C. Scarpa, X. Huang, R. D. Moir, W. D. Jones, D. P. Fairlie, R. E. Tanzi and A. I. Bush, *Journal of Neurochemistry*, 2000, 75, 1219-1233.
10. S. Tandy, K. Bossart, R. Mueller, J. Ritschel, L. Hauser, R. Schulin and B. Nowack, *Environmental science & technology*, 2004, **38**, 937-944.
11. F. Fu and Q. Wang, *Journal of environmental management*, 2011, **92**, 407-418.

12. S. Ebbs, M. Lasat, D. Brady, J. Cornish, R. Gordon and L. Kochian, *Journal of Environmental Quality*, 1997, **26**, 1424-1430.

13. J.-f. Peng, Y.-h. Song, P. Yuan, X.-y. Cui and G.-l. Qiu, *Journal of Hazardous Materials*, 2009, **161**, 633-640.

14. B. Gunawardana, N. Singhal and A. Johnson, *Plant Soil*, 2010, **329**, 283-294.

15. M. E. Dietz and J. C. Clausen, *Environmental science & technology*, 2006, **40**, 1335-1340.

16. J. Good, A. O'Sullivan, D. Wicke and T. Cochrane, *Water Science & Technology*, 2012, 65.

17. W. Hunt, J. Smith, S. Jadlocki, J. Hathaway and P. Eubanks, *Journal of Environmental Engineering*, 2008, **134**, 403-408.

18. C.-h. Hsieh and A. P. Davis*, Journal of Environmental Engineering*, 2005, **131**, 1521-1531.

19. M. Ghaedi, F. Ahmadi and A. Shokrollahi, *Journal of Hazardous Materials*, 2007, **142**, 272-278.

20. İ. Narin, M. Soylak, L. Elçi and M. Doğan, *Talanta*, 2000, **52**, 1041-1046.

21. G. Aragay, J. Pons and A. Merkoçi, *Chemical reviews*, 2011, **111**, 3433-3458.

22. G.-H. Tao and R. Sturgeon, Spectrochimica Acta Part B: *Atomic Spectroscopy*, 1999, **54**, 481-489.

23. S. Mounicou, K. Połeć, H. Chassaigne, M. Potin-Gautier and R. Łobiński, *J. Anal. At. Spectrom.*, 2000, **15**, 635-642.

24. Z. Horváth, A. Lastity, I. Varga, E. Meszaros and A. Molnar, *Talanta*, 1994, **41**, 1165-1168.

25. E. P. Achterberg and C. Braungardt, *Analytica Chimica Acta*, 1999, **400**, 381-397.

26. P. Sonthalia, E. McGaw, Y. Show and G. M. Swain, *Analytica Chimica Acta*, 2004, **522**, 35-44.

27. S. Wang, E. S. Forzani and N. Tao, *Analytical Chemistry*, 2007, **79**, 4427-4432.

28. K. R. Wehmeyer and R. M. Wightman, *Analytical Chemistry*, 1985, **57**, 1989-1993.

29. G. Gillain, G. Duyckaerts and A. Disteche, *Analytica Chimica Acta*, 1979, **106**, 23-37.

30. G. Kefala, A. Economou, A. Voulgaropoulos and M. Sofoniou, *Talanta*, 2003, **61**, 603-610.

31. J. Wang, J. Lu, Ü. A. Kirgöz, S. B. Hocevar and B. Ogorevc, *Analytica Chimica Acta*, 2001, **434**, 29-34.

32. J. Wang, J. Lu, S. B. Hocevar, P. A. Farias and B. Ogorevc, *Analytical Chemistry*, 2000, **72**, 3218-3222.

33. R. P. Buck, *Analytical Chemistry*, 1976, **48**, 23R-39r.

34. M. E. Meyerhoff and Y. M. Fraticelli, *Analytical Chemistry*, 1982, **54**, 27R-44R.

35. M. Meyerhoff and W. Opdycke, *Adv. Clin. Chem*, 1986, **25**, 1-47.

36. E. Bakker, *Electroanalysis*, 1997, **9**, 7-12.

37. R. A. Durst, *Ion-selective electrodes: proceedings*, US National Bureau of Standards; for sale by the Supt. of Docs., US Govt. Print. Off., Washington, 1969.

38. P. T. Kissinger and W. R. Heineman, *Journal of Chemical Education*, 1983, **60**, 702.

39. J. Heinze, *Angewandte Chemie International Edition in English*, 1984, **23**, 831-847.

40. G. A. Mabbott, *Journal of Chemical Education*, 1983, **60**, 697.

40. R. S. Nicholson, *Analytical Chemistry*, 1965, **37**, 1351-1355.

42. A. Pozio, M. De Francesco, A. Cemmi, F. Cardellini and L. Giorgi, *Journal of power sources*, 2002, **105**, 13-19.

43. E. Beit-Yannai, R. Kohen, M. Horowitz, V. Trembovler and E. Shohami, *Journal of Cerebral Blood Flow & Metabolism*, 1997, **17**, 273-279.

44. S. Chevion, E. M. Berry, N. Kitrossky and R. Kohen, *Free Radical Biology* and Medicine, 1997, **22**, 411-421.

45. J. A. Stamford, Z. L. Kruk and J. Millar, *Brain research*, 1984, **299**, 289-295.

46. J. O. Howell, W. G. Kuhr, R. E. Ensman and R. M. Wightman, *Journal of Electroanalytical Chemistry and Interfacial Electrochemistry*, 1986, **209**, 77-90.

47. A. Ewing, R. Wightman and M. Dayton, *Brain research*, 1982, **249**, 361-370.

48. J. E. Baur, E. W. Kristensen, L. J. May, D. J. Wiedemann and R. M. Wightman, *Analytical Chemistry*, 1988, **60**, 1268-1272.

49. B. P. Jackson, S. M. Dietz and R. M. Wightman, *Analytical Chemistry*, 1995, **67**, 1115-1120.

50. D. L. Robinson, B. J. Venton, M. L. Heien and R. M. Wightman, *Clinical chemistry*, 2003, **49**, 1763-1773.

51. M. L. Heien, M. A. Johnson and R. M. Wightman, *Analytical Chemistry*, 2004, **76**, 5697-5704.

52. J. L. Ponchon, R. Cespuglio, F. Gonon, M. Jouvet and J. F. Pujol, *Analytical Chemistry*, 1979, **51**, 1483-1486.

53. M. Armstrong-James and J. Millar, *Journal of neuroscience methods*, 1979, **1**, 279-287.

54. K. Potje-Kamloth, P. Janata and M. Josowicz, *in Contemporary Electroanalytical Chemistry*, Springer, 1990, pp. 199-203.

55. B. D. Bath, D. J. Michael, B. J. Trafton, J. D. Joseph, P. L. Runnels and R. M. Wightman, *Analytical Chemistry*, 2000, **72**, 5994-6002.

56. J. L. Peters, L. H. Miner, A. C. Michael and S. R. Sesack, *Journal of neuroscience methods*, 2004, **137**, 9-23.

57. M. L. Heien, P. E. Phillips, G. D. Stuber, A. T. Seipel and R. M. Wightman, *The Analyst*, 2003, **128**, 1413-1419.

58. P. Takmakov, M. K. Zachek, R. B. Keithley, P. L. Walsh, C. Donley, G. S. McCarty and R. M. Wightman, *Analytical Chemistry*, 2010, **82**, 2020-2028.

59. M. A. Dayton, A. G. Ewing and R. M. Wightman, *Analytical Chemistry*, 1980, **52**, 2392-2396.

60. R. C. Engstrom, T. Meaney, R. Tople and R. M. Wightman, *Analytical Chemistry*, 1987, **59**, 2005-2010.

61. M. A. Dayton, A. G. Ewing and R. M. Wightman, *European Journal of Pharmacology*, 1981, **75**, 141-144.

62. C. W. Atcherley, N. D. Laude, K. L. Parent and M. L. Heien, *Langmuir*, 2013, **29**, 14885-14892.

63. B. Lindström and L. J. Pettersson, *International Journal of Hydrogen Energy*, 2001, **26**, 923-933.

64. N. N. S. Deo and A. H. Chang, *Journal*, 1994.

65. L. Fishbein, *Environmental health perspectives*, 1981, **40**, 43.

66. S. R. Charlton, C. L. Macklin and D. L. Parkhurst, *US Geological Survey Water-Resources Investigations Report*, 1997, 9.

67. A. G. Aslamkhan, A. Aslamkhan and G. A. Ahearn, *Journal of experimental zoology*, 2002, **292**, 507-522.

68. S. P. McElmurry, D. T. Long and T. C. Voice, *Applied Geochemistry*, 2010, **25**, 650-660.

69. M. Bigalke, S. Weyer and W. Wilcke, *Environmental science & technology*, 2010, **44**, 5496-5502.

70. J. Wang and W. D. Marshall, *Analytical Chemistry*, 1994, **66**, 3900-3907.

71 T. R. Harville and R. K. Marcus, *Analytical Chemistry*, 1995, **67**, 1271-1277.

72. T. Zhao, T. Chen, Y. Qiu, X. Zou, X. Li, M. Su, C. Yan, A. Zhao and W. Jia, *Analytical Chemistry*, 2009, **81**, 3683-3692.

73. J. Buffle and M.-L. Tercier-Waeber, *TrAC Trends in Analytical Chemistry*, 2005, **24**, 172-191.

74. M. M. Ardakani, M. Salavati-Niasari, M. K. Kashani and S. Ghoreishi, *Analytical and Bioanalytical Chemistry*, 2004, **378**, 1659-1665.

75. I. Turyan and D. Mandler, *Analytical Chemistry*, 1993, **65**, 2089-2092.

76. P. S. Cahill, Q. D. Walker, J. M. Finnegan, G. E. Mickelson, E. R. Travis and R. M. Wightman, *Analytical Chemistry*, 1996, **68**, 3180-3186.

77. P. Hashemi, E. C. Dankoski, J. Petrovic, R. B. Keithley and R. Wightman, *Analytical Chemistry*, 2009, **81**, 9462-9471.

78. J. Millar, J. A. Stamford, Z. L. Kruk and R. M. Wightman, *European Journal of Pharmacology*, 1985, **109**, 341-348.

79. D. Michael, E. R. Travis and R. M. Wightman, *Analytical Chemistry*, 1998, **70**, 586A-592A.

80. M. A. Laidlaw and G. M. Filippelli, *Applied Geochemistry*, 2008, **23**, 2021-2039.

81. J. O. Nriagu, *Biogeochemistry of Lead in the Environment*, Elsevier/North-Holland Biomedical Press, 1978.

82. H. J. Binns, C. Campbell and M. J. Brown, *Pediatrics*, 2007, **120**, e1285-e1298.

83. S. Zahran, M. A. Laidlaw, S. P. McElmurry, G. M. Filippelli and M. Taylor, *Environmental science & technology*, 2013, **47**, 2839-2845.

84. E. January, 2009.

85. H. Lee, S.-L. Lau, M. Kayhanian and M. K. Stenstrom, *Water research*, 2004, **38**, 4153-4163.

86. D. G. Strawn and D. L. Sparks, *Soil Science Society of America Journal*, 2000, **64**, 144-156.

87. W. Stumm, J. J. Morgan and J. I. Drever, *Journal of Environmental Quality*, 1996, **25**, 1162.

88. L. Sigg, F. Black, J. Buffle, J. Cao, R. Cleven, W. Davison, J. Galceran, P. Gunkel, E. Kalis and D. Kistler, *Environmental science & technology*, 2006, **40**, 1934-1941.

89. K. C. Armstrong, C. E. Tatum, R. N. Dansby-Sparks, J. Q. Chambers and Z.-L. Xue, *Talanta*, 2010, **82**, 675-680.

90. P. Pathirathna, Y. Yang, K. Forzley, S. P. McElmurry and P. Hashemi, *Analytical Chemistry*, 2012, **84**, 6298-6302.

91. G. Li, Z. Ji and K. Wu, *Analytica Chimica Acta*, 2006, **577**, 178-182.

92. N. Khun and E. Liu, *Electrochimica Acta*, 2009, **54**, 2890-2898.

93. B. Baś, M. Jakubowska, M. Jeż and F. Ciepiela, *Journal of Electroanalytical Chemistry*, 2010, **638**, 3-8.

94. B. Sherigara, Y. Shivaraj, R. J. Mascarenhas and A. Satpati, Electrochimica Acta, 2007, **52**, 3137-3142.

95. G. Kefala, A. Economou and A. Voulgaropoulos, The Analyst, 2004, **129**, 1082-1090.

96. V. Guzsvány, H. Nakajima, N. Soh, K. Nakano, I. Švancara, K. Vytřas, L. Bjelica and T. Imato, *Electroanalysis*, 2011, **23**, 1593-1601.

97. P. Silva, M. El Khakani, M. Chaker, A. Dufresne and F. Courchesne, *Sensors and Actuators B: Chemical*, 2001, **76**, 250-257.

98. C. Prado, S. J. Wilkins, F. Marken and R. G. Compton, *Electroanalysis*, 2002, **14**, 262-272.

99. A. C. V. dos Santos and J. C. Masini, *Analytical and Bioanalytical Chemistry*, 2006, **385**, 1538-1544.

100. J. Heyrovský and M. Shikata, *Recueil Des Travaux Chimiques Des Pays-Bas*, 1925, **44**, 496-498.

101. A. Economou, *TrAC Trends in Analytical Chemistry*, 2005, **24**, 334-340.

102. G. Kefala and A. Economou, *Analytica Chimica Acta*, 2006, **576**, 283-289.

103. B. Ninwong, S. Chuanuwatanakul, O. Chailapakul, W. Dungchai and S. Motomizu, *Talanta*, 2012, **96**, 75-81.

104. C. M. Dean, J. J. Sansalone, F. K. Cartledge and J. H. Pardue, *Journal of Environmental Engineering*, 2005.

105. M. K. Aroua, S. Leong, L. Teo, C. Y. Yin and W. M. A. W. Daud, *Bioresource Technology*, 2008, **99**, 5786-5792.

106. M. Püntener, T. Vigassy, E. Baier, A. Ceresa and E. Pretsch, *Analytica Chimica Acta*, 2004, **503**, 187-194.

107. M. R. Ganjali, N. Motakef-Kazami, F. Faridbod, S. Khoee and P. Norouzi, *Journal of Hazardous Materials*, 2010, **173**, 415-419.

108. W. Stumm and J. J. Morgan, *Aquatic chemistry: chemical equilibria and rates in natural waters*, John Wiley & Sons, 2012.

109. E. V. Novotny, D. Murphy and H. G. Stefan, *Science of the Total Environment*, 2008, **406**, 131-144.

110. J. B. Zimmerman and R. M. Wightman, *Analytical Chemistry*, 1991, **63**, 24-28.

111. B. J. Venton, D. J. Michael and R. M. Wightman, *Journal of Neurochemistry*, 2003, **84**, 373-381.

112. Y. Bonfil, M. Brand and E. Kirowa-Eisner, *Analytica Chimica Acta*, 2002, **464**, 99-114.

113. E. D. Gaier, B. A. Eipper and R. E. Mains, *Journal of neuroscience research*, 2013, **91**, 2-19.

114. E. L. Que, D. W. Domaille and C. J. Chang, *Chemical reviews*, 2008, **108**, 1517-1549.

115. Y. H. Hung, A. I. Bush and R. A. Cherny, *JBIC Journal of Biological Inorganic Chemistry*, 2010, **15**, 61-76.

116. I. G. Macreadie, *European Biophysics Journal*, 2008, **37**, 295-300.

117. K. Haarstad, H. Bavor and T. Maehlum, *Water Science & Technology*, 2011, **65**, 76-99.

118. E. Vaiopoulou and P. Gikas, *Water research*, 2012, **46**, 549-570.

119. L. M. Chiodo, S. W. Jacobson and J. L. Jacobson, *Neurotoxicology and teratology*, 2004, **26**, 359-371.

120. S. Charlesworth, E. De Miguel and A. Ordóñez, *Environmental geochemistry and health*, 2011, **33**, 103-123.

121. G. J. Brewer, *Clinical Neurophysiology*, 2010, **121**, 459-460.

122. E. ul Islam, X.-e. Yang, Z.-l. He and Q. Mahmood, *Journal of Zhejiang University Science B*, 2007, **8**, 1-13.

123. J. R. Peralta-Videa, M. L. Lopez, M. Narayan, G. Saupe and J. Gardea-Torresdey, *The international journal of biochemistry & cell biology*, 2009, **41**, 1665-1677.

124. D. M. Ward, K. H. Nislow and C. L. Folt, *Annals of the New York Academy of Sciences*, 2010, **1195**, 62-83.

125. S. Baishaw, J. Edwards, B. Daughtry and K. Ross, *Reviews on environmental health*, 2007, **22**, 91-114.

126. N. E. Selin, *Journal of Environmental Monitoring*, 2011, **13**, 2389-2399.

127. K. S. Ritter, Paul Sibley, Ken Hall, Patricia Keen, Gevan Mattu, Beth Linton, Len, *Journal of Toxicology and Environmental Health Part A*, 2002, **65**, 1-142.

128. R. W. Peters, *Journal of Hazardous Materials*, 1999, **66**, 151-210.

129. J. Kumpiene, A. Lagerkvist and C. Maurice, *Waste management*, 2008, **28**, 215-225.

130. H. Brix, *Water Science and Technology*, 1999, **40**, 45-50.

131. R. Kadlec and S. Wallace, *Edition. Boca Raton, CRCPress*, 2009.

132. O. T. Butler, J. M. Cook, C. F. Harrington, S. J. Hill, J. Rieuwerts and D. L. Miles, *Journal of Analytical Atomic Spectrometry*, 2007, **22**, 187-221.

133. H. M. Anawar, *Talanta*, 2012, **88**, 30-42.

134. K. Fytianos, *Journal of AOAC International*, 2001, **84**, 1763-1769.

135. E. Bakker and E. Pretsch, *Analytical Chemistry*, 2002, **74**, 420 A-426 A.

136. E. Bakker, E. Pretsch and P. Bühlmann, *Analytical Chemistry*, 2000, **72**, 1127-1133.

137. X. Dai, O. Nekrassova, M. E. Hyde and R. G. Compton, *Analytical Chemistry*, 2004, **76**, 5924-5929.

138. M. Tercier-Waeber, J. Buffle, F. Graziottin and M. Koudelka-Hep, 2000.

139. A. A. Mota, J. Buffle, S. Kounaves and M. S. Goncalves, *Analytica Chimica Acta*, 1985, **172**, 13-30.

140. J. Pei, M.-L. Tercier-Waeber and J. Buffle, *Analytical Chemistry*, 2000, **72**, 161-171.

141. J. Barek, A. G. Fogg, A. Muck and J. Zima, *Critical Reviews in Analytical Chemistry*, 2001, **31**, 291-309.

142. Y. Yang, P. Pathirathna, T. Siriwardhane, S. P. McElmurry and P. Hashemi, *Analytical Chemistry*, 2013, **85**, 7535-7541.

143. L. Kiaune and N. Singhasemanon, *in Reviews of Environmental Contamination and Toxicology Volume 213*, Springer, 2011, pp. 1-26.

144. M. E. Hyde and R. G. Compton, *Journal of Electroanalytical Chemistry*, 2003, **549**, 1-12.

145. R. B. Keithley, P. Takmakov, E. S. Bucher, A. M. Belle, C. A. Owesson-White, J. Park and R. M. Wightman, *Analytical Chemistry*, 2011, **83**, 3563-3571.

146. E. J. Parra, P. Blondeau, G. A. Crespo and F. X. Rius, *Chem Commun*, 2011, **47**, 2438-2440.

147. D. Grujicic and B. Pesic, *Electrochimica Acta*, 2002, **47**, 2901-2912.

148. D. Grujicic and B. Pesic, *Electrochimica Acta*, 2005, **50**, 4426-4443.

149. D. Krznaric and T. Goricnik, *Langmuir*, 2001, **17**, 4347-4351.

150. R. Srinivasan and P. Gopalan, *Surface Science*, 1995, **338**, 31-40.

151. K. Shi, K. Hu, S. Wang, C.-Y. Lau and K.-K. Shiu, *Electrochimica Acta*, 2007, **52**, 5907-5913.

152. D. E. García-Rodríguez, L. H. Mendoza-Huizar, C. H. Rios-Reyes and M. A. Alatorre-Ordaz, *Química Nova*, 2012, **35**, 699-704.

153. C. Nila and I. González, *Journal of Electroanalytical Chemistry*, 1996, **401**, 171-182.

154. K. Yoo, B. Miller, X. Shi and R. Kalish, *Journal of the Electrochemical Society*, 2001, **148**, C95-C101.

155. L. Huang, E.-S. Lee and K.-B. Kim, *Colloids and Surfaces A: Physicochemical and Engineering Aspects*, 2005, **262**, 125-131.

156. G. G. Láng, M. Ujvári and G. Horányi, *Journal of Electroanalytical Chemistry*, 2002, **522**, 179-188.

157. J.-J. Lee, B. Miller, X. Shi, R. Kalish and K. A. Wheeler, *Journal of the Electrochemical Society*, 2001, **148**, C183-C190.

158. A. J. Bard and L. R. Faulkner, *Electrochemical methods: fundamentals and applications*, Wiley New York, 1980.

159. D. Mohan and C. U. Pittman, *Journal of Hazardous Materials*, 2006, **137**, 762-811.

160. M. Corapcioglu and C. Huang, *Water research*, 1987, **21**, 1031-1044.

161. M. Seredych, D. Hulicova-Jurcakova, G. Q. Lu and T. J. Bandosz, *Carbon*, 2008, **46**, 1475-1488.

162. S. Biniak, M. Pakula, G. Szymanski and A. Swiatkowski, *Langmuir*, 1999, **15**, 6117-6122.

163. D. McPhail and B. Goodman, *Biochemical Journal*, 1984, **221**, 559.

164. J. Nagaj, K. Stokowa-Sołtys, E. Kurowska, T. Frączyk, M. Jeżowska-Bojczuk and W. Bal, *Inorganic chemistry*, 2013, **52**, 13927-13933.

165. A. E. Ross and B. J. Venton, *The Analyst*, 2012, **137**, 3045-3051.

166. J. G. Roberts, K. L. Hamilton and L. A. Sombers, *The Analyst*, 2011, **136**, 3550-3556.

167. L. Miguel-Chinchilla, E. Gonzalez and F. A. Comin, *Environ Monit Assess*, 2014, **186**, 5247-5259.

168. Y. G. Gu, Q. S. Li, J. H. Fang, B. Y. He, H. B. Fu and Z. J. Tong, *Ecotoxicol Environ Saf*, 2014, **105**, 7-12.

169. J. Zobrist, M. Sima, D. Dogaru, M. Senila, H. Yang, C. Popescu, C. Roman, A. Bela, L. Frei, B. Dold and D. Balteanu, *Environmental science and pollution research international*, 2009, **16 Suppl 1**, S14-26.

170. L. Ritter, K. Solomon, P. Sibley, K. Hall, P. Keen, G. Mattu and B. Linton, *Journal of toxicology and environmental health. Part A*, 2002, **65**, 1-142.

171. K. S. Murray, D. T. Rogers and M. M. Kaufman, *Journal of environmental quality*, 2004, **33**, 163-172.

172. C. H. Burton, *Livestock Science*, 2007, **112**, 208-216.

173. A. Cestonaro do Amaral, A. Kunz, R. L. Radis Steinmetz and K. C. Justi, *Journal of environmental management*, 2014, **141**, 132-137.

174. K. Page, M. J. Harbottle, P. J. Cleall and T. R. Hutchings, *The Science of the total environment*, 2014, **487**, 260-271.

175. M. B. McBride, B. K. Richards, T. S. Steenhuis, J. H. Peverly, J. J. Russell and S. Suave, *Mobility and solubility of toxic metals and nutrients in soil fifteen years after sludge application*, 1997.

176. B. K. Richards, T. S. Steenhuis, J. H. Peverly and M. B. McBride, *Environmental pollution (Barking, Essex : 1987)*, 1998, **99**, 365-377.

177. N. Prat, J. Toja, C. Sola, M. D. Burgos, M. Plans and M. Rieradevall, *The Science of the total environment*, 1999, **242**, 231-248.

178. C. Solà, M. a. Burgos, Á. Plazuelo, J. Toja, M. Plans and N. s. Prat, *Science of The Total Environment*, 2004, **333**, 109-126.

179. J. Nason, D. Bloomquist and M. Sprick, *Journal of Environmental Engineering*, 2012, **138**, 734-742.

180. M. Ferreira, S. L. Lau and M. K. Stenstrom, *Water environment research : a research publication of the Water Environment Federation*, 2013, **85**, 793-805.

181. C. Dean, J. Sansalone, F. Cartledge and J. Pardue, *Journal of Environmental Engineering*, 2005, **131**, 632-642.

182. P. P. Hernandez, C. Undurraga, V. E. Gallardo, N. Mackenzie, M. L. Allende and A. E. Reyes, *Biological research*, 2011, **44**, 7-15.

183. B. A. Chowdhury and R. K. Chandra, *Progress in food & nutrition science*, 1987, **11**, 55-113.

184. P. C. Stanley and V. C. Wakwe, *The Nigerian postgraduate medical journal*, 2002, **9**, 199-204.

185. G. Du Laing, J. Rinklebe, B. Vandecasteele, E. Meers and F. M. G. Tack, *Sci Total Environ*, 2009, **407**, 3972-3985.

186. M. F. Leal and C. G. Van Den Berg, *Aquatic Geochemistry*, 1998, **4**, 49-75.

187. C. M. G. van den Berg and J. R. Donat, *Analytica Chimica Acta*, 1992, **257**, 281-291.

188. R. Mugabe, T. J. Nyangababo and K. H. *Schr⊘der, International Journal of Environmental Studies*, 1998, **55**, 247-253.

189. Y. Cheng, D. J. Schiffrin, P. Guerriero and P. A. Vigato, *Inorganic Chemistry*, 1994, **33**, 765-769.

190. P. Flash, *Journal of Chemical Education*, 1994, **71**, A6.

191. R. Aydin, U. Ozer and N. Turkel, *Turk. J. Chem.*, 1997, **21**, 428-436.

192. M. J. Potter, M. K. Gilson and J. A. McCammon, *Journal of the American Chemical Society*, 1994, **116**, 10298-10299.

193. D. L. Parkhurst, and Appelo, C.A.J., 2013, **book 6**, 497 p.

194. J. D. Allison, D.S. Brown, and K.J. Novo-Gradae, , 1990, p. 106 p.

195. M. A. Mercê ALR, Szpoganicz B, Levy NM, and Felcman J, *J. Braz. Chem. Soc*, 1996, **7(4)**.

196. R. M. Smith, A. E. Martell, R. J. Motekaitis and p. Standard Reference Data, *Journal*, 2004.

197. D. B. McPhail and B. A. Goodman, *Biochem J*, 1984, **221**, 559-560.

198. H. E. Mash, Y.-P. Chin, L. Sigg, R. Hari and H. Xue, *Analytical chemistry*, 2002, **75**, 671-677.

199. M. T. Vasconcelos, M. A. Azenha and O. M. Lage, *Anal Biochem*, 1996, **241**, 248-253.

200. D. Wyrzykowski, B. Pilarski, D. Jacewicz and L. Chmurzyński, *J Therm Anal Calorim*, 2013, **111**, 1829-1836.

201. P. Pathirathna, S. Samaranayake, C. W. Atcherley, K. L. Parent, M. L. Heien, S. P. McElmurry and P. Hashemi, *The Analyst*, 2014, **139**, 4673-4680.

202. D. P. Manica, Y. Mitsumori and A. G. Ewing, *Anal Chem*, 2003, **75**, 4572-4577.

203. I. Kostic, T. Andelkovic, R. Nikolic, A. Bojic, M. Purenovic, S. Blagojevic and D. Andelkovic, *J.Serb.Chem.Soc*, 2011, **76(9)**, 1325-1336.

204. B. Halliwell, *in Free radicals in the brain*, Springer, 1992, pp. 21-40.

205. D. J. Waggoner, T. B. Bartnikas and J. D. Gitlin, *Neurobiology of disease*, 1999, **6**, 221-230.

206. V. Desai and S. G. Kaler, *The American journal of clinical nutrition*, 2008, **88**, 855S-858S.

207. H. E. Allen and D. J. Hansen, *Water Environment Research*, 1996, **68**, 42-54.

208. G. K. Pagenkopf, R. C. Russo and R. V. Thurston, *Journal of the fisheries board of Canada*, 1974, **31**, 462-465.

209. W. Sunda, Massachusetts Institute of Technology and Woods Hole Oceanographic Institution, 1975.

210. H. Gampp, M. Maeder, C. J. Meyer and A. D. Zuberbühler, *Talanta*, 1985, **32**, 257-264.

211. W. C. Swope, H. C. Andersen, P. H. Berens and K. R. Wilson, *The Journal of Chemical Physics*, 1982, **76**, 637-649.

212. C. B. Jacobs, I. N. Ivanov, M. D. Nguyen, A. G. Zestos and B. J. Venton, *Analytical Chemistry*, 2014, **86**, 5721-5727.

213. E. House, J. Collingwood, A. Khan, O. Korchazkina, G. Berthon and C. Exley, *Journal of Alzheimer's disease: JAD*, 2004, **6**, 291-301.

214. M. Barry, D. M. Flynn, E. A. Letsky and R. Risdon, *BMJ*, 1974**, 2**, 16-20.

215. S. Flora, M. Mittal and A. Mehta*, Indian Journal of Medical Research*, 2008, **128**, 501.

216. P. Caravan, J. J. Ellison, T. J. McMurry and R. B. Lauffer, *Chemical reviews*, 1999, **99**, 2293-2352.

217. E. J. Werner, A. Datta, C. J. Jocher and K. N. Raymond, *Angewandte Chemie International Edition*, 2008, **47**, 8568-8580.

218. P. C. Goffinet, Journal, 1983.

219. C. D. Bragg, Journal, 1984.

220. W. E. Morf, *The principles of ion-selective electrodes and of membrane transport*, Elsevier, 2012.

221. J. Bjerrum and P. Andersen, *Metal ammine formation in aqueous solution*, Munksgaard, 1945.

222. P. Gans, A. Sabatini and A. Vacca, *Talanta*, 1996, **43**, 1739-1753.

223. H. K. Frensdorff, *Journal of the American Chemical Society*, 1971, **93**, 600-606.

224. R. Wimmer, F. L. Aachmann, K. L. Larsen and S. B. Petersen, *Carbohyd Res*, 2002, **337**, 841-849.

225. A. Mercê, A. Mangrich, B. Szpoganicz, N. Levy and J. Felcman, *JOURNAL OF THE BRAZILIAN CHEMICAL SOCIETY*, 1996, **7**, 239-245.

226. S. Sauvé, M. McBride and W. Hendershot, Archives *of Environmental Contamination and Toxicology*, 1995, **29**, 373-379.

227. J. Buffle, F. L. Greter and W. Haerdi, *Analytical Chemistry*, 1977, **49**, 216-222.

228. D. Lake, P. Kirk and J. Lester, *Journal of Environmental Quality*, 1984, **13**, 175-183.

229. P. Pathirathna, Siriwardhane, T., McElmurry S. P , Hashemi P, *The Analyst*,2016.-under review

230. R. Nalbandyan, *Neurochemical research*, 1983, **8**, 1211-1232.

231. H. Porter and S. Ainsworth, *Journal of Neurochemistry*, 1961, **7**, 20-25.

232. F. Stevenson and Y. Chen, *Soil Science Society of America Journal*, 1991, **55**, 1586-1591.

233. M. Ghaedi, F. Ahmadi and M. Soylak, *Journal of Hazardous Materials*, 2007, **147**, 226-231.

ABSTRACT

A NOVEL, ULTRA-FAST ELECTROCHEMICAL TOOL TO STUDY SPECIATION OF TRACE METALS IN AQUEOUS SOLUTION

by

PAVITHRA PATHIRATHNA

May 2016

Advisor: Dr. Parastoo Hashemi

Major: Chemistry (Analytical)

Degree: Doctor of Philosophy

Trace metals play important roles in biological and ecological systems. In biology, trace metals act as catalytic or structural cofactors and regulate biochemical processes. In the environment, natural and anthropogenic sources of trace metals mobilized into natural waters where they can create harmful and persistent pollution. Trace metal chemistry in physiological and environmental systems can fluctuate rapidly which makes it difficult to clearly define trace metals' roles in these systems with traditional analytical methods. Furthermore, these systems are often chemically harsh and physically delicate (e.g. the brain), factors that add to the challenge of analysis in real systems. Fast scan cyclic voltammetry is explored in the context of rapid, minimally invasive and robust analysis of Cu^{2+} and Pb^{2+} in aqueous samples with carbon fiber microelectrodes.

Unique Cu^{2+}-specific and Pb^{2+}-specific waveforms were generated with optimized potential windows and scan rates to provide sub-second analysis of these two trace metals. An array of electrochemical and spectroscopic techniques was employed to discover the underlying mechanisms of the ultra fast FSCV response. Adsorption was explained as the fundamental mechanism for the rapid FSCV signal and the thermodynamic properties of adsorption of Cu^{2+} onto CFMs were evaluated with fast scan controlled adsorption voltammetry in different matrices. In aquatic systems and soils, metals commonly exist in complexed forms with organic and inorganic ligands. It is generally the free, unbound metal that is the most toxic, thus metal speciation is a critical factor when considering metal pollution. Free Cu^{2+} concentrations and the solution formation constant, K_fs, provide valuable speciation information. We show that FSCV and FSCAV can be utilized to study copper speciation. Mathematical relationships were constructed from experimental data to predict free Cu^{2+} concentrations and the overall K_fs of a solution with a range of model ligands, representing a range of Cu^{2+}- ligand K_fs expected to be encountered naturally. These findings showcase the power of FSCV as a real-time biocompatible, eco-friendly speciation sensor with excellent sensitivity and a temporal resolution of milliseconds.

AUTOBIOGRAPHICAL STATEMENT

Pavithra Pathirathna

EDUCATION

2011 - 2016	Wayne State University Detroit, MI	Ph.D., Chemistry
2009 - 2011	University of Kelaniya Sri Lanka	B.Sc., Chemistry

HONORS

2015	Best graduate student oral presentation, ANACHEM/SAS Detroit Section Symposium, Livonia, MI
2015	Esther and Stanley Kirschner General Chemistry Teaching Award (Best General Chemistry Teaching Assistant), Wayne State University, MI
2014	Honor Citation for Teaching Service in Chemistry, Wayne State University, MI
2013	Graduate Student Professional Travel Award, Wayne State University, MI
2012	Paul and Carol C. Schaap Endowed Distinguished Graduate Student Fellowship, Wayne State University, MI
2009	Silver Medalist, Inter University Chemistry Competition organized by Royal Chemical Society, Sri Lanka

SELECTED PUBLICATIONS

1. **P. Pathirathna**, T. Siriwardhane, S. P. McElmurry and P. Hashemi, *The Analyst*, 2016 - Under Review.
2. T. Siriwardhane, **P. Pathirathna** , A. Sulkanen, A. Tremonti, S. P. McElmurry and P. Hashemi, *Analytica Chimixa Acta*, 2015 - Under Review.
3. **P. Pathirathna**, S. Samaranayake, C. W. Atcherley, K. L. Parent, M. L. Heien, S. P. McElmurry and P. Hashemi, *The Analyst*, 2014, **139**, 4673-4680.
4. Y. Yang, **P. Pathirathna**, T. Siriwardhane, S. P. McElmurry and P. Hashemi, *The Analytical Chemistry*, 2013, **85**, 7535-7541.
5. **P. Pathirathna**, Y. Yang,K. Forzley, S. P. McElmurry and P. Hashemi, *Analytical Chemistry*, 2012, **84**, 6298-6302.